Initial Investigation of Reinforced Concrete Filled Tubes for use in Bridge Foundations

WA-RD 776.1

Charles Roeder
Dawn Lehman

June 2012

Washington State Department of Transportation
Office of Research & Library Services

WSDOT Research Report

Research Report
Agreement T4118, Task 58
Bridge Foundations

INITIAL INVESTIGATION OF REINFORCED CONCRETE FILLED TUBES FOR USE IN BRIDGE FOUNDATIONS

by

Charles Roeder
Professor

Dawn Lehman
Associate Professor

Department of Civil and Environmental Engineering
University of Washington, Box 352700
Seattle, Washington 98195

Washington State Transportation Center (TRAC)
University of Washington, Box 354802
University District Buildin
1107 NE 45th Street, Suite 535
Seattle, Washington 98105-4631

Washington State Department of Transportation
Technical Monitor
Bijan Khaleghi
Bridge Design Engineer, Bridge Administration Section

Prepared for

The State of Washington
Department of Transportation
Paula J. Hammond, Secretary

June 2012

TECHNICAL REPORT STANDARD TITLE PAGE

1. REPORT NO.	2. GOVERNMENT ACCESSION NO.	3. RECIPIENT'S CATALOG NO.
WA-RD 776.1		

4. TITLE AND SUBTITLE	5. REPORT DATE
INITIAL INVESTIGATION OF REINFORCED CONCRETE FILLED TUBES FOR USE IN BRIDGE FOUNDATIONS	June 2012
	6. PERFORMING ORGANIZATION CODE
7. AUTHOR(S)	8. PERFORMING ORGANIZATION REPORT NO.
Charles Roeder, Dawn Lehman	
9. PERFORMING ORGANIZATION NAME AND ADDRESS Washington State Transportation Center (TRAC) University of Washington, Box 354802 University District Building; 1107 NE 45th Street, Suite 535 Seattle, Washington 98105-4631	10. WORK UNIT NO.
	11. CONTRACT OR GRANT NO. Agreement T4118, Task 58
12. SPONSORING AGENCY NAME AND ADDRESS Research Office Washington State Department of Transportation Transportation Building, MS 47372 Olympia, Washington 98504-7372 Project Manager: Kim Willoughby, 360.705.7978	13. TYPE OF REPORT AND PERIOD COVERED Research Report
	14. SPONSORING AGENCY CODE

15. SUPPLEMENTARY NOTES

This study was conducted in cooperation with the U.S. Department of Transportation, Federal Highway Administration.

16. ABSTRACT:

The Washington State Department of Transportation (WSDOT) frequently employs deep pile or caisson bridge foundations for its bridge structures. Deep pile and drilled shaft foundations are increasingly important for seismic design in Washington state, because of increased seismic design load demands in bridge design specifications. A common caisson is a reinforced concrete filled tube caisson. Although these types of foundation elements are common, there are few guidelines on their design. As a result, current WSDOT design methods are conservative and neglect the many benefits provided by composite action of the concrete and the steel tube, which may result in increased cost and size of the foundation. Recent research on composite concrete filled steel tubes (CFT) shows significant benefit for applications using CFT elements, in particular that CFT elements can develop more lateral resistance and greater inelastic deformation capacity with less deterioration of resistance than reinforced concrete elements of the same weight and diameter. Hence the use of this composite action permits smaller diameter and shorter caisson foundations resulting in cost savings associated with a smaller piles and drilled shafts, less material and reduced construction time and cost. This research involves consideration of the composite properties of CFT members with internal reinforcement, and this special case of internally reinforced CFT is identified as RCFT in this report.

The research study used analytical tools verified using past experimental and analytical research on CFT members and foundation connections without internal reinforcement. The research included comprehensive review of past research results including experiments and analysis of CFT and RCFT elements and connections. Design models were evaluated and compared to prior test results to determine their accuracy and reliability. A comprehensive analytical study was performed to extend this prior research to current WSDOT RCFT applications. The analytical studies were calibrated to past experimental results to document their accuracy, and the analysis included development of basic design models, fiber or section based analysis, and detailed continuum based models. No experiments were included in this initial study, but observations from prior experimental research were to be used to support the work. The goals of this preliminary study were to develop initial answers to uncertainly in the design process of these components and their connections to permit the WSDOT to begin to employ the benefits of composite action for these sub-structural systems. To that end, specific design recommendations from this preliminary research study are provided. Finally, an overview of the additional research needed to further develop the deep foundation system is provided.

17. KEY WORDS	18. DISTRIBUTION STATEMENT
Concrete Filled Tubes, Caissons, Connections	No restrictions. This document is available to the public through the National Technical Information Service, Springfield, VA 22616

19. SECURITY CLASSIF. (of this report)	20. SECURITY CLASSIF. (of this page)	21. NO. OF PAGES	22. PRICE
None	None		

DISCLAIMER

The contents of this report reflect the views of the authors, who are responsible for the facts and the accuracy of the data presented herein. The contents do not necessarily reflect the official views or policies of the Washington State Department of Transportation or Federal Highway Administration. This report does not constitute a standard, specification, or regulation.

Table of Contents

List of Figures

List of Tables

Notation

A_b - Area of internal reinforcing bars in RCFT
A_c - Area of concrete
A_s - Area of steel
CFT - Concrete filled tube
C_{max} - Compressive force in concrete due to combined axial and bending
C_s - Compressive force in steel tube due to combined axial and bending
D - Diameter of the tube
D_o - Outside diameter of annular ring or diameter of corrugated tube
E = Elastic modulus
EI_{eff} - Effective EI of CFT or RCFT
F_{EXX} - Tensile strength of weld electrode
F_y - Yield strength of steel
F_{yb} - Yield strength of steel reinforcing bars in RCFT
F_{ys} - Yield strength of steel tube
F_u - Tensile strength of steel
I = Moment of inertia
K - Effective length coefficient
M - Bending moment
M_u - Factored bending moment
P - Axial load
P_e - Euler buckling load
P_o - Ultimate axial crushing load
P_u - Factored axial load
PSDM - Plastic stress distribution method
R - Curvature parameter for nonlinear model of RCFT and CFT
RC - Reinforced concrete
RCFT - Concrete filled tube with internal reinforcement
V_u - Factored shear design force
c - One half chord length of the compressive block for PSDM
c_b - One half chord length for the internal reinforcing bars for PSDM
f'_c - Compressive strength of concrete
f'_{cf} - Compressive strength of concrete fill in CFT or RCFT
h - Depth required for punching shear of footing
l - Column length for determining Kl/r
l_e - Embedment length for cone pullout of full-strength CFT foundation connection
r - Radius of gyration
r_b - Mean radius of internal reinforcement
r_{im} - Mean radius of internal reinforcement
r_m - Mean radius of tube
s - Maximum spacing of shear reinforcing in cone pullout region
t - Thickness of the tube
y - Vertical distance of neutral axis from center of tube in plastic stress distribution method
Δ - Column deflection for nonlinear model of CFT and RCFT

δ - Secondary deflection for computing P-δ moments
ϕ - Resistance factor
λ - Ratio of $\frac{Kl}{r\pi}\sqrt{\frac{F_y}{E}}$
ρ - Ratio of flexural reinforcement
ρ_i - Ratio of internal reinforcement
θ - Connection rotation for full strength CFT or RCFT connection
θ_b - Angle to axis location y in the reinforcing bars
θ_s - Angle to axis location y in the tube

CHAPTER 1

INTRODUCTION

The Washington State Department of Transportation (WSDOT) frequently employs deep pile or caisson bridge foundations for its bridge structures. An example of a foundation system is illustrated in Figure 1.1; this foundation is the Pier No. 4 of the Ebey Slough project. This pile extends approximately 238 ft below the base of the bridge pier. The pile is a 6-ft in diameter steel tube with 1-in. minimum wall thickness, and the top 87 ft are filled with concrete and reinforced with 32 #14 longitudinal bars. Therefore, this foundation includes a reinforced concrete filled tube caisson element. Other deep foundations may be large diameter drilled shafts with a steel tube inserted into the shaft. Both the drilled shafts and tubular piles are filled with reinforced concrete to complete the sub-structure element, and form the connection to the piers of the bridge substructure.

Although these types of foundation elements are common, there are few if any guidelines on their design; in particular, design guidance on the inclusion of the steel tube in the strength and stiffness calculations is lacking. The current AASHTO Bridge Design Code for bridge piles and/or shafts does not adequately describe how to design a pile or shaft that uses a steel casing and reinforced concrete fill. As a result, current design methods are conservative and neglect the many benefits provided by composite action of the concrete and the steel tube. As a result, the cost and size of the foundation may be much larger than necessary.

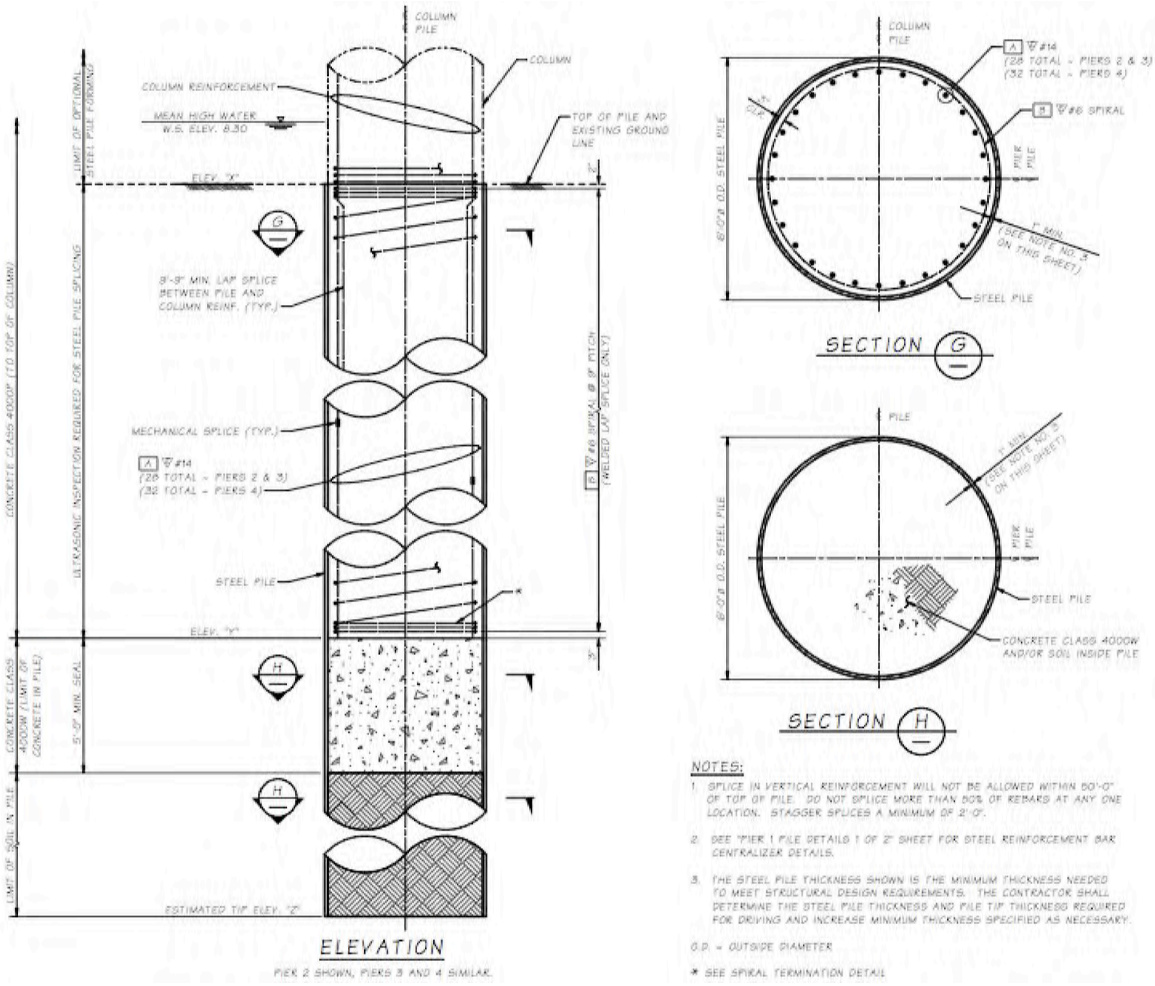

Figure 1.1. Pier No. 4 Caisson Ebey Slough

Recent research on composite concrete filled steel tubes (CFT) shows significant benefit for applications using CFT elements. The steel tube serves as formwork and reinforcement for the concrete fill. The concrete fill restrains local and global buckling and significantly increases resistance and inelastic deformation capacity. Recent analysis and experiments performed for the California Department of Transportation (CALTRANS) has shown that CFT elements can develop more lateral resistance and greater inelastic deformation capacity with less deterioration of resistance than reinforced concrete elements of the same weight and diameter.

Hence the use of this composite action permits smaller diameter and shorter caisson foundations resulting in cost savings associated with a smaller piles and drilled shafts, less material and reduced construction time and cost.

Deep pile and drilled shaft foundations are increasingly important for seismic design in Washington state, because of increased seismic design load demands in bridge design specifications. Recent University of Washington research has shown great economic benefit in employing the composite resistance and stiffness of the resulting CFT member, and this research project was a first step to permitting WSDOT engineers to fully utilize these benefits. This research involves consideration of the composite properties of CFT members with internal reinforcement, and this special case of internally reinforced CFT is identified as RCFT in this report.

SCOPE OF THE RESEARCH

This research is an analytical study that builds upon past experimental and analytical research on CFT members and foundation connections. The research was closely coordinated with WSDOT engineers, and the broad goals of the research were established in a meeting with WSDOT engineers on November 17, 2009. Eleven primary research priorities were established during that meeting. They were as follows:

1. To develop analytical models with hand solution equations
2. To develop design examples using the outcome of the analytical model
3. To consider both the single shaft-single column case, and CFT pile cap connections
4. To ensure that any analytical model includes both steel casing and internal reinforcement
5. To determine minimum casing thickness for structural and pile

driving

6. To recommend the relative proportion of internal reinforcement vs. casing in composite section
7. To develop connection details for attachment of the steel casing to the pile cap
8. To develop stress-strain or moment-curvature models for RCFT composite sections, which included the strength of the casing, the internal reinforcement, and the concrete
9. To investigate casing manufacturers and availability for type and size
10. To investigate the use of spirally welded steel tubes
11. To determine corrosion rate for steel casing.

The research included comprehensive review of past research results including experiments and analysis of CFT and RCFT elements and connections. Design models were evaluated and compared to prior test results to determine their accuracy and reliability. A comprehensive analytical study was performed to extend this prior research to current WSDOT RCFT applications. The analytical studies were calibrated to past experimental results to document their accuracy, and the analysis included development of basic design models, fiber or section based analysis, and detailed continuum based models. No experiments were included in this initial study, but observations from prior experimental research were to be used to support the work. The goals of this preliminary study were to develop initial answers to the 11 issues noted above and to permit WSDOT engineers to begin employing the benefits of composite action for these sub-structural systems.

In view of the practical goals of this research, the researchers met with WSDOT engineers at regular intervals throughout the study to discuss progress and refine the requirements of WSDOT engineering practice. These meetings were held on March 28,

2010; June 8, 2010 and February 24, 2011. During the February 24, 2011, meeting, supplement funding and a time extension were provided to permit analysis of typical WSDOT pile-to-pile-cap connection details. Discussions from these meetings were incorporated into the research and were used to establish the recommendations provided here.

SCOPE OF THE REPORT

This report summarizes the results of the preliminary study. Chapter 2 provides an abbreviated summary of current design methods, past experimental and analytical research on CFT applications, and comparison of this past research to design and evaluation methods. Chapter 3 summarizes the extended analytical research performed with this study. Here the results from CFT research are analytically extended to reinforced concrete filled tube (RCFT) applications. Alternative analytical methods for RCFT are demonstrated, and comparisons of the expected performance of RCFT and CFT are provided. Chapter 4 provides recommendations from this preliminary research study. It addresses issues, including the 11 issues noted earlier, and provides a design example that demonstrates how the use of composite action could benefit WSDOT engineers. Chapter 5 summarizes the design recommendations and recommended analytical procedures for CFT and RCFT. Finally, Chapter 6 provides a summary and conclusions from the work and the additional research needed to further develop the deep foundation system.

CHAPTER 2

CURRENT DESIGN MODELS FOR AND PREVIOUS RESEARCH ON CFT

CFT offers many practical advantages, but it has had limited use in US construction with much wider use in Asia. Relative to conventional structural systems, such as reinforced concrete and steel, CFT components offers increased strength and stiffness. The concrete infill provides stiffness and strength in compression. The steel tube provides large tensile and compressive capacity, and the fill restrains local and global buckling. The inelastic deformation capacity of the CFT system is increased by the confinement of the concrete fill by the thin, ductile steel tube, and this significantly contributes to the seismic performance. Furthermore, CFTs are economical, reducing labor requirements and permitting rapid construction, because the steel tube serves as formwork and reinforcement to the concrete fill. The concrete fill can be placed without vibration using self-consolidating concrete (SCC).

CFT may employ either circular or rectangular tubes. Rectangular CFT is used more frequently in practice, because their shape permits more direct steel-to-steel connections, but circular CFT is more applicable to deep bridge foundations and offers several major advantages. Shear stress transfer between the steel and concrete is needed to develop composite action, and prior research (Roeder et al. 2009, and Roeder et al. 1999) shows that circular CFT provides greater bond stress transfer, better confinement, and increased shear reinforcement to the concrete fill than rectangular CFT. When the bond stress for CFT members is limited, modest bending moments and some structural

connection details dramatically enhance bond stress transfer. As a result, shear connectors are seldom required for these conditions. However, careful attention must be paid to the bond stress requirements for CFT components with high axial load and little or not bending moment. A secure interface between the concrete and the steel is required, and therefore concrete shrinkage must be minimized.

While circular CFT offers great benefits, it is less frequently used, because the design provisions and the structural connections for circular CFTs are not well defined. The following section summarizes the current design methods and connection details for circular CFT.

CURRENT DESIGN METHODS FOR CFT

Strength and stiffness are important design properties, and the American Institute of Steel Construction (AISC) LRFD and the American Concrete Institute (ACI) 318 Specifications (AISC 2005, ACI 2008) provide expressions to estimate these engineering parameters for CFT members. However, the two specifications provide quite different design limits and expressions for CFT. The American Association of State Highway and Transportation Officials (AASHTO) LRFD Specifications and the Seismic Design Guidelines (AASHTO 2009 and 2007) also provide design rules for CFT, which are also different from the AISC and ACI provisions.

Expressions to Predict Flexural Resistance

Chapter I of the AISC Specification (2005a) permits the use of (1) the plastic stress distribution or (2) the strain-compatibility method for predicting the flexural and axial resistance of circular CFT components. The plastic-stress distribution method

assumes that the section develops a uniform compressive stress of $0.95f'_c$ in the concrete and the full yield stress, F_y, of the steel in tension and compression as illustrated in Figure 2.1a. The $0.95f'_c$ concrete stress is larger than the coefficient of $0.85f'_c$ typically used for a Whitney stress block calculation in recognition of the beneficial effects of concrete confinement in circular CFT. With this method, axial load and bending resistance pairs are determined by satisfying equilibrium over the cross-section for each possible neutral axis location to establish the axial-moment (P-M) diagram, as shown in Figure 2.1a. Small D/t results in larger resistance, because the area of steel is larger relative to the amount of concrete, but larger D/t values result in significantly increased bending moment for modest axial loads, as shown in Figure 2a, because of the increased contribution of concrete fill in compression. Figure 2.1b demonstrates these same effects in dimensionless form.

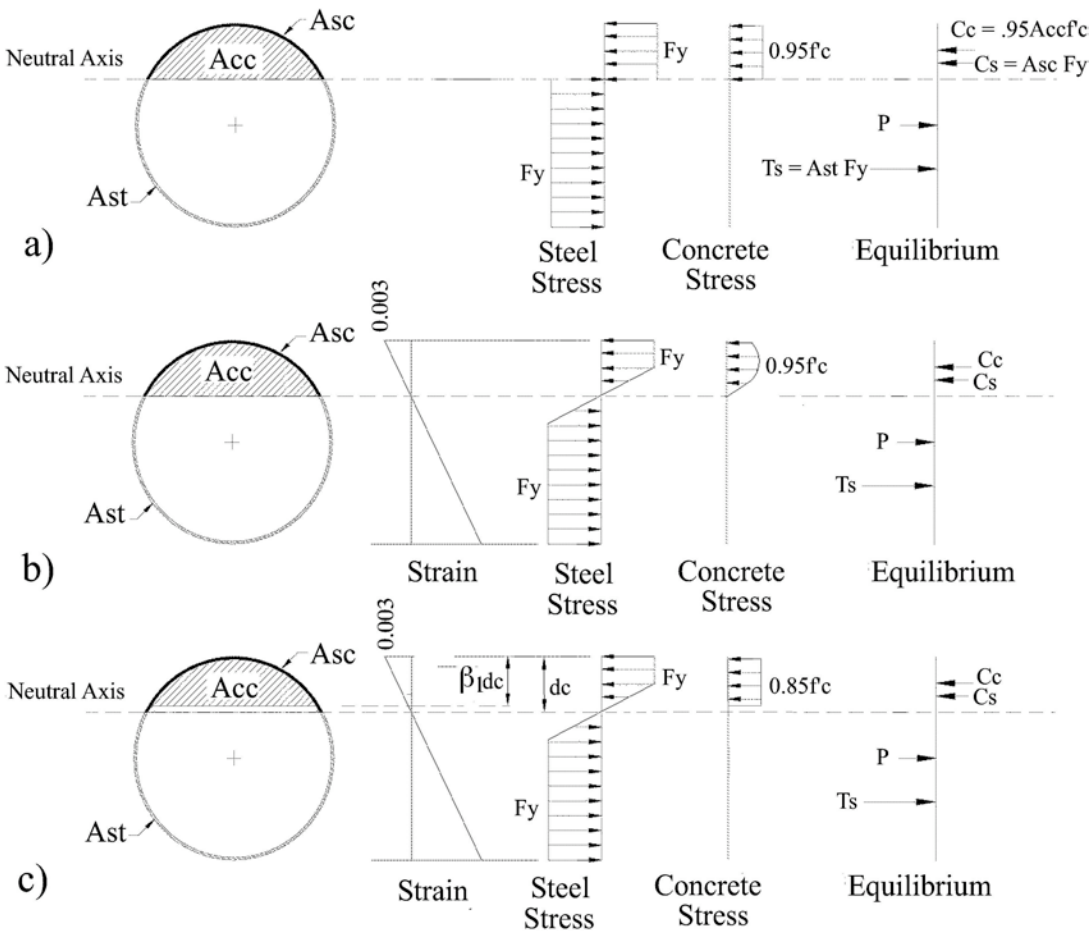

Figure 2.1 Models for prediction of resistance of CFT; a) Plastic Stress Distribution Method, b) AISC Strain Compatibility Method, and c) ACI Method

The AISC strain compatibility method is adapted from a conventional flexural strength calculation used to predict the flexural strength of a reinforced concrete section. It employs a linear strain distribution. The material models include an elastic-perfectly plastic curve to model the steel and a parabolic curve for the concrete. By satisfying the constitutive and equilibrium relations, the flexural strength is determined for a maximum compressive strain in the concrete of 0.003 mm/mm. The ACI design procedure, shown in Figure 2.1c, is similar to the AISC strain compatibility method, except that it is permitted to use an equivalent rectangular stress block with a 0.85f'c compressive stress

acting over a depth $\beta_1 c$, where β_1 depends on the concrete strength. In the expression, c is the depth from the location of the maximum compressive strain to the neutral axis depth.

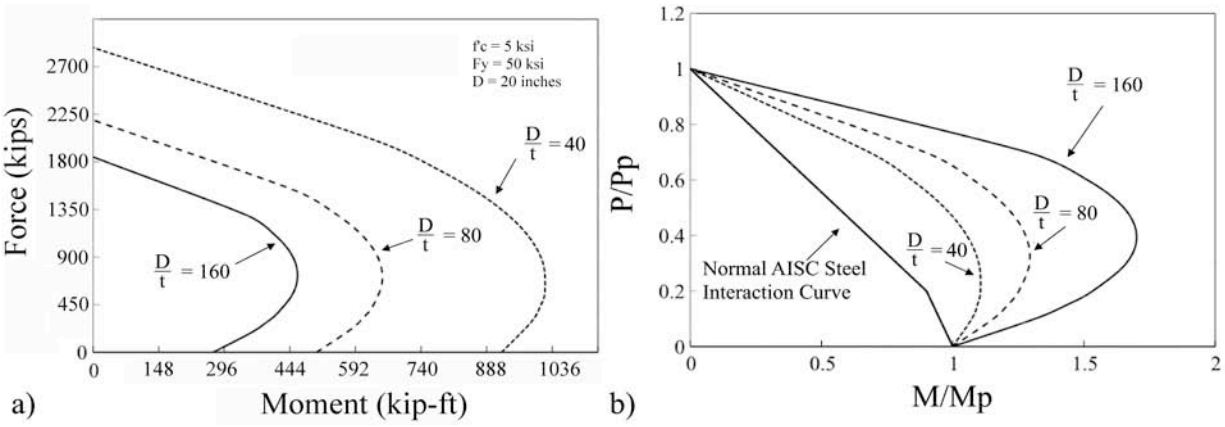

Figure 2.2 Axial load-bending moment interaction curves for CFT: (a) plastic stress distribution, (b) normalized

The AASHTO LRFD (AASHTO 2005) Specifications (Sections 6.9.5 and 6.12.2) address the design of circular CFT, but these provisions are less sophisticated than the AISC or ACI provisions. The pure moment capacity is limited to the plastic bending capacity of only the steel section, and the axial load capacity is controlled by the yield stress of the steel and a uniform concrete stress of $0.85f'_c$. The axial load and bending moment interaction curve is essentially the interaction curve used by AISC for steel wide flange sections, as illustrated in Figure 2.2b. The AASHTO Guide Specification for LRFD Seismic Bridge Design (Section 7.6) provides a design method that is similar to the AISC plastic stress distribution method.

Stability Limits

The D/t slenderness limit is employed to limit local buckling of the tube to assure development of the plastic capacity of the member. This limit is larger than the limit for a hollow section since the concrete fill restrains local buckling.

Again there is wide variation in these local slenderness limits among the codes. The following equations show the results from the three codes.

$$\frac{D}{t} \le 0.15\frac{E}{F_y} \qquad \text{(AISC Provisions)} \qquad \text{(Eq. 1a)}$$

$$\frac{D}{t} \le \sqrt{\frac{8E}{F_y}} \qquad \text{(ACI Provisions)} \qquad \text{(Eq. 1b)}$$

$$\frac{D}{t} \le 2\sqrt{\frac{E}{F_y}} \qquad \text{(AASHTO LRFD Provisions)} \qquad \text{(Eq. 1a)}$$

These local stability limits yield very different results. For a circular CFT with a steel yield stress of 50 ksi, the limits are approximately 87, 68, and 48 for the AISC, ACI and AASHTO provisions, respectively.

Column buckling is addressed in the AISC (Section I2-1b) and AASHTO provisions by:

$$P_{cr} = 0.658^{\frac{P_o}{Pe}} P_o \qquad \text{for stocky columns where } P_e < .44P_o \qquad \text{(Eq. 2a)}$$

$$P_{cr} = 0.877P_e \qquad \text{for slender columns where } P_e > .44P_o \qquad \text{(Eq. 2b)}$$

$$P_o = 0.95 f_c^{'} A_c + F_y A_s \qquad \text{(Eq.2c)}$$

In the expressions, P_e is the elastic buckling load by the Euler equation, and A_c and A_s are areas of the concrete and steel, respectively. The resistance factor is 0.75 for circular CFT columns, and hence the provisions would never permit a column with axial load ratio,

P/P_o, greater than 0.75 in interaction curves such as Figure 2.2. ACI does not directly consider column buckling, but a minimum eccentricity and moment magnifier are employed to achieve a similar effect.

Effective Stiffness

The effective member stiffness, EI_{eff}, of CFT is needed to define buckling capacity and determine deflections, but there is also significant variation in the design specifications:

$$EI_{eff} = E_s I_s + C_3 E_c I_c \qquad \text{by AISC Provisions} \qquad \text{(Eq. 3a)}$$

where $$C_3 = 0.6 + \left(\frac{A_s}{A_c + A_s} \right) \qquad \text{(Eq. 3b)}$$

$$EI_{eff} = E_s I_s + \frac{.2 E_c I_g}{1 + \beta_d} \qquad \text{by ACI Provisions} \qquad \text{(Eq. 3c)}$$

$$EI_{eff} = E_s I_s + 0.4 \left(\frac{E_c A_c}{A_s} \right) I_s \qquad \text{by AASHTO Provisions} \qquad \text{(Eq. 3d)}$$

In the expressions, A, E, and I are the area, elastic modulus, and moment of inertia of the section for the respective materials. The subscripts c, s, and g refer to properties of the concrete, steel and gross concrete sections, respectively. The contribution of internal reinforcement is included in the specification provisions, but the effect is not included in some equations discussed in this chapter, because the CFT experiments used here do not include internal reinforcement, the effects of additional internal reinforcement. The β_d in Eq. 3c is usually approximately 1.0, and so the AASHTO and AISC provisions predict a larger effective stiffness than the ACI provisions.

PREVIOUS EXPERIMENTAL RESULTS

This research program did include experimental study of CFT component or connections. However, numerous previous experimental studies were performed on circular CFT, and these previous results were used to evaluate the accuracy and validity of design models. More than 1800 CFT tests were identified. The focus of this study is on circular concrete filled tubes with realistic sizes. This constraint was used to develop criteria to eliminate non-compliant specimens. Specifically, tests that were not included in this study included (a) rectangular sections, (b) tests subjected to axial load only, (c) tests failing through an irrelevant failure mode such as weld fracture, (d) tests on tubes of very small (less than 4-in.) diameter, (f) those from reports that provided inadequate information to understand the tests or the specimen behavior, or (g) tests on hollow tubes used as control or reference specimens.

The resulting database compiled for this research consisted of 122 circular CFT specimens gathered from 16 test programs and 20 publications as summarized in Table 2.1. Comprehensive information on each test, including the test set-up and configuration, material properties of the steel and concrete, and detailed information regarding specimen behavior including strength, stiffness, cyclic behavior, deterioration of resistance, and inelastic deformation capacity, was assembled (Bishop 2009).

Table 2.1 Circular CFT test data

Source	Diameter (in)	D/t	P/P_o	Kl/r	Number of Specimens	Test Information
Boyd, Cofer & McLean (1995)	8	73-107	10-14%	32-33	5	Foundation Connection
Chronister (2007)	20	80	11-21%	23-24	4	Foundation Connection
Elchalakani et al. (2001)	100-110	40 - 110	0	--	4	Flexural
Elremaily and Azizinamini (2002)	325	34 - 56	20-42%	17-18	6	Beam Column
Fujimoto, et al. (2004)	6-12	34-101	15-80%	9-19	11	Eccentrically Loaded Col.
Furlong (1967)	4-6	36-98	23-63%	21-23	10	Eccentrically Loaded Col.
Han et al. (2006)	100-200	47-105	0	--	18	Flexural
Kingsley (2005)	20	80	9%	23-24	1	Foundation Connection
Marson and Bruneau (2004)	320-405	43-74	19-33%	33-44	4	Foundation Connection
Morino et al. (1997)	9.5	27-53	40-70%	16-25	12	Beam-Column
O'Shea and Bridge (2000)	10.5-11	59-226	78-86%	23-26	6	Flexural
Prion and Boehme (1994)	6	89	15-55% 74-82% 0	21-39 80 --	7 4 5	Beam-Column Eccentrically Loaded Col. Flexural
Thody (2006).	20	80	0	--	6	Flexural Tests
Wheeler and Bridge (2006)	16-18	63-72	0	--	6	Flexural Tests
Williams (2006)	20	80	9%	23-24	2	Foundation Connection
Zhang et al. (2009)	13	57-110	29-59%	28-30	12	Foundation Connection

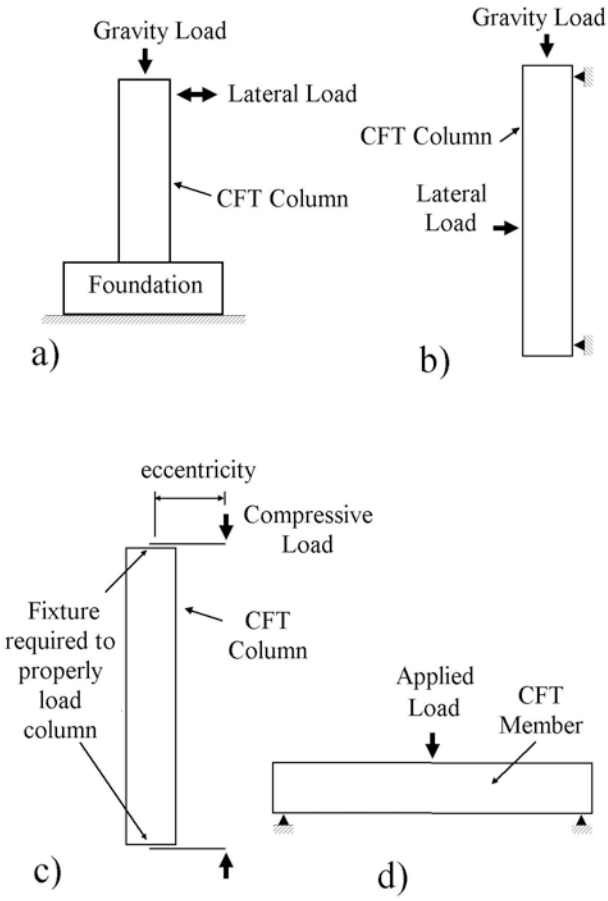

Figure 2.3. Schematic of CFT test configurations; a) connection test, b) beam-column test, c) eccentrically loaded column test, d) flexural test

The tests were divided into four broad categories as shown in Figure 2.3: (1) CFT foundation connection tests, (2) beam-column tests, (3) eccentrically loaded column tests, and (4) pure bending (flexure only) tests. Flexural and beam-column tests typically had 3- or 4-point loading with or without an axial load, while beam-column tests had a concentrically applied axial load to evaluate combined load resistance and P-δ effects. There were 28 CFT foundation tests, 31 eccentrically loaded tests, 26 beam-column tests, and 37 flexural tests with no axial load. The D/t ratio varied between 27 and 226; the

diameter, D, varied between 4 and 20 in., with most test specimens having diameters of less than 12 inches. The database included a wide range of concrete and steel strengths

These experimental data were used to analyze, compare, and evaluate alternative design models. Initial analysis of the 122 tests showed clear consistency among the flexural tests, axially loaded tests, and the beam-column tests. However, there was significant inconsistency and variability within the eccentrically loaded column tests, and between the eccentrically loaded column tests and the other three types of tests. This inconsistency was examined in detail. Figure 2.3c shows that eccentrically loaded tests must be loaded to provide a uniform bending moment over the column length with the only deviation caused by P-δ effects. However, this is difficult to achieve in practice because the test apparatus must properly distribute the stresses to both the steel and concrete elements at each end of the specimen. If this stress distribution is achieved, failure will always occur at mid-height of the column where the maximum moment occurs. If this is not achieved, local failure will occur at the end of the column, and some eccentrically loaded column specimens clearly demonstrated this improper end failure. It was often impossible to separate the eccentrically loaded specimens with improper failure from those with proper end loading. As a result, all eccentrically loaded test specimens were excluded from the database, since some were not consistent indicators of CFT performance. The remaining 91 specimens were used for the continued evaluation of CFT behavior.

CFT Column-to-Foundation Connection Tests

CFT connections for deep foundation applications was a question of interest to WSDOT, and this research was coordinated with a CALTRANS research study, which

included experimental work to investigate seismically resistant foundation connections for CFT. Therefore, that foundation connection work is briefly summarized here. Most of these tests are included in the database on 91 CFT elements noted above, but these tests are described in a greater detail here because of their applicability to the WSDOT research program.

CFT offers many advantages for economical and rapid construction, and the column-to-foundation connection illustrated in Figure 2.4 offers potential benefits for both CFT bridge piers and deep foundation connections. The connection employs a flange or annular ring, which is welded to the end of the tube with a complete joint penetration (CJP) or full strength fillet weld, as shown in Figure 2.4c. The hollow ring projects outside and inside the tube by 16 and 8 times the flange thickness, respectively. There are no reinforcing bars in the tube or dowels penetrating from the tube into the foundation.

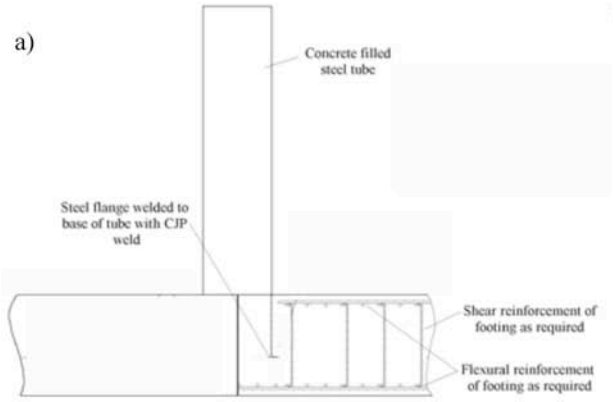

Figure 2.4 Proposed monolithic CFT pier or column foundation connections

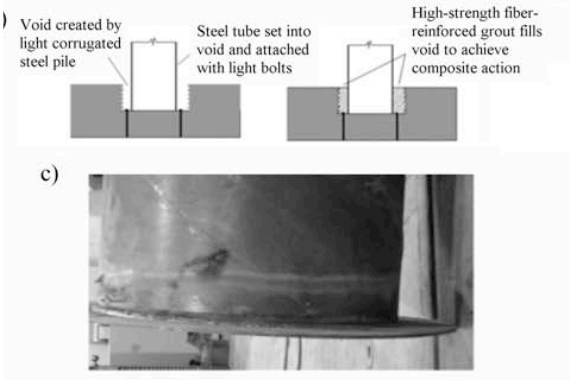

Figure 2.5 Proposed isolated CFT pier or column foundation connections with close-up of annular ring

The tube is embedded into the foundation in one of two ways, as depicted in Fig. 2.4 and 2.5. The embedded tube is anchored with the annular ring (Fig. 2.5(, so sufficient concrete depth is needed to sustain the stresses associate with pullout and push-thru the foundation element. If these are achieved, the tube and the ring primarily contribute to the connection stiffness and resistance. Figure 2.4 shows a monolithic connection, in which the flange and tube end are embedded directly into the foundation or pile cape with the embedded option. Figure 2.5 shows the isolated connection, in which the footing is cast with a recess formed by a corrugated steel pipe. The recess has an inside diameter that is slightly larger than the outside diameter of the annular ring. With this recessed option, the tube is placed in the recess after the foundation concrete has been cast. After placement, the gap between the tube and the corrugated pipe is filled with high-strength, low-shrinkage, fiber-reinforced grout. For both options, the steel tube is filled with low shrinkage self consolidating concrete to complete the member and connection.

A series of large-scale experiments evaluated the performance of this foundation connection (Kingsley 2005, Williams 2007, Chronister 2008, and Lee 2011). Figure 2.5 shows the dimensions and geometry of a typical specimen. The embedded depth of the

tube, l_e, the shear reinforcement in the foundation, the axial load ratio, and the properties of the steel tube were varied between specimens as shown in Table 2.2, since these were potential design issues and major parameters in the research study.

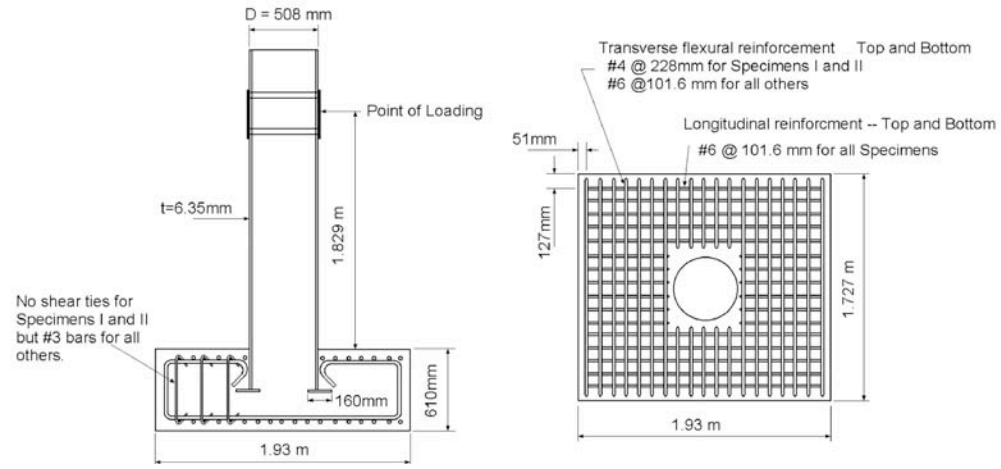

Figure 2.6 Typical test specimen

Table 2.2 Summary of test specimens and results

Spec.	l_e/D	Study Parameter	F_y (MPa)	F_u (MPa)	f'_c (MPa)	Max. Drift	Max. Load (kN)	Failure Mode
1	0.6	Embedded w/light shear reinforcement	520	605	76	8.5%	581	Cone pullout
2	0.6	Embedded w/ significant shear reinforcement	520	605	76	9.5%	599	Cone pullout
3	0.9	Embedded	520	605	69	8.0%	735	Ductile tearing of tube
4	0.6	Recessed	520	605	69	7.8%	618	Partial pullout
5	0.9	Embedded	520	605	78	9.0%	749	Ductile tearing
6	0.75	Recessed	520	605	82	9.6%	770	Ductile tearing
7	0.75	Recessed - punching shear w/225mm depth	520	605	64	NA	3413	Monotonic punching
8	0.75	Recessed - punching shear w/225mm depth	520	605	65	NA	3044	Cyclic punching
9	0.9	Recessed - galvanized	520	605	69	8.5%	770	Ductile tearing
10	0.9	Recessed - galvanized w/near fault cyclic deformation	520	605	67	10.5%	797	Ductile tearing
11	0.9	Recessed - increased axial (2737 kN)	520	605	64	10.4%	743	Ductile tearing
12	0.9	Recessed - Increased axial (3649 kN)	520	605	69	9.5%	788	Ductile tearing
13	0.8	Embedded - straight seam tube	340	417	60	11.6%	538	Ductile tearing
14	0.775	Recessed - straight seam tube	340	417	65	10.4%	530	Ductile tearing
15	0.775	Recessed - evaluation of l_e	355	540	54	10.2%	512	Ductile tearing
16	0.8	Recessed - evaluation of l_e	355	540	60	7.3%	521	Ductile tearing
17	0.7	Recessed - evaluation of l_e	355	540	68	7.4%	601	Ductile tearing w/ footing cracking
18	0.6	Recessed - evaluation of l_e	355	540	70	7.4%	587	Ductile tearing w/ increased footing damage

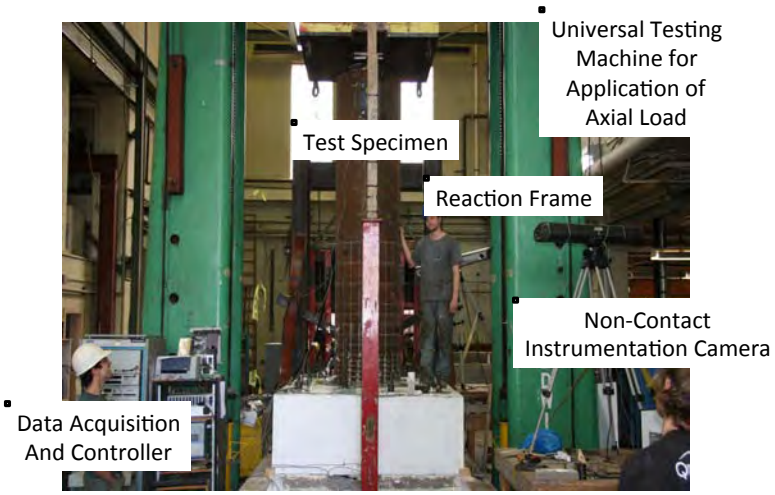

Figure 2.7 Specimen and test set-up

Most tests evaluated the connection under axial compression and cyclic lateral load, and the self-reacting test frame was placed under the 2,400 kip Baldwin Universal Testing Machine, as shown in Figure 2.7. Most specimens had a compressive load of approximately 400 kips, which was approximately 10 percent of the crushing compressive capacity of the CFT member, but larger loads were used for a few tests to evaluate punching shear. The compressive load was applied using the Baldwin Test Machine through a dimpled, lubricated Polytetrafluoroethylene (PTFE) sliding surface with a #8 mirror finish stainless steel mating surface. The sliding assembly rested on a spherical bearing to permit end rotation. Therefore, P-δ effects were directly simulated in the test, and the friction was minimized. A 220-kip MTS actuator applied the cyclic lateral loading, and the displacement history was based upon ATC-24 protocol (ATC 1992) or a near fault variation of this cyclic deformation history.

Connections with very shallow embedment, such as Specimen 1, developed relatively poor performance with cone pullout failure, as shown in Figure 2.8. Cracking initiated in the footing at the column-footing interface at very small deformations, and

this cracking spread from the column base, parallel and perpendicular to the direction of loading with increasing deformation. This ultimately led to the severe foundation cracking and cone pull out, as shown in Figure 2.8b. The maximum horizontal load was reached at 2.4 percent drift, and dramatic deterioration of resistance was noted as shown in Figure 2.8a. The maximum resistance was smaller than the plastic capacity of the composite section but approached the theoretical yield force of the tube.

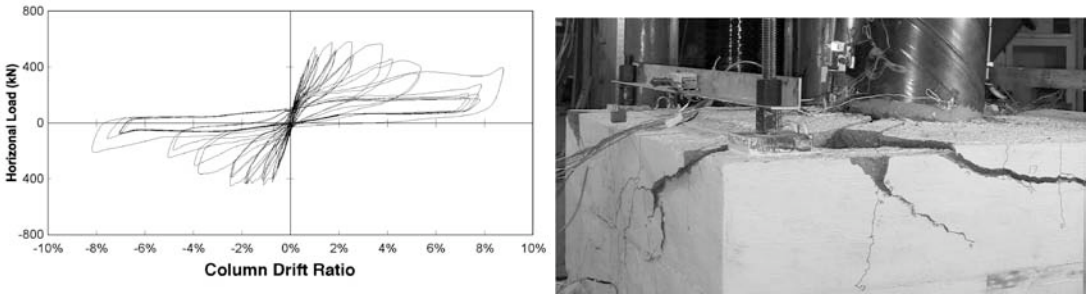

a) b)

Figure 2.8. Specimen-I performance: a) force-deflection response, b) photo of footing damage at end of the test

Most specimens had adequate embedment depth needed to provide excellent ductility and inelastic deformation capacity with virtually no damage to the footing. Specimen III used as an example of this behavior. Very small hairline foundation cracks formed at 0.5 percent drift, but these foundation cracks remained smaller in width, larger is spacing, and were not widely distributed in comparison to Specimen I. Tensile yielding of the tube of Specimen III was clearly observable at 1.3 percent drift at a horizontal load of 134 kips. The maximum horizontal load of 165 kips was reached at 2.4 percent drift. After this drift, the shear force decreased; however this decrease was solely a result of the P-δ moments, as shown in Figure 2.9a. The maximum resistance exceeded the ultimate plastic capacity of the composite CFT member. At 4-percent drift, local buckling of the

tube was clearly visible, and ductile tearing initiated at the highly strained region of the buckle at 6 percent drift. The concrete fill inside the tube at the column base had crushed at this deformation level. The test was terminated at 8-percent drift because of significant tearing around the perimeter of the steel tube at the local buckled region, as shown in Figure 2.9. The specimen sustained virtually not damage to the footing as can be seen in Figure 2.9b.

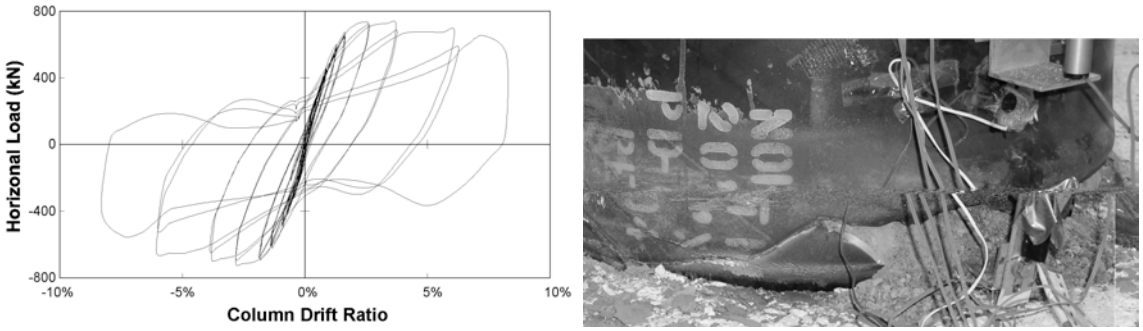

a) b)

Figure 2.9. Specimen-III; a) force-deflection response, b) ductile tearing of tube at the local buckle at the end of the test.

Similar behavior, including the progression of yielding, buckling, and tearing, was noted in other tests. Specimens with inadequate embedment sustained damage to the footing, reduced ductility and inelastic deformation capacity, and deterioration in resistance. Specimens with greater embedment depth developed the full composite resistance and plastic capacity of the CFT member and attained large inelastic deformations prior to connection failure. Local buckling of the thin wall tubes was first observed at 3 percent to 4 percent drift, and maximum lateral resistance (including reduction for P-δ effects) occurred at similar drift levels. Degradation in resistance (including P-δ effects) was insignificant until approximately 6 percent drift. After multiple cycles of severe buckling, deformation tears initiated in the peak of the buckle and grew around the perimeter of the buckled tube with multiple cycles of increasing

deformation. Failure of the tube was noted at drift levels of between 8 and 10.5 percent. These deformation levels are significantly larger than those that can be obtained with reinforced concrete piers and caissons. Furthermore, somewhat larger drift levels were often achieved with lower yield strength steel.

A simplified cone pull-out model, shown in Figure 2.10, is currently being developed to establish the required embedment depth needed to assure ductile behavior with these CFT connections. The model considers the concrete strength and the diameter, wall thickness, and tensile strength of the tube to establish this required embedment length.

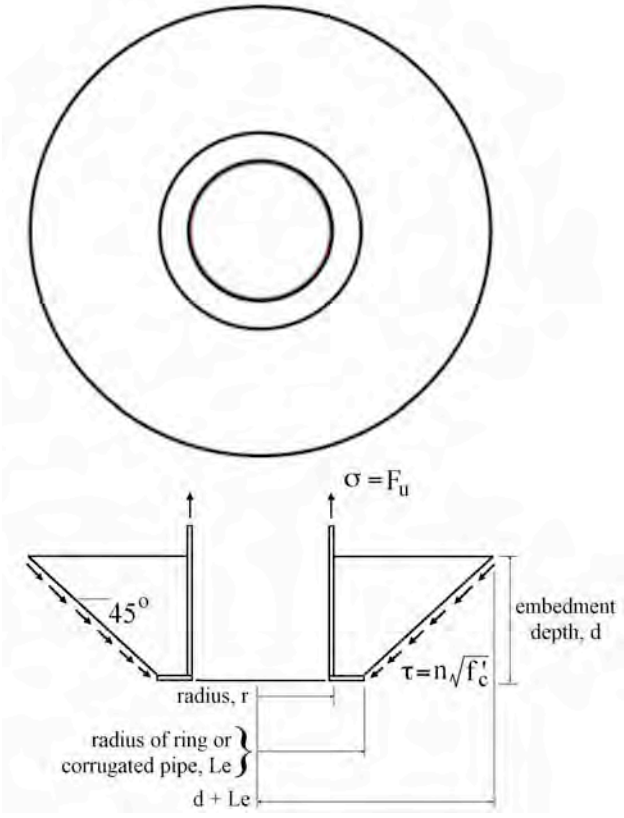

Figure 2.10. Cone pull-out model for establishing embedment depth

ANALYSIS AND EVALUATION OF SIMPLIFIED DESIGN MODELS

The measured resistances of the 91 circular CFT specimens in the database were compared to the resistances predicted by the design models shown in Figure 2.1. The plastic stress distribution method is easier to use and is viewed as providing consistently conservative predictions of resistance (e.g., Marson and Bruneau 2004, Kingsley 2005). As a result, the method was studied in detail.

The moment resistance was computed by applying the measured axial load to the specimen cross-section, the measured material properties of the steel and concrete, and the stress distribution illustrated in Figure 2.1a to determine the bending moment. Figures 2.11a and b show the ratio of measured moment capacity to the predicted moment capacity by the plastic stress distribution method as functions of the axial load ratio (P/P_o) and the local slenderness of the tube, respectively. A ratio greater than 1.0 indicates a conservative prediction.

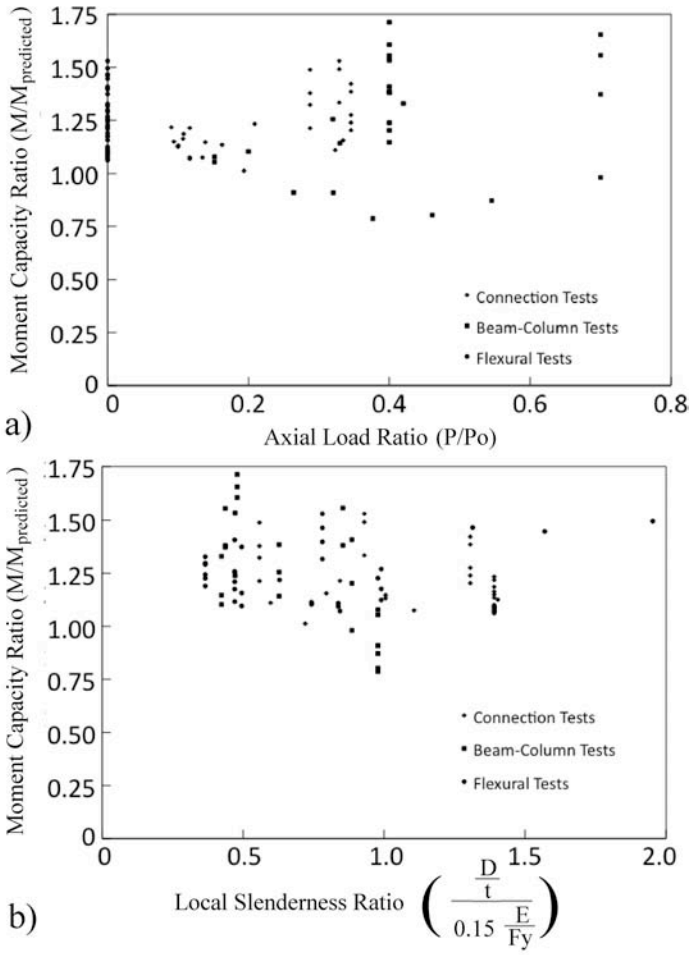

Figure 2.11. Comparison of measured to predicted plastic stress distribution moment resistance a) as a function of P/P_o, and b) as a function of D/t of the tube

The mean ratio of measured-to-predicted moment capacity was 1.24 with a standard deviation of 0.18, and there was consistency in the mean and standard deviations for the three separate test groups. A few beam-column specimens fell slightly below 1.0, but these specimens all approached the maximum D/t slenderness limit permitted by current design specifications, as shown in Figure 2.11b. Furthermore, several of those tests also had large Kl/r values, which indicates that global column buckling reduced the resistance and must be considered explicitly. Simply applying the plastic stress method

for slender components did not meet the code specification. Finally, Figure 2.11b shows that the AISC local slenderness limit (Eq. 1a) was generally adequate to assure development of the full composite resistance of CFT members, since their full capacity was developed for many CFT members that greatly exceeded the current AISC slenderness limit. This clearly indicates that the ACI and AASHTO D/t slenderness limits are overly conservative for circular CFT.

The ACI and AISC strain-compatibility methods are sectional analysis methods that will be discussed in greater detail in the next section. These analysis methods were significantly less accurate than the plastic stress distribution method, and they were more difficult to use. The mean ratio of the measured-to-predicted moment capacity for the ACI method was 1.65 and the standard deviation was 1.14, and the AISC strain compatibility method had similar variations. The larger standard deviation was caused by the greater scatter in the predictions, since the method slightly overestimated the bending capacity in a few cases but also underestimated the bending capacity by several hundred percent in other cases. The primary reason for the inaccuracy of the ACI strain compatibility method is the 0.003 compressive strain limit. For conventional reinforced concrete, this 0.003 strain limit provides a lower-bound estimate to spalling of the concrete cover, but the concrete cover is eliminated with CFT, since all concrete is well confined. The current AASHTO LRFD resistance predictions are even more conservative than the ACI strain-compatibility method.

Simplified Closed Form Solution of Plastic Stress Distribution Method

The plastic stress distribution method provides a practical solution for predicting the resistance of CFT. The method is relatively simple, but it currently involves trial and

error assumptions as to the neutral axis location. As a result, a closed-form solution was derived by application of equilibrium of the plastic stress distribution through integration over the cross section, as illustrated in Eq. 4 and Figure 2.12.

$$r_m = r - \frac{t}{2} \qquad \text{(Eq. 4a)}$$

$$\theta = \sin^{-1}\left(\frac{y}{r_m}\right) \qquad \text{(Eq. 4b)}$$

$$c = r_i \cos\theta \qquad \text{(Eq. 4c)}$$

$$P = F_y t r_m \left\{(\pi - 2\theta) - (\pi + 2\theta)\right\} + \frac{0.95 f_c'}{2}\left\{(\pi - 2\theta) r_i^2 - 2yc\right\} \qquad \text{(Eq. 4d)}$$

$$M = 0.95 f_c' c\left\{\left(r_i^2 - y^2\right) - \frac{c^2}{3}\right\} + 4F_y tc\frac{r_m^2}{r_i} \qquad \text{(Eq. 4e)}$$

A positive value of P implies a compressive force, and y and θ are positive with the sign convention shown in Figure 2.12. The variable y varies between plus and minus r_i, and the P-M curve can be generated by solving the equations for various points over this range.

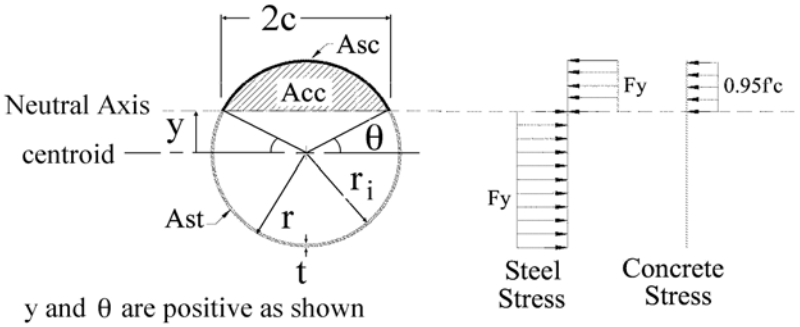

Figure 2.12. Geometry used for closed form derivation of stress distribution prediction

The interaction curve developed by the plastic stress distribution method does not consider column buckling, and the buckling load must be determined from Eqs. 2a and

2b. On the basis of the effective length of the column, the load effectively truncates the M-P diagram, as shown in Figure 2.1c.

Composite Stiffness

The effective stiffness, EI_{eff}, of circular CFT is also important, because it is used to evaluate deflections, deformations, and buckling capacity. Equations 3 show the AISC, ACI, and AASHTO models used to estimate EI_{eff} for CFT. Comparison of these equations shows that the AISC provisions predict a larger value of EI_{eff} than ACI, and AASHTO stiffness is always larger than the AISC stiffness with the difference depending upon the D/t of the tube. Fifty circular CFT tests that provided the force-deflection, moment-curvature, or moment-rotation response data were identified, and the EI_{eff} determined from those specimens were compared to the design models of Eqs. 3a through 3d.

With the AISC provisions, the average ratio of the measured to the predicted flexural stiffness was 0.57 for flexural tests and 0.87 for combined compression and flexural tests. With the ACI provisions, the corresponding results were 0.95 and 1.36, respectively. This indicates that the ACI provisions provide a relatively good prediction of flexural stiffness for flexural members, but significantly underestimate the stiffness for members with combined bending and compression. The AISC expression overestimates the flexural stiffness but provides increasing accuracy on CFT members with significant compressive axial load. These observations are logical because beam-columns with increasing axial load engage more of the concrete in compression, which should increase EI_{eff}.

Proposed Simplified and Improved Stiffness Model for CFT

All of the current stiffness models can be expressed as:

$$EI_{eff} = E_s I_s + C' E_C I_C \qquad \text{(Eq. 5a)}$$

Each codified expression uses a different values of C' but the values is always less than 1.0 in each design provision. It should be noted that C' takes different forms such as C3 in the AISC Provisions (Eq. 3b) and a function of the concrete for ACI and AASHTO (Eqs. 3c and 3d). This variable is used to represent the contribution of the concrete fill to the CFT stiffness. The test data show that C' should be larger for increased compressive load.

Using these results as a guide, the data were revisited to develop a more accurate and representative equation. A number of simple functions were considered, and Eq. 5b was ultimately developed as the best fit to the experimental data:

$$C' = 0.15 + \frac{P}{P_0} + \frac{A_S}{A_S + A_C} < 0.9 \qquad \text{(Eq. 5b)}$$

This expression is more consistently accurate and has a smaller standard deviation than all other current models, and on average it provides a conservative (lower) estimate to the secant stiffness that is achieved in experimental results at 90 percent of the ultimate load. This conservatism is important because increased stiffness provides increased estimates of buckling load. Figure 2.13 compares the measured stiffness to the stiffness predicted by Eq. 5. The ratio is significantly closer to 1.0 than those obtained for comparisons of the measured to predicted stiffness by the AISC and ACI equations. The scatter remains significant but is much smaller than those noted with the AISC, ACI, or AASHTO provisions.

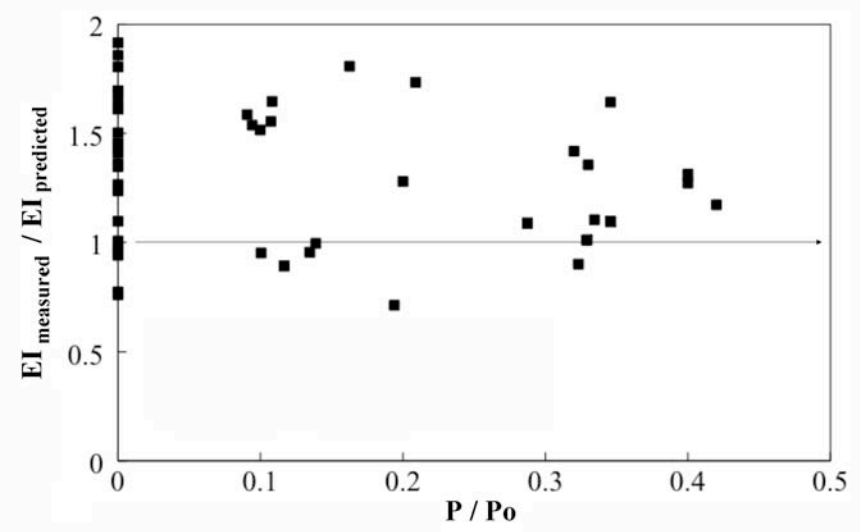

Figure 2.13. Comparison of proposed stiffness models to measured stiffness

SECTION AND FIBER-BASED MODELS FOR FLEXURAL STRENGTH

Section and fiber-based cross-section analyses models (including the strain compatibility methods) are commonly used for reinforced concrete bridge piers, and these methods were also evaluated. Multiple methods including XSECTION (a cross-section developed by Caltrans) were evaluated, but the OpenSees platform was utilized for the bulk of the work, since it clearly duplicated the results from other analytical tools and permitted greater versatility in the analysis (Mazzoni et al. 2005). Sectional analysis methods typically consider the confinement of concrete and strain hardening of steel, which are not directly considered in the plastic stress distribution method. However, the moment resistance is a function of the strain or curvature, and so the flexural resistance defined by these methods requires a realistic and reliable failure limit state, such as the 0.003 in/in compressive strain limit.

To study the effectiveness of the fiber or sectional analysis methods, a wide range of analyses were performed (Bishop 2009) with kinematic strain hardening ratios of the

steel between 0.4 and 1.5 percent along with different models for simulating the confined concrete stress strain response (Thody 2005, Mander et al. 1988, Inai et al. 2004), and different strain, curvature, or deformation limits. The Thody model (2005) was based on several specific CFT test results (Kingsley 2005, Williams 2007). The Inai model (2004) was empirically developed from a wider range of past CFT experiments, and the Mander model (1988) is a commonly used model for reinforced concrete with limited applicability to CFT.

Figure 2.14 provides a comparison of the models with the measured moment-curvature response for a typical flexural specimen. The Thody empirical model for CFT provided the best theoretical approximation of the measured behavior for this test, but the Inai model for CFT more consistently predicted the response for most CFT specimens. However, the Inai model did not capture the maximum moment at the measured curvature in the experiments because it failed to simulate deterioration resulting from severe local buckling of the CFT specimen. Strength deterioration in CFT is a result of large local buckling of the tube and tube tearing, rather than spalling or cracking of the concrete, and local buckling is not captured with sectional analysis methods. The Mander confinement concrete model did not provide a good representation of either the moment-curvature behavior or the increased resistance of CFT members. It frequently predicts early deterioration of resistance because of spalling that cannot occur in CFT members.

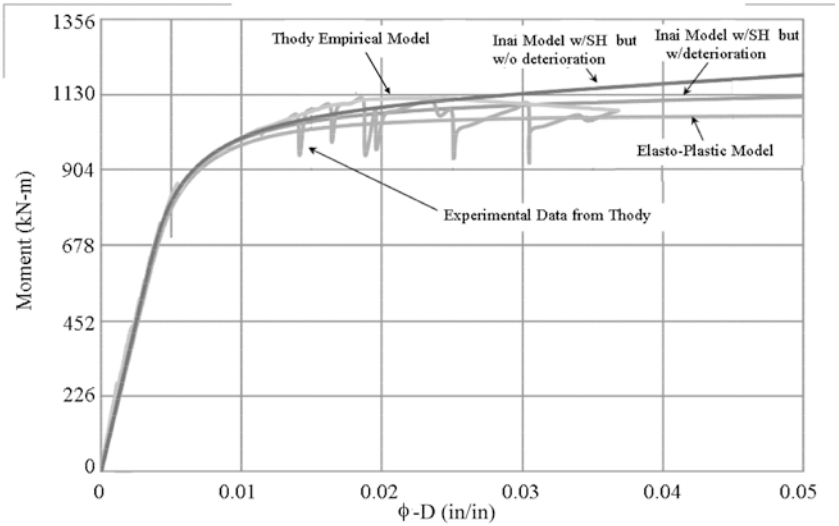

Figure 2.14. Measured vs. predicted moment-curvature behavior using different concrete models in a fiber-based cross-section analysis

The maximum resistance predicted with fiber-based cross-section analysis depends upon the constitutive model and the limiting strain, curvature, or deformation. A wide range of limits—including tensile and compressive strain in steel (ε_{st} and ε_{sc}), compressive strain in the concrete (ε_{cc}), curvature (ϕ), dimensionless form of curvature consisting of the product of the curvature and the diameter of the tube (ϕ*D), and combinations of the above were evaluated.

Figure 2.15 illustrates the average dependence of the moment strength ratio on the curvature for all 91 specimens for several of these evaluations with the best available CFT sectional model (the Inai model) with bilinear steel behavior used with (Figure 2.15a) and without strength deterioration (Figure 2.15b). The figure shows the mean maximum moment strength ratio as a function of the dimensionless curvature for each of the test set-up categories in the three test categories. The figure shows that the accuracy of the predicted maximum resistance improves for larger curvatures, and on average the strength is underestimated by the most accurate sectional analysis method. The Inai

model without strength deterioration provides improved accuracy for the predicted resistance (Figure 2.15b), but the accurate prediction occurred at an average ϕ*D of 0.077. At this large deformation, the flexural capacity was predicted within 3 percent, with a standard deviation of 0.14, but no single test specimen in the database came close to actually achieving this large ϕ*D limit. While the predicted resistance is accurate, the deformation behavior associated with this prediction is totally unrealistic. This was a common failing of all sectional analysis methods, and Inai model performed consistently better than other methods. Loss of compressive capacity of CFT occurs only after severe local buckling, but sectional analysis methods cannot capture local buckling.

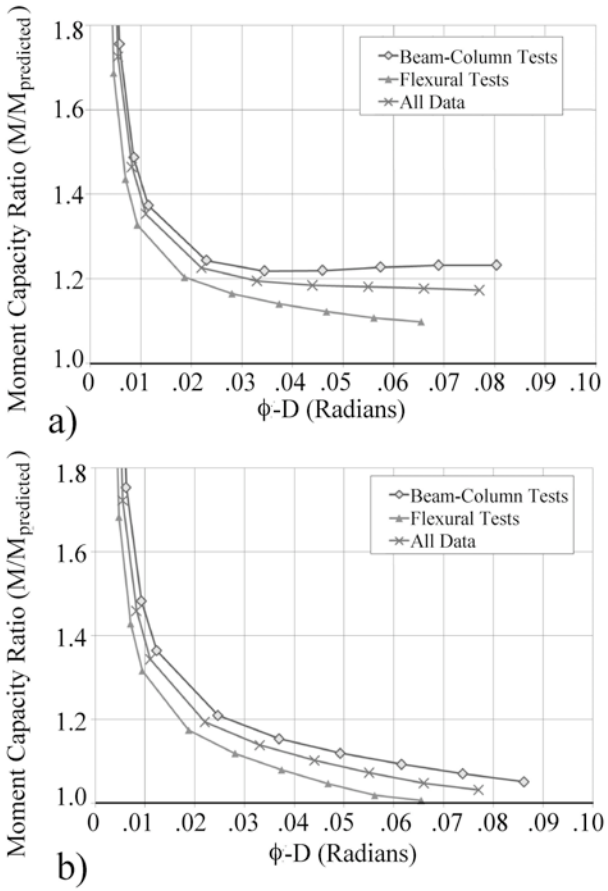

Figure 2.15. Evaluation of fiber-based cross-section nodel noment prediction using Inai concrete constitutive model; a) with deterioration, and b) without strength deterioration

The Inai model without strength deterioration is the most accurate cross-sectional analysis model; Table 2.3 shows the relative accuracy of various failure limits with this model. The 0.003 compressive strain limit for the concrete fill greatly underestimates the strength of circular CFT. The experiments indicated that buckling and tearing of the steel tube contributed to strength deterioration; therefore, maximum strains in the steel tube were used as potential limit states. A compressive steel strain of $5\varepsilon_y$ and a tensile steel strain of $10\varepsilon_y$ resulted in a mean strength ratio of 1.12 and 1.13, respectively, with the same standard deviations of 0.15. Similar results were found using a ϕ*D value of 0.03 (mean ratio of 1.12 and standard deviation of 0.14). However, none of these limits provided good comparison with the strains coinciding with actual deterioration of resistance in the experiments

Table 2.3. Comparison of calculated moment strength ratios for fiber-based sectional analysis

Limit State	Measured-to-Predicted Flexural Strength Ratio			
	Mean	Min	Max	Std. Dev.
ϕ*D = 0.03	1.12	0.72	1.55	0.14
ε_{cc} = 0.003 mm/mm	1.64	0.97	9.18	1.17
$\varepsilon_{sc}/\varepsilon_y - 5$	1.12	0.76	1.55	0.15
$\varepsilon_{st}/\varepsilon_y = 10$	1.13	0.68	1.48	0.15

CONTINUUM (FE) ANALYSIS METHODS

Finite element (FE) analyses of selected experiments were conducted. While sectional analysis did not provide a good prediction of the experimental behavior, nonlinear continuum analysis models provided very good correlation but at great cost in time and complexity (Moon et al. 2010). The analyses were conducted using the analysis program ABAQUS (2005). The 4-node shell element with reduced integration (S4R) and 8-node solid element (C3D8R) were used to construct the finite element model for CFT

shown in Figure 2.16. Critical modeling aspects of CFT include concrete confinement and bond stress between the steel shell and concrete fill, and these issues were addressed with GAP elements simulating the interface between steel tube and concrete infill. These GAP elements

- Permit separation between the steel and concrete surfaces under tensile stress,
- Prevent penetration of the concrete into the steel, and
- Provide bond stress between the concrete by combining the confining contact stress with a coefficient friction to develop shear stresses at the interfaces.

CFT bond stress is primarily transferred through friction (Roeder et al. 2010). The GAP element available in ABAQUS is ideal for simulating the transfer mechanism. Parametric analyses were conducted to evaluate variation in the coefficient of friction. Evaluation of the experimental results indicated that a coefficient of friction of 0.47 provided the most accurate estimate over the full performance range of CFT.

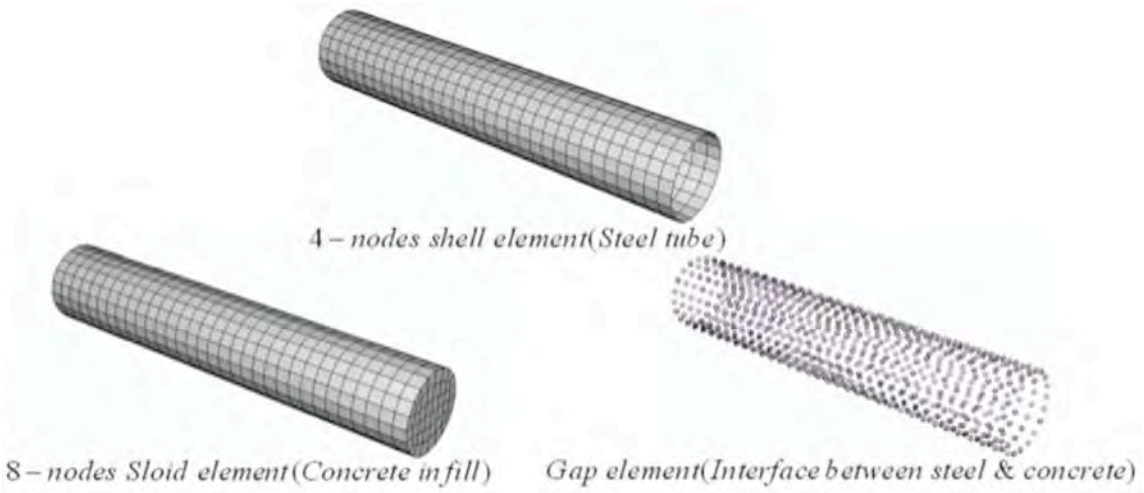

Figure 2.16. ABAQUS finite element mesh and model

The constitutive models were calibrated to the measured properties for each CFT experiment. The ABAQUS concrete damaged plasticity model was employed, and the tri-linear stress-strain relationship with isotropic strain hardening was employed for steel. The concrete damaged plasticity model results in a non-symmetric material stiffness matrix because the nonlinear behavior does not use an associated flow rule. The stress-strain relationship (see Figure 2.17a) for unconfined concrete model was used because the confinement is generated by the compressive stress transferred through the gap element. This provides a more rational and realistic measure of true confinement. The dilation angle of the material, ψ, is an important parameter with the concrete damaged plasticity model, and ψ was selected as 20° on the basis of calibration analyses performed in the study.

An example of the steel model is illustrated in Figure 2.17b. The solution method was selected to obtain an acceptable rate of convergence, and the STABILIZE option provided by ABAQUS with the asymmetric matrix storage and solution scheme was employed.

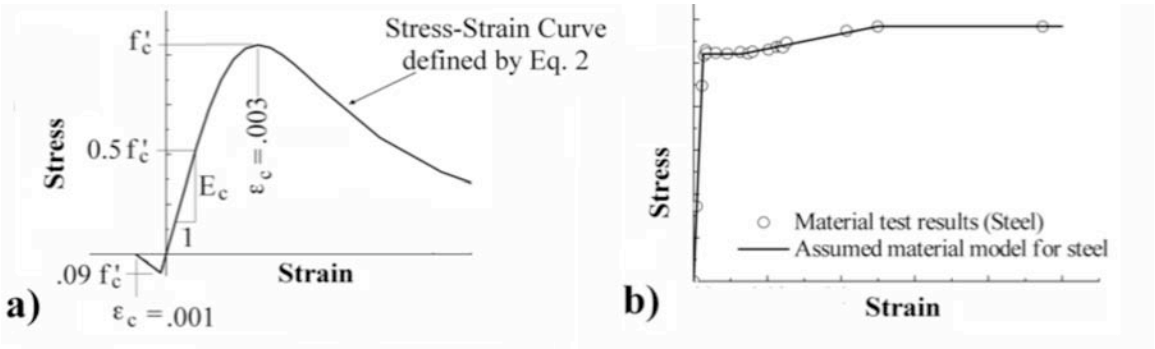

Figure 2.17. Typical material models for analysis; a) concrete, b) steel

A mesh refinement study was completed to assure convergence of the nonlinear analyses. Analyses with a finite element mesh scaled to have 8, 12, 16, and 20 elements

around the perimeter of the tube were performed, and changes were insignificant between the 16- and 20-element mesh. As a result, a 20-element mesh was selected for this analytical study.

Theoretical predictions of the nonlinear finite element models were compared to test specimens under axial load, shear, and flexure, and combined axial and bending. Figure 2.18 shows typical comparisons of the computed behavior to the measured axially loaded experimental behavior. Figure 2.19 shows typical comparison of the continuum analysis for tests with fixed axial load, monotonically increasing bending moment associated, and P-δ moments. The continuum model provides conservative but reasonably accurate estimates of the maximum resistance in all cases. It captures deterioration of resistance because the model accurately simulates both global and local buckling, and it provides a realistic estimate of the strain or deformation at the maximum load capacity.

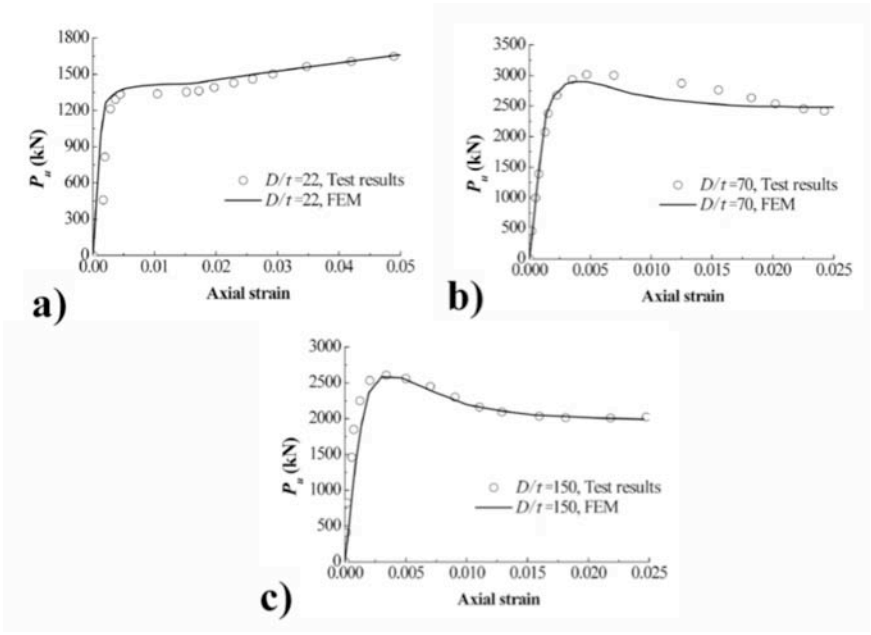

Figure 2.18. Comparison with compression test results of Schneider (1998); (a) *D*/*t*=22; (b) *D*/*t* =70; and (c) *D*/*t* =150

These evaluations were completed for many of the 91 specimens included in the database. The continuum finite element model was documented as a very accurate and reliable model for CFT. The ABAQUS continuum finite element model (FEM) on average slightly underestimated the moment capacity of the tubes for all conditions, but the estimate was more accurate than the plastic stress distribution method. Earlier it was noted that the plastic stress distribution method underestimated the maximum flexural resistance of beam-columns by an average of approximately 24 percent. Strain compatibility and section or fiber methods resulted in larger average errors and much larger scatter in the predicted results. The FEM analysis also resulted in conservative predictions of the flexural capacity of beam-columns with and without axial load, but the error and scatter were smaller than those resulting from the plastic stress distribution method. The plastic stress distribution method underestimated the capacity predicted by the continuum finite element analysis by an average of approximately 10.4 percent. Therefore, the continuum model underestimated the measured flexural capacity by an average of approximately 12.3 percent.

The FEM accurately predicted the initiation of local buckling in the tube, and it accurately predicted crack development in the concrete within the tube. The accuracy was verified by comparison with experimental results for multiple specimens. Figure 2.20 shows the predicted concrete crushing cracking and the observed concrete damage in one specimen. The FEM analysis illustrated these damaged areas by the inability to transfer stress through the crushed and cracked zone. The continuum model also showed the deterioration of resistance noted in the test specimens after severe buckling occurred. Finally, the ABAQUS analysis provided a basis for estimating the ultimate failure

deformation of CFT elements, but the comparison with experimental results was clearly much weaker for this case. While the continuum analysis is accurate, it is very costly in time and computation and is not suitable for most typical bridge foundation projects. Hence, the plastic stress distribution method is more attractive.

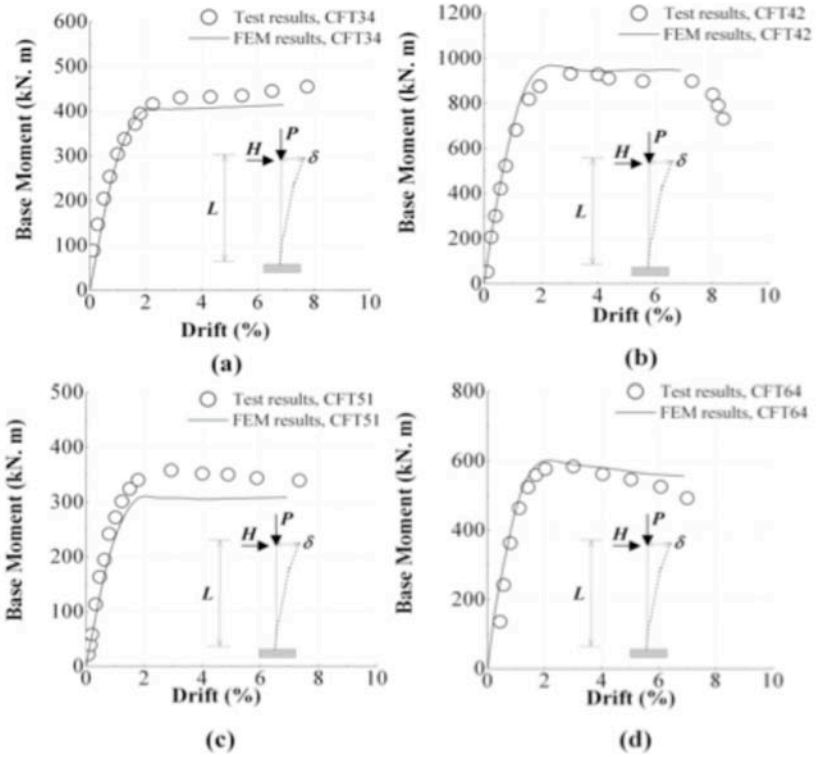

Figure 2.19. Verification of the FE model for CFT under combined loading (tests by Marson and Bruneau (2004)

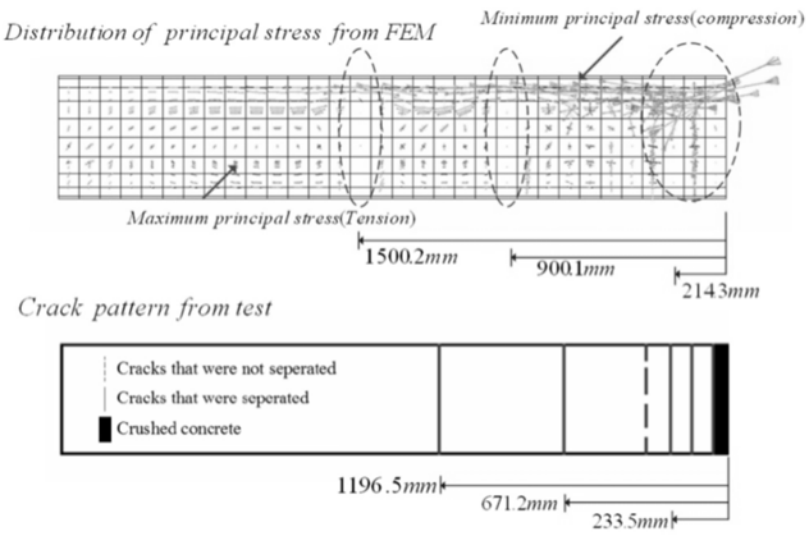

Figure 2.20. Verification of crack development predictions

CHAPTER 3

INVESTIGATION OF RCFT RESPONSE AND DESIGN

RCFT structural elements are concrete filled tubes with internal longitudinal reinforcement, or reinforced concrete filled tubes (RCFTs). Typically, this reinforcement is placed to increase the strength or connect the CFT component. In some cases, corrosion of the exterior steel tube is a design concern, and internal reinforcement is used for some or all of the flexural strength contribution of the steel. Although this is a common structural engineering solution, few experiments have investigated the behavior of RCFT elements. For the most part, the experimental studies that have investigated RCFTs cannot be used because the tests employ different conditions, or the research reports do not provide sufficient information to verify or evaluate the research results.

To study the behavior and develop design expressions for RCFT components, an extensive analytical research study was conducted. These analytical investigations used the modeling approaches presented in Chapter 2. The continuum modeling approach was used to investigate the behavior. The design expressions were then evaluated and modified to include the effect of the internal reinforcement.

Chapter 2 showed that detailed non-linear continuum finite element analysis methods are a suitable tool for predicting CFT performance. These analyses require considerable effort and time for development and completion. However, in lieu of testing, this approach represents a method to investigate the response of these systems. Non-linear continuum analyses were used as a primary evaluation tool in this RCFT research.

In Chapter 2, it was noted that the plastic stress distribution method provided conservative but reliable predictions of the maximum resistance of CFT. The accuracy of these models were evaluated by comparing the predicted resistance to the experimental results, and it was shown that the inelastic plastic stress distribution method was

- Significantly easier to use than other design models, and
- More accurate with less variation in the computed results than other design models.

A closed-form solution of the method was derived for use in a computer spreadsheet to develop P-M interaction curves. Here, the plastic stress distribution method will be extended and adapted to RCFT applications.

Models based on strain-compatibility with nonlinear material-specific constitutive models, often referred to as fiber models, resulted in considerable scatter and inaccuracy in the predicted results. Use of these models is not recommended primarily for the following reasons:

- Fiber or moment-curvature models require a strain or deformation limit to determine the maximum resistance; however, these models do not simulate local buckling, which is the primary mode of deterioration of resistance and ultimate failure of CFT elements. Uncertainty in the predicted resistance is to be expected.
- Fiber models are relatively more difficult to use in comparison to the plastic stress distribution method.

As a result, strain compatibility or sectional analysis methods will not be emphasized in this chapter; however, they may be employed from time to time as checks of the relative accuracy of other methods.

Chapter 2 also documented the accuracy of various models for predicting the stiffness of CFT elements, and an improved method was proposed. This stiffness method will be evaluated for RCFT components.

CONTINUUM ANALYSIS OF RCFT

The continuum analysis models provided improved accuracy for CFT experiments because they conservatively estimated the ultimate capacity, accurately predicted local buckling that ultimate led to failure of the CFT member, and estimated the maximum moment capacity to within 10.4 percent of the experimental value. The modeling procedures for the RCFT elements were similar to those of the CFT models described in Chapter 2, but additional elements were added to include the effects of reinforcing bars, as shown in Figure 3.1. As with previous CFT analyses, nonlinear shell elements were used to model the steel tube, 8-node solid elements were used to model the concrete fill, and gap elements models the steel tube-concrete fill interface.

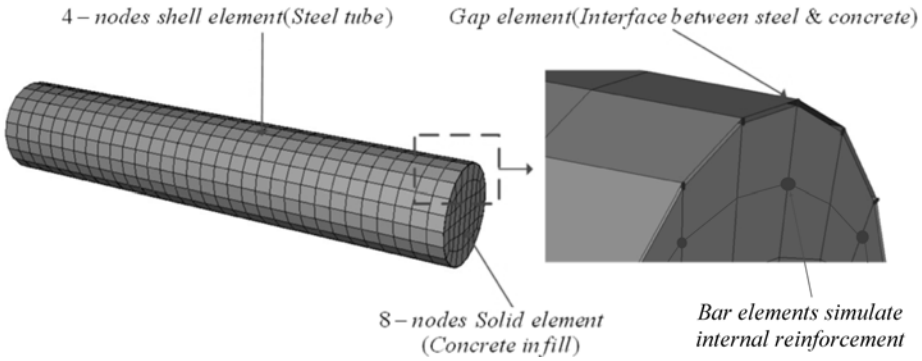

Figure 3.1 Finite element model for RCFT members

The general accuracy of the continuum FEM method was documented by comparison to CFT experiments presented in Chapter 2 because of the lack of RCFT test. However, as with the CFT application, a closed form solution to the RCFT equation was developed, and this solution represents a quicker and easier method of analysis for design practice. The accuracy of the plastic stress distribution method for RCFT was documented by comparison to the nonlinear FEM analysis. Analyses were performed on tubes of 20- and 60-in. diameters. The D/t ratios were between 50 and 120, and internal reinforcement ratios, ρ, were between 0 and 2 percent of the gross area of the member. Analyses were performed with RCFT under flexure (3-point loading), buckling under axial load, and beam-columns loaded under combined axial and bending. Periodic comparisons were made to experimental results to document the accuracy of various calculations, but in all cases the experimental comparisons were for CFT members (or RCFT with ρ equal to 0.0).

Figure 3.2 shows a typical result from the continuum analysis. In the figure, the moment-drift results of three configurations are shown. All three configurations used a tube with a D/t ratio of 80. In each case, the moment is normalized to the theoretical moment capacity of a hollow tube. This normalization provides insight into the contribution of the concrete in enhancing the flexural strength through compression and resistance to local buckling. The bottommost line (solid) indicates a concrete filled tube without internal reinforcement. The remaining two lines show the flexural response of a tube with 1 percent and 2 percent internal reinforcement. The radius of the internal reinforcement (r_{bm}) and the tube (r_m) is 0.8. The strength enhancement of the tube with 1 percent reinforcement is small. The strength enhancement of the tube with 2 percent

internal reinforcement is larger, as expected. In all cases, this enhancement will depend on the relative equivalent longitudinal reinforcing ratio of the tube and internal reinforcement and their relative radial geometries. However, the results show that the internal reinforcement only provides a modest increase in strength.

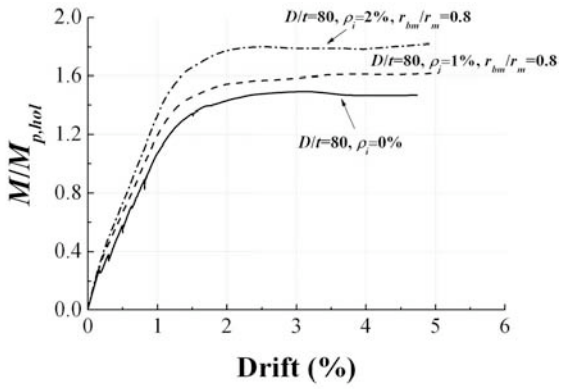

Fig. 3.2 Normalized moment-drift relationship of CFT under bending.

COMPARISON WITH DESIGN EXPRESSIONS

Appropriate design expressions for CFT were discussed in Chapter 2. These included expressions to predict the flexural strength (plastic stress distribution method), the flexural stiffness, and the axial capacity. Here these expressions were evaluated using the results from the FE analyses to evaluate their appropriateness for use with RCFT components.

The plastic stress distribution method was adapted to RCFT by the approximation illustrated in Figure 3.3. There are n internal reinforcing bars inside the tube centered at a radius, r_m, as shown in the figure. The internal reinforcing bars are replaced by an internal tube with a mid-thickness radius equal to r_{bm} and a thickness that exactly matches the total area of the rebar (nA_b), as shown in the figure.

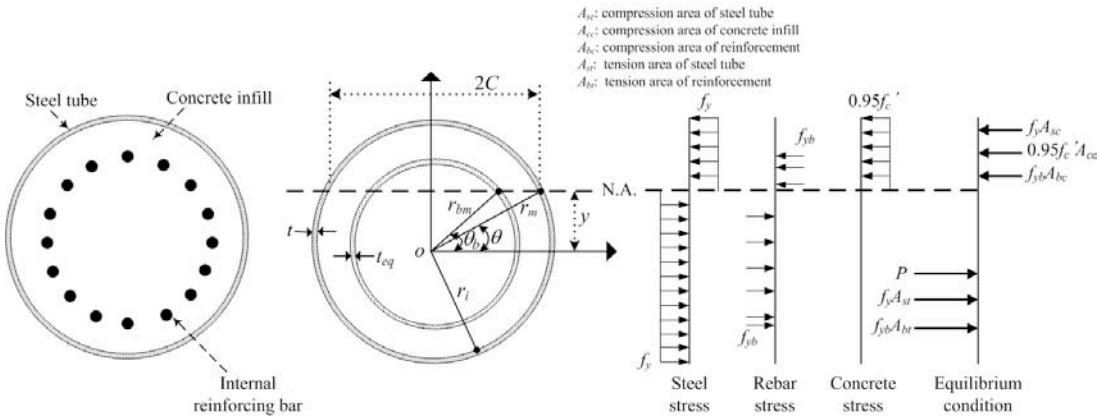

Figure 3.3 Geometry for derivation of plastic stress distribution method with internal reinforcing

$$r_m = r - \frac{t}{2} \qquad \text{(Eq. 6a)}$$

$$\theta_s = \sin^{-1}\left(\frac{y}{r_m}\right) \qquad \text{(Eq. 6b)}$$

$$\theta_b = \sin^{-1}\left(\frac{y}{r_b}\right) \qquad \text{(Eq. 6c)}$$

$$c = r_i \cos\theta_s \qquad \text{(Eq. 6d)}$$

$$c_b = r_b \cos\theta_b \qquad \text{(Eq.6e)}$$

$$t_b = \frac{n A_b}{2\pi r_b} \qquad \text{(Eq. 6f)}$$

$$P = F_{ys} t r_m \left\{(\pi - 2\theta_s) - (\pi + 2\theta_s)\right\} + t_b r_b \left\{F_{yb}(\pi - 2\theta_b) - \left(F_{yb} - .95 f_c'\right)(\pi + 2\theta_b)\right\}$$

$$+ \frac{0.95 f_c' c}{2}\left\{(\pi - 2\theta_s) r_i^2 - 2yc\right\} \qquad \text{(Eq. 6g)}$$

$$M = 0.95 f_c' c\left\{\left(r_i^2 - y^2\right) - \frac{c^2}{3}\right\} + 4 F_{ys} t c \frac{r_m^2}{r_i} + 4 F_{yb} t_b c_b r_b \qquad \text{(Eq. 6h)}$$

These equations were programmed into a spreadsheet to develop P-M interaction curves for a wide range of RCFT applications. Figure 3.4 illustrates an example calculation. The figure shows the interaction curve of a 30-in. diameter, 0.375-in. wall

thickness tube. The specified material properties were 50 ksi steel with 8 ksi concrete fill. CFT with and without internal reinforcement were analyzed. The internal reinforcement was 16 No. 9 bars at a radius of 12 inches with a yield strength of 60 ksi. The internal reinforcement ratio, ρ_i, is 2.3 percent flexural steel, which increases the steel (relative to the tube only) by 45.3 percent. However it only increases the total resistance by 14 to 23 percent, depending on the level of axial load. Steel placed in the tube contributes much greater bending and axial resistance to the member than an equivalent amount of internal reinforcement because the steel tube reinforces the concrete at the optimal location.

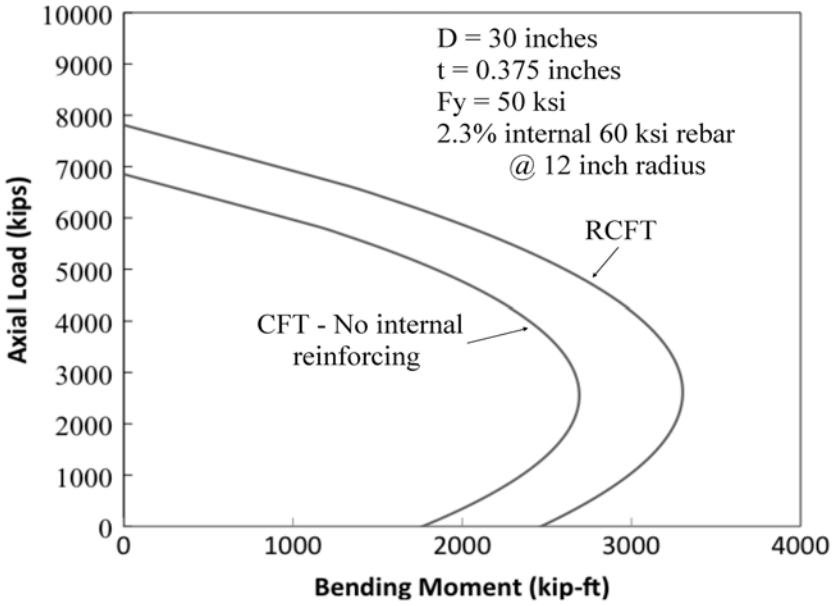

Figure 3.4 Typical RCFT P-M interaction curve and comparison to CFT curve

Experimental verification of the plastic stress distribution method for CFT members showed that the plastic-stress distribution method provides a conservative estimate of the resistance, and on average it underestimates the maximum moment capacity by 24 percent. Since experimental results were not available for investigation of

the response of RCFT, the continuum analysis results were used. As seen for the CFT, the results provided strong support for use of the plastic stress distribution method for determining the maximum resistance of RCFT members with no column buckling. Figure 3.5 shows typical results from the parameter study. In all cases the moment capacity from the FEM analysis is normalized to the moment capacity predicted by the plastic stress distribution method shown above. The plots consider variation in D/t ratio of the tube and the reinforcing ratio of the internal reinforcement. The results are similar to the results for the CFT components. The plastic stress distribution method is consistently 10 to 15 percent lower than that achieved by the continuum analysis, and the conservatism does not depend on the amount of internal reinforcement in the member. Prior comparison has shown that the continuum analysis underestimates the moment capacity achieved with CFT members by about 10 percent, and so these results suggest that experimental results on RCFT members are expected to produce moment capacity that is 20 to 25 percent larger than the capacity predicted by the plastic stress distribution method.

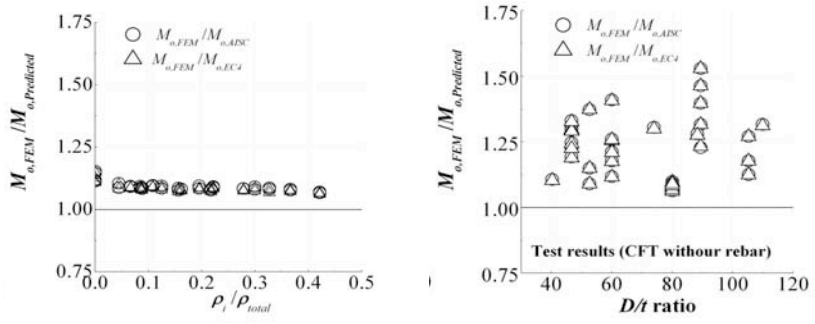

Figure 3.5 Results of parametric study of RCFT under bending: $M_u/M_{u,PSDM}$ vs. (a) ρ (b) D/t ratio;

The effective stiffness, EI_{eff}, of the RCFT member is an important engineering design parameter. To evaluate the effectiveness of the available stiffness expressions to predict the flexural stiffness of RCFT, the results from the FEM analyses were compared to the predicted stiffness by using various design models. For these comparisons, the full elastic stiffness of the internal reinforcing was considered in the design models.

Figure 3.6 shows comparisons obtained from the parameter study. As was similar for RCFT and reinforced concrete members, the flexural stiffness depends on the level of the demand (prior to yield or near cracking) and the level of axial load. Stiffness values at small levels (pre-cracking) of flexural loading are consistently larger than stiffness values at high (approximately yield) flexural loading. Figures 3.6a and 3.6c provide analytical simulated flexural stiffness values corresponding to 10 percent of the expected plastic moment capacity ($0.1M_p$). At these load levels, all of the methods, including the AISC method (Eqs 3a and 3b) and the proposed improved method (Eqs 5a and 5b), underestimate the stiffness.

Figures 3.6b and 3.6d compare the FEM stiffness obtained at 90 percent of the expected plastic stress distribution moment capacity ($0.9M_p$). The AISC method overestimates the stiffness; the proposed improved method provides an accurate estimate. A primary application of the effective stiffness is to calculate the buckling capacity of RCFT, and hence the stiffness values established at the 90 percent of the expected ultimate capacity are rational. In addition, for gravity load and elastic seismic analyses, the demand is expected to be close to the yield strength. Both suggest that a target effective stiffness that approximates 90 percent of the plastic moment strength is

appropriate for design. As a result, the proposed improved method of stiffness prediction (Eqs. 5a and 5b) is the recommended procedure for this research.

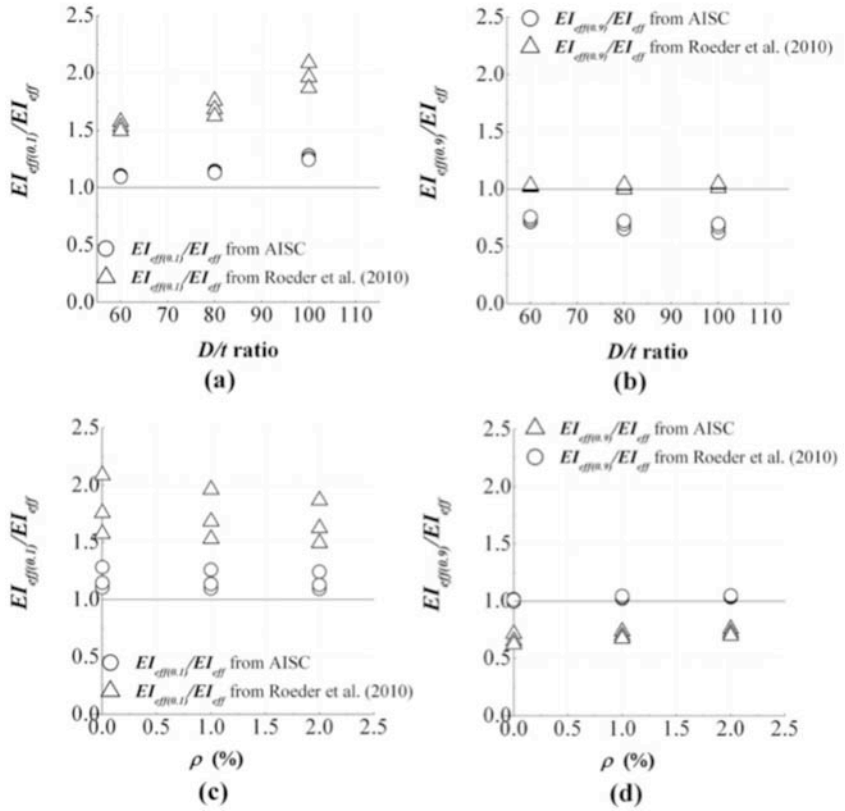

Figure 3.6 Results of parametric study of CFT under bending: (a) $EI_{eff(0.1)}/EI_{eff}$ vs. D/t ratio; (b) $EI_{eff(0.9)}/EI_{eff}$ vs. ρ; (c) $EI_{eff(0.1)}/EI_{eff}$ vs. D/t ratio; and (d) $EI_{eff(0.9)}/EI_{eff}$ vs. ρ.

Analyses were performed on RCFT under pure axial load to evaluate the accuracy of expression to predict the axial response of buckling load predictions. Again, analytical simulated results were used for comparison with the RCFT. Figure 3.7 shows the documented comparison of past experiment results for CFT (or RCFT with ρ of 0.0) and the AISC buckling equations (Eqs. 2a and 2b). Note that the stability parameter, λ, is defined as:

$$\lambda = \frac{Kl}{r\pi}\sqrt{\frac{F_y}{E}} \qquad \text{(Eq. 6)}$$

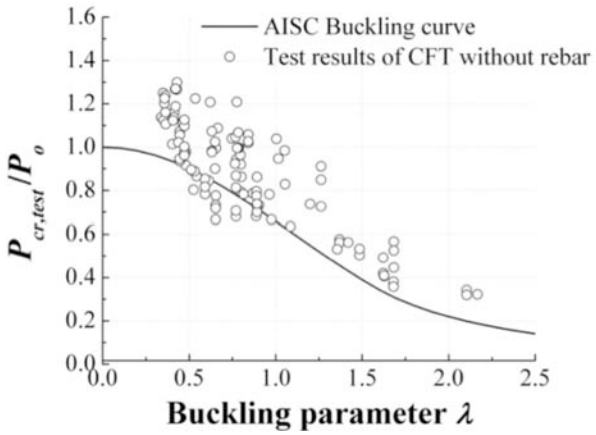

Figure 3.7 Comparison of measured buckling resistance to AISC prediction for CFT

The figure shows that the AISC equation is generally conservative, but there is considerable scatter in the test results, and a fair number of specimens fall below the design equation for small to intermediate slenderness values. In this evaluation, the effective length coefficient, K, provided by the authors was used in this evaluation. However, achieving specific boundary conditions in experiments is difficult, and significant variation in the true boundaries must be expected.

As a result, several compressively loaded specimens that were well documented in the published research were analyzed in greater detail to better understand the buckling issue. Figure 3.8 shows the analysis of different slenderness ratios. Columns with small slenderness, Kl/r (or λ), values develop larger compressive loads, but the load may be lost very rapidly with local or global buckling. Further specific tests were evaluated in detail, and it was determined that these results did not match many of these values,

suggesting that the lower capacities were likely caused by errors made in specimen fabrication. This was verified for other nominally identical tests by the same researcher in the same test program achieved acceptable compressive resistance. The results of this analysis indicated that the AISC provisions are an accurate indicator of CFT buckling capacity. Figure 3.9 shows that the buckling capacities predicted by the continuum FEM analysis are similar to the AISC provisions.

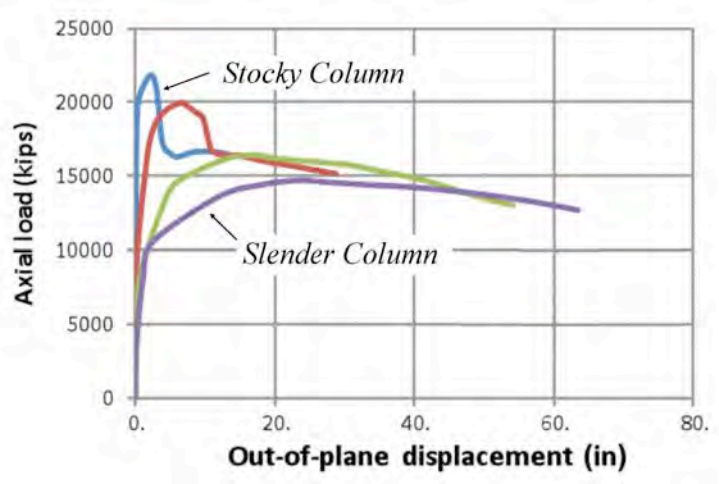

Figure 3.8 Theoretically predicted compressive buckling capacity for CFT columns

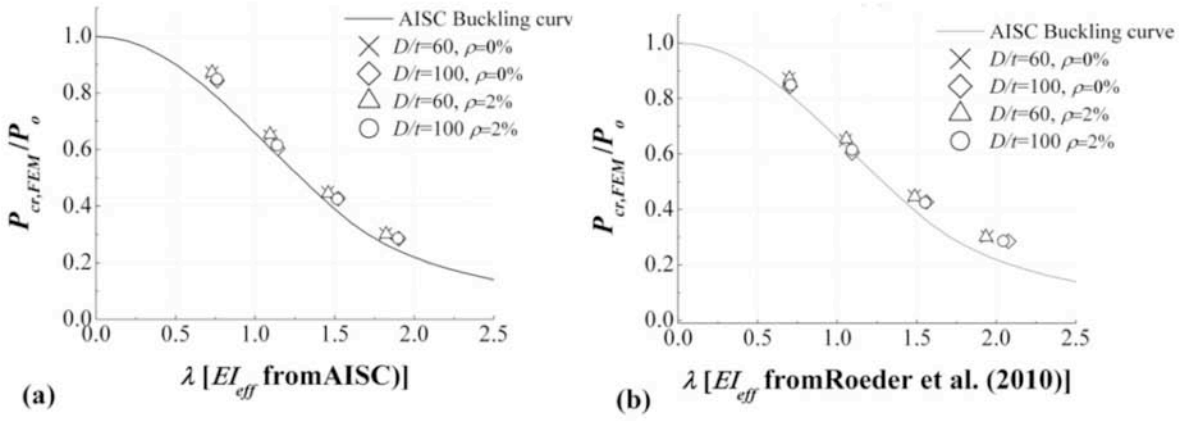

Figure 3.9 Results of parametric study of CFT under axial load: (a) $P_{cr,FEM}/P_o$ vs. λ based on AISC (2005); and (b) $P_{cr,FEM}/P_o$ vs. λ based on Roeder et al. (2010).

AXIAL LOAD-MOMENT INTERACTION CURVES FOR RCFT

Design interaction curves for CFT also vary with design provisions. To evaluate the accuracy of each, available interaction curves were compared with the nonlinear FEM analysis parameter investigation. Finally, these analytical results were compared to newly proposed models for RCFT axial load-bending moment interaction including column buckling.

The continuum finite element analyses were used to simulate RCFT behavior under flexure and buckling. Figure 3.10 shows typical results of two RCFT columns. The solid line was derived from the plastic stress; this analysis does not include member-buckling effects and provides the ideal capacity of the section. In comparison, two analyses were conducted for each column, one with and one without P-δ effects. It can be seen that column buckling clearly limits the compressive capacity of the column (note that in all cases, the compressive strength including P-δ effects is less than the squash load, P_0). The plastic stress distribution method provides a reasonable interaction curve to compute the capacity at lower axial loads (Figure 3.10b) and at higher axial loads for less slender columns (Figure 3.10a). However, at larger axial loads and as the slenderness ratio increases, the interaction curve from the PSDM overestimates the capacity. Therefore the design curve must account for this capacity reduction resulting from P-δ effects.

*D=60in, D/t=60, ρ_i=2%, f_y=50ksi, f_{yb}=50ksi, and f_c'=5ksi

For L/D=8, λ=0.73

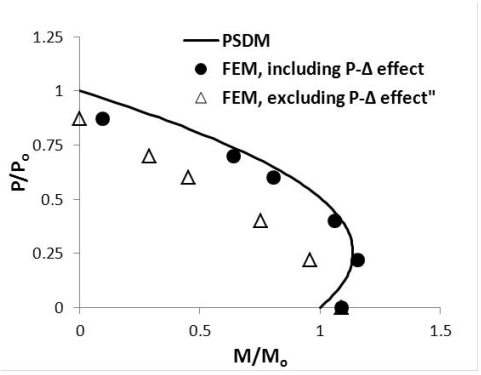

For L/D=12, λ=1.09

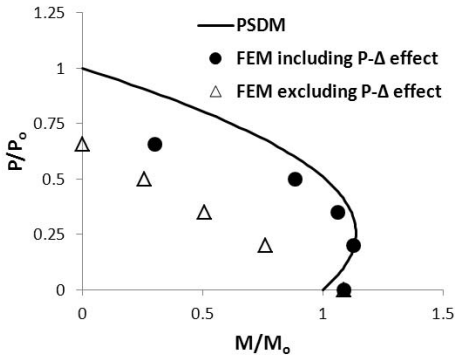

Figure 3.10 Effect of P-δ moments on the combined load strength interaction

A comparison with available interaction curves was made. Although the AISC specification permits use of the interaction curve employed with wide flange sections, that curve is very conservative and inappropriate for CFT and is not discussed here. Figure 3.11a shows an alternative curve permitted in AISC. This curve uses the normal plastic stress distribution method interaction curve as its basis. The buckling capacity of the CFT column is determined and defined as point A' in the figure. Point A is the pure axial strength, computed using the plastic stress distribution interaction curve without the inclusion of second-order effects. Point B is the pure flexural strength (zero axial load), again computed using with the plastic stress distribution method. Point C is the vertical intersection of point B (pure moment) and the plastic stress distribution interaction curve; in other words, point C is the axial capacity corresponding to the pure flexural strength. Using Point C as a basis, Point C' is computed by the ratio of the axial resistances, A'/A. The final interaction curve is formed by connecting points A', C' and B.

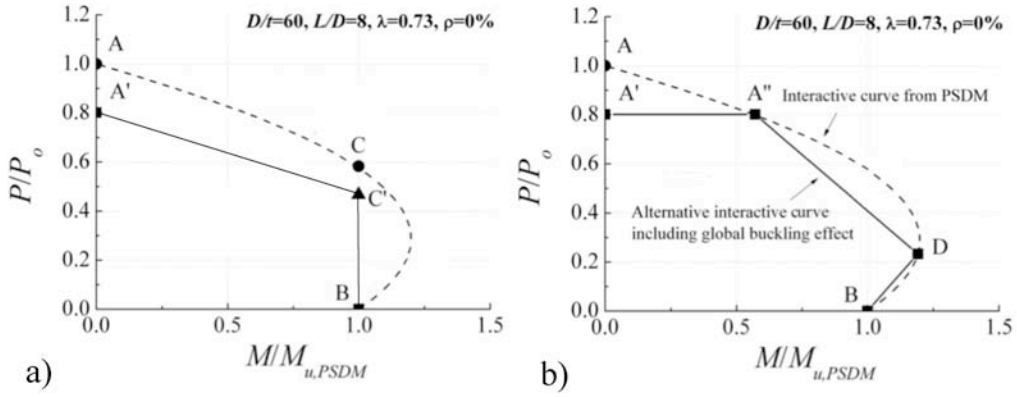

Figure 3.11 Interaction curves including effects of buckling

Figure 3.12 shows a series of theoretical predictions by the nonlinear continuum analysis, and the interaction curve permitted by AISC. It can be seen that the AISC procedure is conservative, in particular for CFT elements with relatively small compressive load. This makes the AISC method unsuitable for many seismic applications where the expected axial load is low and an accurate estimate of the flexural strength is needed to design adjacent elements.

A new method was developed for establishing an accurate yet practical method for developing P-M interaction curves for CFT and RCFT elements. The method was developed as a result of several observations, including the following:

- The AISC curve is conservative and does not reflect the capacity of these components.
- The plastic stress distribution interaction curve represents the moment demand, including P-δ moments, but cannot simulate the lower capacity resulting from member buckling.
- The AISC design provisions provide a reasonable method by which to estimate the axial strength of a slender column susceptible to overall buckling.

Using these results as a basis, a new interaction curve is proposed, and is shown in Figure 3.11b. The proposed curve is specially designed to take the benefits from both plastic-stress distribution method and current design codes. As defined in AISC, the points *A* and *B* are axial and flexural capacity of the CFT, respectively, without considering global buckling effects and computed from plastic-stress distribution method. Point *C* corresponds to the location that results in the same moment capacity as point *B* but with axial load, and points *A'* & *C'* can be obtained by multiplying the length effect reduction factor, which is defined as $P_{cr}/P_{o,AISC}$. Point *D* corresponds to an axial strength of one half of that determined for point *C'*. In the proposed curves, axial strength is limited to point *A'*, and the intersection of the *P-M* interaction curve from the plastic-stress distribution method and the parallel line with the *x* axis through point *A'* is defined as *A''*. Finally, by connecting points *A'*, *A''*, *D*, and *B*, an alternative *P-M* interaction curve can be constructed

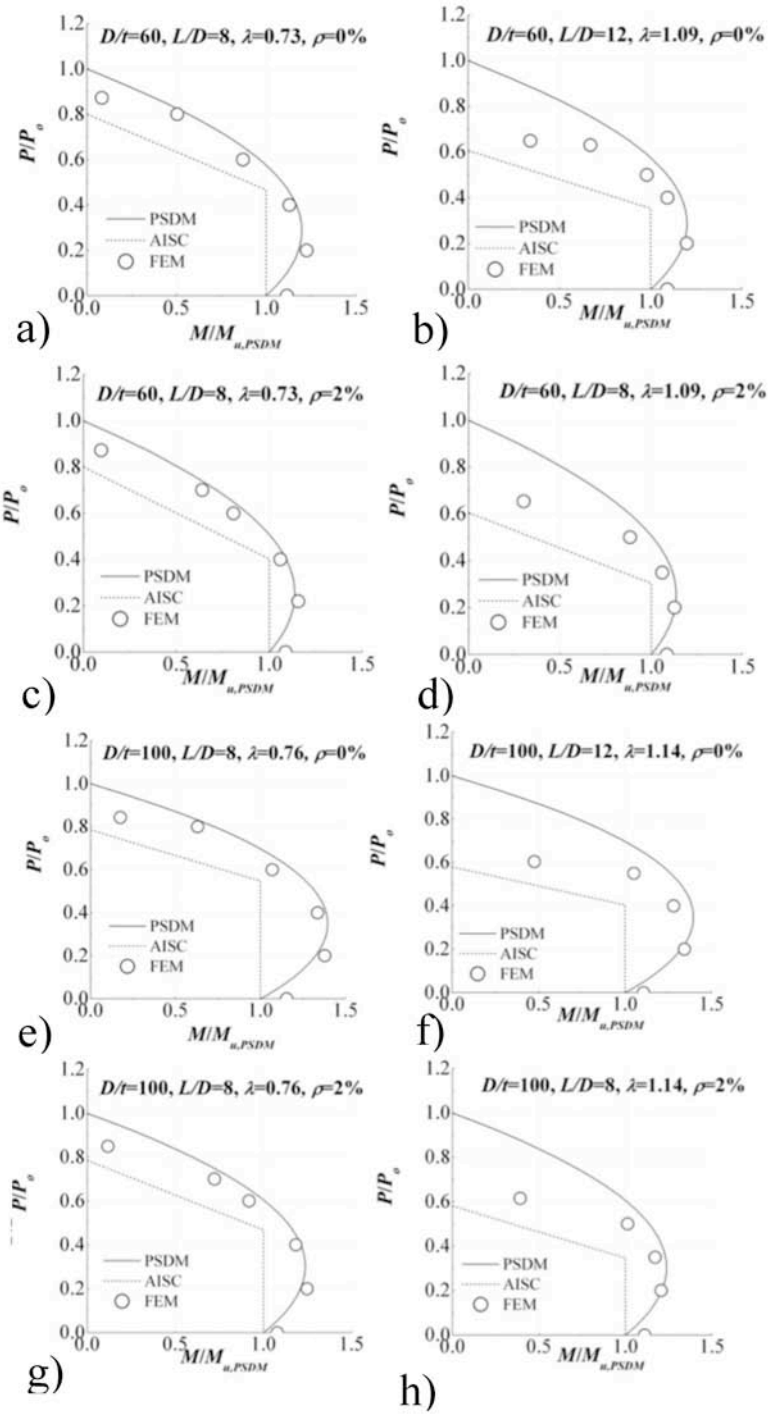

Figure 3.12 Comparisons of the AISC interaction curve to interaction predicted by continuum model

Figure 3.13 provides a comparison of the resistance interaction predicted by the continuum model with the proposed interaction curve. The proposed interaction curve is conservative, but considerably more accurate than the AISC model.

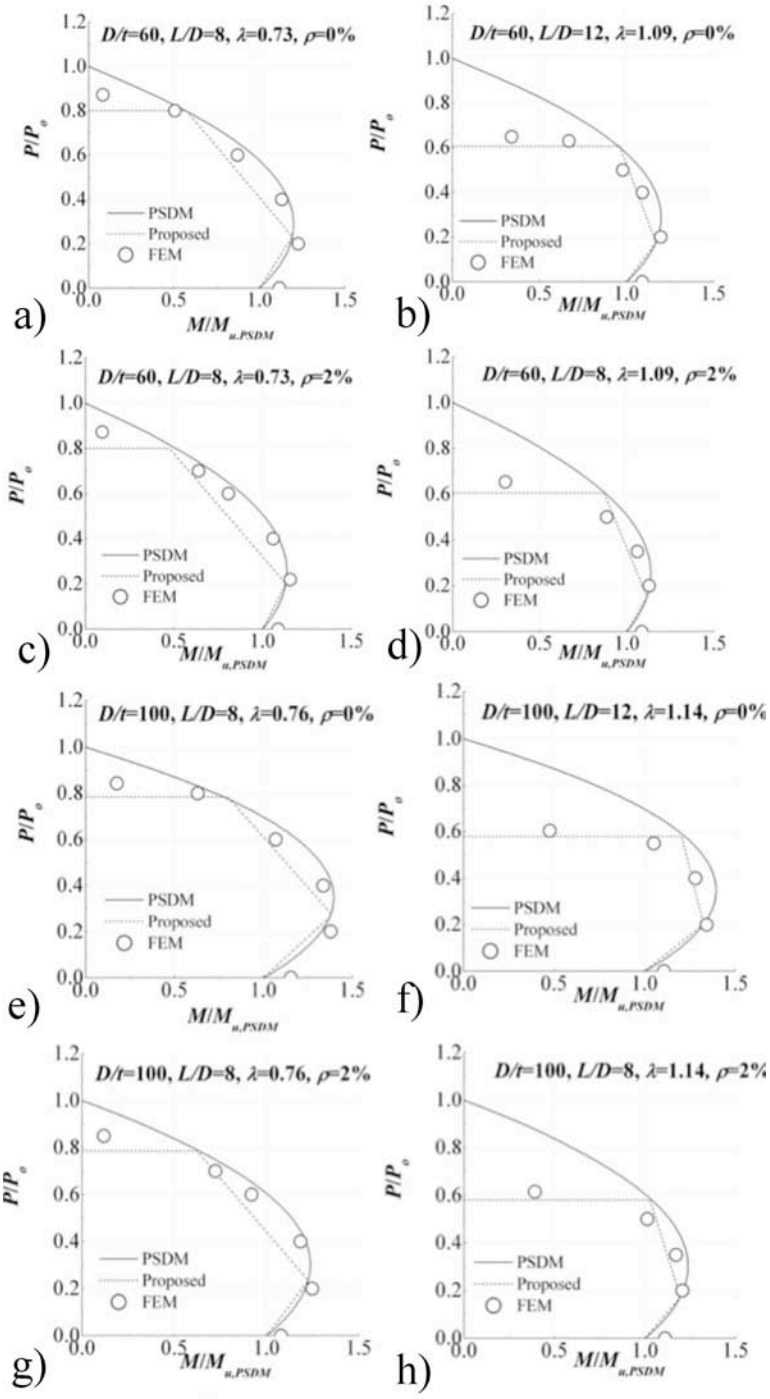

Figure 3.13 Comparisons of the proposed interaction curve to interaction predicted by continuum model

RCFT CAISSON-TO-PILE CONNECTIONS

The connection of a drilled shaft to a reinforced concrete pier in WSDOT is likely to take the form illustrated in Figure 1.1. Experiments have not been performed on this connection. These experiments are required to investigate response, including the required transfer length to reach both the yield and ultimate moment capacity of the RCFT. In this initial phase, supplemental funding was provided to complete a series of nonlinear analyses of the connection.

The objective of these analyses was to begin to study the RCFT response. A parametric study was established to investigate salient parameters on the response. Analyses were performed on the general configuration of the baseline model, which is shown in Figure 3.14, with deviations from the primary model parameters for the parametric study. The analyses were performed with an ABAQUS nonlinear continuum FEM, which was verified by using the experimental results from previous CFT tests. The study parameters included the following:

- The diameter and wall thickness of the tube
- The diameter of the reinforced concrete pier
- The number and size of reinforcing bars in the pier
- The coefficient of friction between the concrete fill and the steel tube wall (This was done because discussions indicated that the caisson may not be fully cleaned in some locations, and the bond stress transfer would be correspondingly reduced.)
- The length of the tube
- The length the reinforced concrete pier reinforcing extended into the tube, and

- The axial load in the column.

The lateral load on each analysis was monotonically increased until the nonlinear model predicted deterioration in resistance. The target response mode resulting in deterioration in resistance was a development of a flexural hinge in the reinforced concrete pier; however, other failure modes were noted. Most significantly, excessively short embedment of the rebar into the tube resulting from deterioration of resistance occurred as a result of pull-out or slip of the concrete fill in the tube. In most cases, slip of the concrete fill relative to the tube did not cause a complete failure of the connection. Instead there was a sharp drop in bending resistance that was recovered with increasing deformation. The bar pullout deterioration typically had more severe consequences.

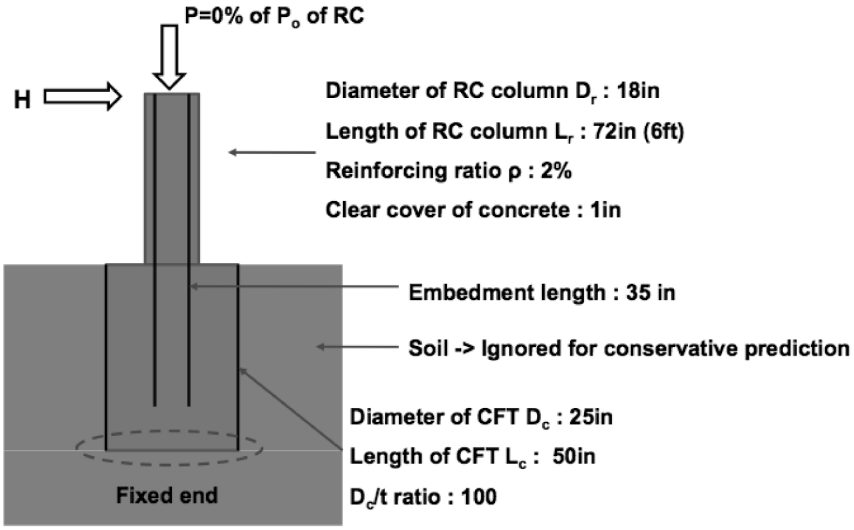

Figure 3.14 Basic analytical model for caisson-to-column connection

The critical area for inelastic deformation in these analyses is the base of the reinforced concrete (RC) bridge pier, since that is the target region for inelastic deformation during extreme seismic events. The analytical model for the CFT used the approach described in Chapter 2, which was previously calibrated to past tests on CFT elements.

For this model, further verification was required for the simulation of the reinforced concrete (RC) pier. A specimen that was tested during a previous WSDOT research program (Pang et al. 2007) was used to validate the modeling approach. Figure 3.15 compares the simulated results from the nonlinear FEM analysis and the experimental results. For the global response, the measured and predicted results are similar, as indicted in the figure. Local comparisons were also made, including tensile cracking of the concrete, spalling of the concrete, and damage in concrete relative to large rebar elongation, as noted with bond stress deterioration; all of these response modes compared well. This RC pier comparison led to considerable confidence in the theoretical predictions.

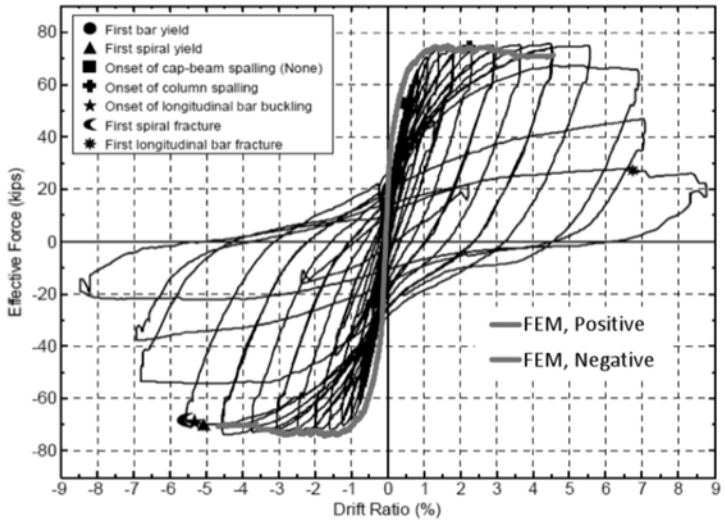

Figure 3.15 Comparison of theoretical and experimental behavior for RC pier

The results were evaluated with consideration for the following: (1) global deformations, (2) relative movement or slip between the steel tube and concrete fill, (3) inelastic deformation in the hinge region of the RC pier, and (4) the distribution of stress

and strain in the RC pier and the steel and concrete fill of the CFT in the critical region of interest.

Figure 3.16 shows typical analytical results. In all analyses, a crack developed in the concrete fill in the CFT below the end of the RC pier rebar, as depicted in Figure 3.14. For a shorter embedment, this cracking is expected, since large stresses would be distributed from the reinforcing bar to the confined concrete. However, for longer embedment depths, the actual formation or impact of this crack is questionable, since it may be a function of the boundary conditions of the analyses. Only with complementary experimental testing is it possible to completely investigate this issue. The slip and cracking were typically small; however, the size and extent of the crack, the resulting slip, and the load and deformation at which cracking initiated varied with different connection design parameters. In particular, the effect of the cracking and amount of slip depended on the axial load and anchored length of the reinforcing bars. Compressive load on the RC pier increased the moment capacity of the pier, as expected, and also delayed the initiation of cracking and slip and reduced the magnitude of the cracking and slip. The extension or embedment length of the RC pier reinforcement into the CFT had a significant impact on the performance of the system.

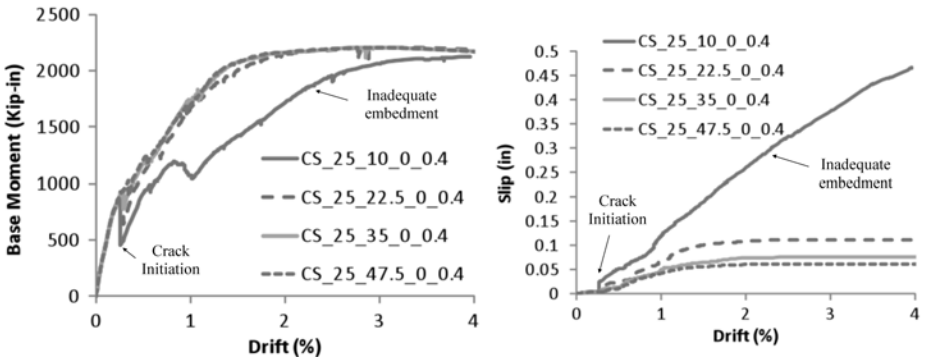

Figure 3.16 Effect of RC pier reinforcement embedment length

Figure 3.16 shows the results of four different analytical models with four different embedment depths for the reinforcing bar. The embedment depths used were 10 in., 22.5 in., 37 in., and 47.5 in. Two types of results are shown. Figure 3.16a shows the force-drift response. Figure 3.16b shows the force-slip response. The results indicate that if the embedment length was too short, i.e., the RC pier did not reach its theoretical flexural strength, the slip was excessive. However, if the embedment length was adequate (the flexural capacity was reached), the effect was very small, as shown in the figure. Excessively short embedment length dramatically changed the stress and strain distribution within the concrete fill and the steel tube in the critical load transfer region.

The relative diameter of the CFT in comparison to the RC pier affected the response, although to a lesser extent. Larger diameter CFT reduced and delayed slip and cracking in the section. This appears to be caused by the fact that the larger diameter of the CFT reduces the stress demands in the steel tube, concrete fill, and shear stress transfer between the two materials.

Figure 3.17 shows the results of a partial study on the impact of the coefficient of friction on the response. Two different embedment depths are shown, one that is less than the ACI required ($0.77l_d$) and one that is more than twice the ACI required ($2.77l_d$). As shown in the figure, reduced friction between the steel and concrete fill increased slip; cracking was increased as well. However, the differences are not large, and for well-anchored reinforcement, they are negligible. This is in good agreement with previous observations on CFT tests with a greased inside wall of the tube (Roeder, Lehman and Thody 2009). The friction developed at this slip interface is largely sustained by binding

action within the tube because of differential stiffness of the concrete fill and the steel tube, and hence the frictional resistance is quite reliable, regardless of the friction value if the bending moment is significant.

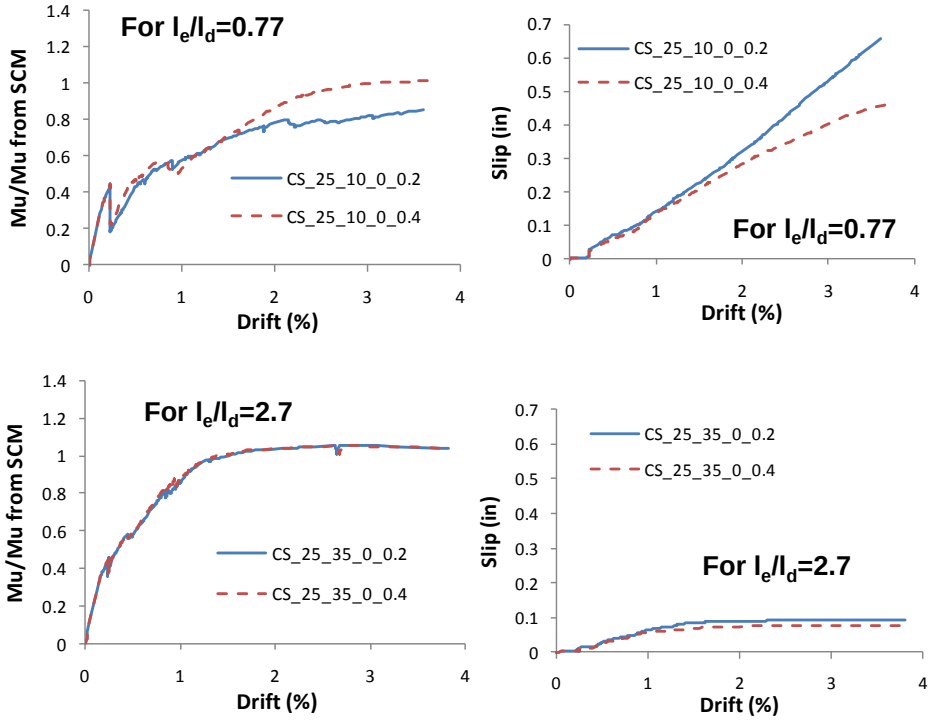

Figure 3.17 Impact of coefficient of friction on response and slip

CHAPTER 4

DESIGN AND BEST PRACTICE RECOMMENDATIONS FOR RCFT

The research results are used to provide recommendations for the 11 primary research issues raised in the initial WSDOT discussions related to this research program and summarized in Chapter 1. The recommendations are based upon the work summarized in chapters 2 and 3, but additional analysis with these same analytical procedures is added in some cases. Each of the 11 issues is addressed in a subsection below. However, several sections do not have specific subsections, since they are addressed elsewhere.

ANALYTICAL MODELS WITH HAND SOLUTIONS

The plastic stress distribution method is recommended for determining the basic material resistance of both CFT (Eq. 4) and RCFT (Eq. 6) components. For stiffness, EI_{eff}, of both CFT and RCFT, it is recommended that Eqs. 5a and 5b be employed. These stiffness values should be used in Eq. 2 to establish the axial capacity, including geometric nonlinearities, of both CFT and RCFT elements.

The axial load-bending moment (P-M) interaction curve including stability effects should employ the interaction curve construction illustrated in Fig. 3.11b. If this curve is employed, the resistance of both RCFT and CFT will be conservatively predicted, and the mean or expected moment resistance predicted by the model will be approximately 24 percent larger than the predicted moment capacity for any given axial load. An EXCEL computer spread sheet was developed to construct the above interaction curve.

Note that item 4 of the initial 11 items is included in the above discussion.

DESIGN EXAMPLES WITH THE ANALYTICAL MODELS

Design information was provided regarding the Ebey Slough drilled shaft illustrated in Fig. 1.1. The information indicated that the factored design axial on the pile at the strength limit state was 2424 kips, and the factored axial load, shear force, and bending moment at the extreme limit state were 800 kips, 303 kips, and 12,070 kip-ft, respectively. These design parameters were used to evaluate the Ebey Slough example and to demonstrate benefits of the composite action of the RCFT member. As noted earlier, the steel tube is 60 in. in diameter and 1 in. thick, and it contains 32 No. 14 bars for internal reinforcement with 6 in. of cover. The shaft is entirely underground, and therefore, consideration of buckling or stability is not required. Under these conditions, the plastic stress distribution method was employed to evaluate the total capacity of the caisson. For these calculations the yield strength of the tube steel and internal reinforcement were approximated as 50 and 60 ksi, respectively. The concrete compressive strength was approximated as 4 ksi. For the strength limit state, the full composite RCFT caisson has an axial capacity 29,000 kips. For the extreme load limit state with 800 kips compressive load, the bending capacity would exceed 32,000 kip-ft. Resistance factors are required for the final design check, but the total combined RCFT caisson clearly is more than three times the strength required by the design demands.

As an alternative design, the internal reinforcement was entirely removed, and the tube diameter was reduced to 5 ft. The tube wall thickness was retained as 1 in. because of the assumed requirements of driving, but 0.375 in. of this wall thickness was ignored

because of potential corrosion over the life of the foundations. For this design condition, the axial load capacity for the strength limit state is 16,130 kips, and the moment capacity for the extreme load limit state is 12,430 kip-ft. This design corresponds approximately to the required capacity, but the component requires 31 percent less concrete and 33 percent less steel, yet it has adequate resistance to develop the design loads with 0.375 in. of sacrificial steel for potential corrosion.

Additional savings may be possible because of the reduced driving or drilling costs with the smaller diameter shaft. Clearly soil strength and connection issues are not considered, but this example illustrates a huge potential cost saving in the design of piles and drilled shaft caissons.

SINGLE-SHAFT COLUMN AND CFT PILE CASE—CONNECTION DETAILS

The single-shaft drilled shaft and caisson and the CFT pile are fundamentally similar elements, and the resistance and stiffness of the member are basically defined by the RCFT and CFT recommendations noted above. The primary difference between the two applications is the connection of the pile or drilled shaft to the pier or pile cap. These two basic issues are discussed here, since they are fundamentally related.

This research did not include funding for the experimental research. However, this WSDOT research was closely coordinated with a CALTRANS research project on CFT bridge piers, and it is possible to build upon that parallel study. The CALTRANS research has supported the development of a foundation connection of CFT bridge piers to a reinforced concrete footing or pile cap. The research shows that this connection can develop the full composite resistance of the CFT member and achieve large inelastic

deformation capacity with minimal deterioration of resistance. The connection of a CFT bridge pier is simply the inverted case of a CFT pile connected to a pile cap. Hence, the CFT pile-to-pile cap connection can be formed as shown in Figure 4.1.

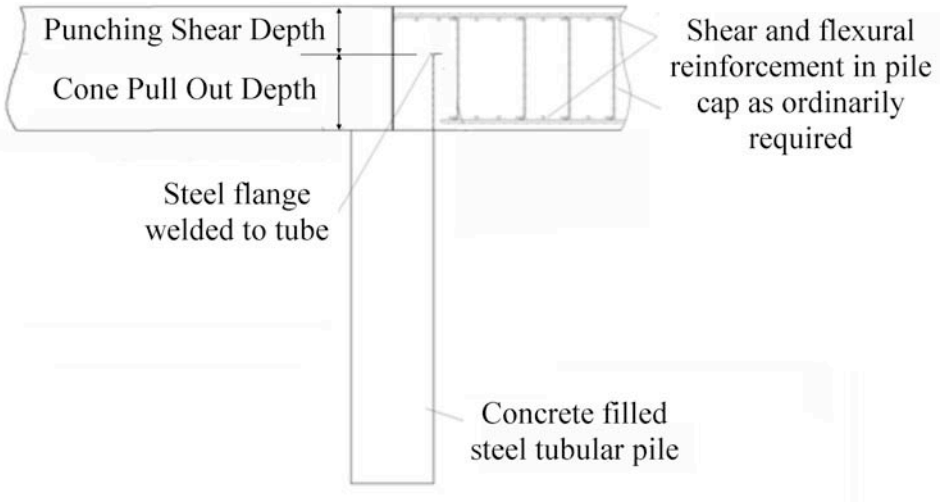

Figure 4.1 Proposed pile-to-pile cap connection

Stresses sustain by the steel tube are transferred to the surrounding concrete through bearing and bond. The majority of the stress transfer is accomplished by an annular ring, which is welded to the end of the steel tube. The design of the ring is as follows:

- The ring thickness should equal the pile thickness.
- The ring should project 16 times the thickness outside the tube and 8 times the thickness inside the tube.

The pile cap reinforcement is designed for bending and shear of the pile cap using conventional methods. The pile cap thickness should also be selected to meet bending and shear requirements, but it must also be adequate to develop the steel tube and to

accommodate the punching shear and cone pull-out, which result from the large compressive stresses sustained by the annular ring.

The minimum punching shear depth should be defined on the basis of the maximum compressive load on the pile using the outside diameter of the annular ring. Using the cone pull-out geometry illustrated in Figure 2.10, the required depth for cone pull-out, l_e, is defined as:

$$l_e = (-D_o + \sqrt{(D_o^2 + 2DtF_u/(n\sqrt{f_c'})})/2 \quad \text{(Eq. 7)}$$

In this equation, l_e is the minimum embedment depth, F_u is the ultimate tensile strength of the steel tube in psi, and D is the outside diameter of the steel tube. D_o is the outside diameter of the flange or annular ring, and f'_c is the concrete strength in psi. The recommended value of n is 6, based on prior experimental results (Lee 2010). Note that this equation is in the later stages of development, since experiments are still in progress, and further revisions are possible. However, this is a conservative equation, and it is expected that any further revisions will serve to make the minimum embedment length shorter.

The connection of a drilled shaft to a reinforced concrete pier in WSDOT is likely to take the form illustrated in Fig. 1.1. Experiments have not been performed on this connection. These experiments are required to investigate response, including the required transfer length to reach both the yield and ultimate moment capacity of the RCFT. In this initial phase, supplemental funding was provided to complete a series of nonlinear analyses of the connection. The objective of these analyses was to begin to study the RCFT response. A parametric study was established to investigate salient

parameters on the response. Analyses were performed on the general configuration of baseline model with variations on specific study parameters. The study parameters and conclusions made for each based on the analyses are provided below.

1. **Geometry of the tube (D/t ratio)**. Analyses were performed for a wide range of D/t ratios. When the reinforcing embedment was sufficient, the D/t ratio did not affect the overall response. Figure 4.2 shows a wide range of D/t ratios. In all cases, the normalized moment strength was the same.

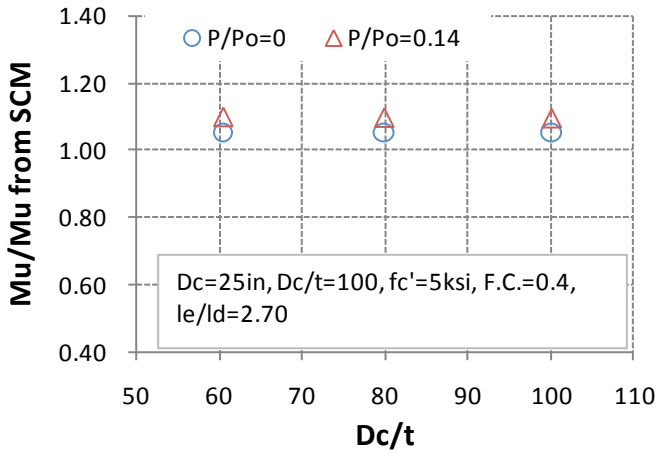

Figure 4.2 Impact of D/t ratio on the strength of pier-to-caisson connection

2. **The relative diameter of the tube and the reinforced concrete pier**. A more limited study was performed on the parameter, and the results indicated, again, that if the reinforcing bars are fully anchored, this parameter does not affect the performance.
3. **The number and size of reinforcing bars in the pier**. The number of reinforcing bars in the pier has only a minimal impact on the response, as shown in Figure 4.3. As suggested by the analysis results, fewer bars may allow a slightly shorter embedment; however this difference is minimal relative to other parameters and therefore is not

taken into account in the analysis. However, the size of the reinforcing bar influences the required anchorage depth. In all cases, the minimum anchorage depth of the reinforcing bar is twice the ACI limit.

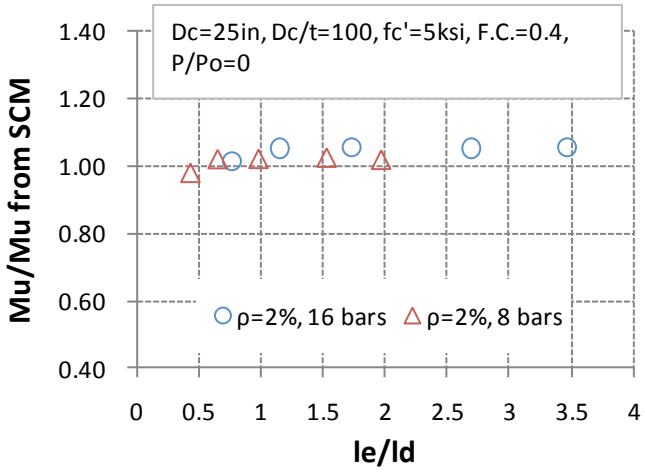

Figure 4.3 Impact of number of reinforcing bars on connection strength

4. **The coefficient of friction between the concrete fill and the steel tube**. This parameter was varied to simulate the internal condition of the tube. Discussions with engineers at WashDOT indicated that the caisson may not be fully cleaned in some locations and the bond stress transfer would be correspondingly reduced. This parameter is influential for shorter embedment depths. However, for longer embedment depths, the coefficient of friction does not affect the response significantly. This suggests that the contamination within the tube must be quite severe to cause a dramatic effect on performance
5. **The length of the tube**. Studies show that the required length of the tube is a function of the required embedment depth of the longitudinal reinforcement. These two design requirements are linked.

6. **The length that the reinforced concrete pier reinforcing extends into the tube**. This is the most important parameter. If the reinforcing bar is short (shorter than twice the ACI required length or the tube diameter), the connection will fail to achieve its full capacity. This is demonstrated in Fig, 3.16. However, if these design requirements are met, the response is stable. In addition, as noted by the previous items, a sufficient embedment depth minimizes the influence of the other parameters.
7. **The axial load in the column**. The analyses indicated that the axial load has an influence on the formation of the crack at the base of the longitudinal reinforcing bars, the amount of slip, and strength and stiffness, as would be expected from a cross-section analysis. However, for a well-anchored RC pier, these effects are minimal.

There is good confidence in these analyses, but experimental verification to support and document the analysis is needed. However, the recommendation from this experimental research is that the proposed pier-to-caisson connection is likely to be highly effective if the proper embedment length is maintained. The embedment length is compared to the minimum development length for rebar in the ACI-08 specifications (ACI 318-08 Section 12.2). The ACI development length was not fully effective in developing the strength. On the basis of these limited evaluations, the recommended length is the larger of (1) 2 times the ACI development length (ACI 2008) and (2) the outside diameter of the tube.

MINIMUM CASING THICKNESS

The minimum casing thickness is an important engineering issue for both driving and structural applications. This issue was a regular topic of discussion during the progress meetings. From these discussions it was agreed that the minimum thickness required for driving is a contractor decision.

For structural integrity, it is recommended that the minimum wall thickness of the casing for structural applications be defined by Eq. 1a. This equation will assure that the ultimate resistance proposed by the plastic stress distribution method can be achieved. Nonlinear continuum FEM analysis suggests that a more slender tube is possible for some applications, but this work is insufficiently advanced to justify a change at this time.

RELATIVE PROPORTION OF INTERNAL TO CFT REINFORCEMENT

The amount and placement of the internal reinforcement make it less effective than the reinforcing provided by the steel tube. Hence, it is recommended that the design rely primarily on the capacity of the CFT member. Use of longitudinal reinforcement may be required to satisfy other considerations, including connections and regions of the caisson for which the steel tube has been terminated. However, in most cases the addition of longitudinal reinforcement will not enhance the strength or stiffness of the RCFT, and in many cases it can be neglected in the strength and stiffness calculations. However, the steel tube, when corrosion effects are taken into account, has a significant effect on strength and stiffness and should be included in the engineering calculations in most cases.

STRESS-STRAIN AND MOMENT-ROTATION CURVES

As noted previously, the simplest and most accurate method of predicting the performance of CFT and RCFT is the plastic stress distribution method (Eqs. 6 for RCFT and Eqs. 4 for CFT) combined with buckling and stability checks (Eqs. 2) and the flexural stiffness (Eqs. 5) model.

A simple elasto-plastic moment-rotation behavior, such as illustrate in Fig. 4.4a, is proposed to simulate the connection response. The rotation can be considered as a concentrated end rotation with little loss of accuracy in performance. This simple elasto-plastic model has a sharp transition between elastic and plastic behavior, which is different than commonly used with fiber or section models.

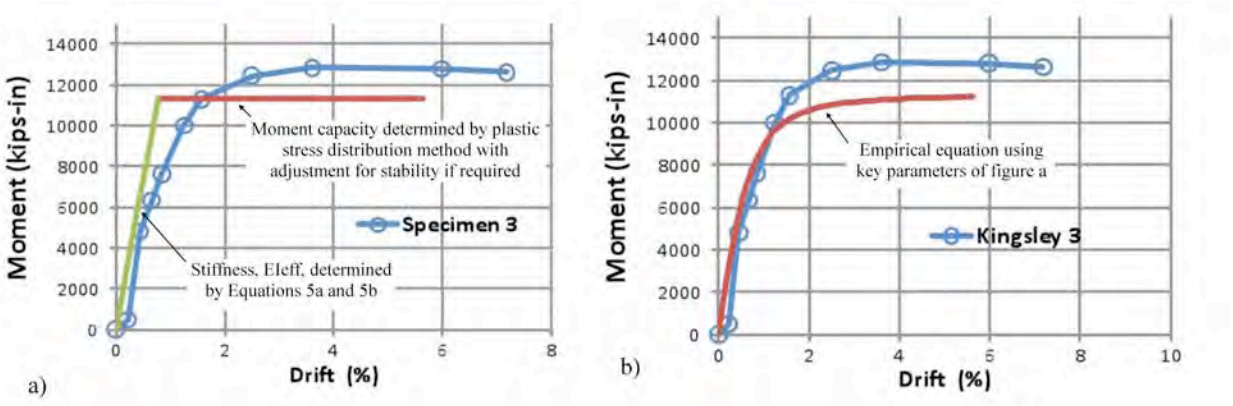

Figure 4.4 Proposed models for nonlinear deformation of CFT and RCFT elements

CFT and RCFT applications provide a slow transition to nonlinearity because of the progression of yielding in the steel around the circumference of the tube and the nonlinear performance of concrete. Hence, an alternative model with a smooth transition between elastic and plastic behavior is proposed, illustrated in Fig. 4.4b, and it is based on the Giuffre and Pinto model (1970). This second model also uses the moment

resistance, M_p, obtained from the plastic stress distribution method and the elastic stiffness model, but the moment rotation behavior is defined by an empirical curve:

$$M = \left[\frac{\theta}{\left(1+\theta^R\right)^{1/R}} \right] M_u \qquad \text{(Eq. 7a)}$$

where

$$\theta = \frac{\Delta}{\Delta_p} \qquad \text{(Eq. 7b)}$$

$$\Delta_p = M_u / K \qquad \text{(Eq. 7c)}$$

In the expressions, K is the elastic stiffness of the deflection parameter, Δ, and it depends on EI_{eff}, the boundary conditions, and mechanics of the application. The variable R is an empirical term calibrated to the experimental results, and R=4 is recommended on the basis of a comparison to past CFT experiments. Both models are simple to employ, and they result in better accuracy than that achieved by sectional analysis. The models were compared to a large number of experimental results, and Fig. 4.5 illustrates some of these comparisons.

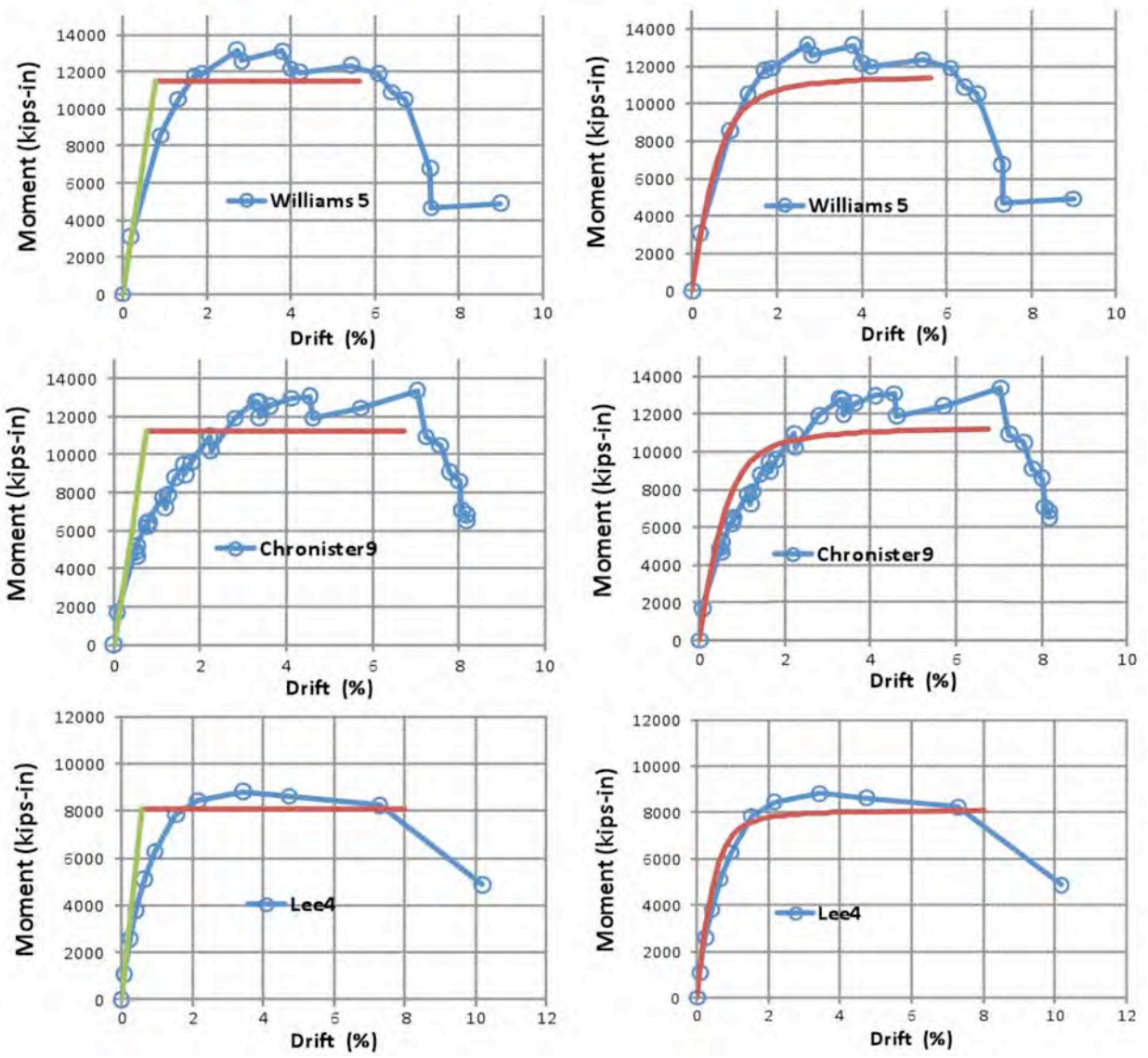

Figure 4.5 Comparison of proposed model and experimental results

CORROSION AND OTHER ISSUES

Other issues, including the availability of tube suppliers, different tube manufacturing methods, and corrosion, were included among the original 11 issues. However, during periodic discussions with WSDOT engineers, these issues became lower priority concerns. The CFT and RCFT applications for deep foundations normally

require large diameter tubes, and spirally welded tubes are likely more rapidly obtained and more widely available in these large diameters. Northwest Pipe and Skyline Steel are two suppliers of such pipe in this region. WSDOT has already modified its specification to include spiral welded tube. Straight seam welded tube may be available for CFT piles because of their smaller diameter. Tests have been performed on straight seam tubes, and the inelastic performance was found to be comparable.

Corrosion is an important engineering issue. AASHTO LRFD section 10.7.5 addresses corrosion and deterioration of steel piles. It is noted that corrosion depends on many factors, such as salt water intrusion, chemistry and pH of the soil, local effects such as industrial waste, and any coatings or protection. It is also recognized that sacrificial steel, corrosion resistant steel alloys, galvanization, and other cathodic protection may be employed. This research recognizes the issues of corrosion and deterioration, but corrosion was not a focus of this study. However, this study showed that the use of the composite benefits of CFT and RCFT is huge in comparison to the internal reinforcement currently employed. Furthermore, the tube thickness will typically be controlled by pile driving or handling of the tube during construction of the drilled shaft. As a result, the composite action provided by employing CFT and RCFT behavior will likely produce shafts that are stronger and stiffer than required by design.

Here, a sacrificial thickness method is recommended to compute the strength and stiffness of the RCFT, in only a part of the tube thickness in the CFT and RCFT evaluation. This recognizes that a significant portion of the tube thickness may be lost to corrosion, while the pile retains sufficient resistance for its intended application.

Furthermore, corrosion is likely only over a specific length of the pile or drilled shaft, depending upon the conditions permitting corrosion.

Hot-dipped galvanization can be used on these tubes to dramatically extend their life. Tests have been performed on CFT with galvanized steel, and the galvanization clearly has no detrimental impact on the composite action or structural performance.

CHAPTER 5

DESIGN EXPRESSIONS FOR CFT AND RCFT PILES AND CAISSONS AND FULLY RESTRAINED PILE CAP CONNECTIONS

INTRODUCTION

CFTs have engineering properties that offer strength and stiffness beyond a conventional reinforced concrete (RC) member. The research reported herein was undertaken to develop engineering expressions to fully use CFT piles and caissons in bridge construction, which include the steel shell. The research has shown that (1) CFT elements can sustain multiple cyclic drifts to large levels with minimal damage and (2) the expected strength and stiffness of RCFT is approximately that of CFT components and can be estimated using similar tools. However, RCFT offers very little advantage beyond that achieved with CFT, while adding considerable cost and complexity. As a result, RCFT is recommended only as a transition between CFT and RC elements.

The prior CALTRANS and ARMY research programs studied two types of fully restrained connections for CFT pier-to-foundation connections. One of those two connections are readily usable as CFT pile-to-pile cap connections, as illustrated in Fig. 5.1. This connection employs a flange or annular ring, as shown in Fig. 5.2. This annular ring is attached to the top of the CFT pile, and it is then partially embedded into the pile cap. This anchored connection resists flexural loading from the pile through strutting action to the bottom of the pile cap (resulting from the portion tube of the CFT column that is in tension) and the top of the pile cap (resulting from the portion of tube of the CFT column that in compression). The tests show this connection

is both simple to construct and fully effective in transferring the flexural strength of the CFT column.

Transition connections between RC concrete caissons and CFT caissons have not been tested, but considerable analysis has been performed. Models have been developed to predict the strength of the RCFT elements, and this RCFT behavior may be used to provide increased strength over a significant length of the pile relative to conventional RC construction. Figure 5.3 shows a proposed connection between a CFT or RCFT pile and an RC pile segment. This is expected to provide good performance, but the maximum resistance is limited to the capacity of the RC element for connections with adequate anchorage.

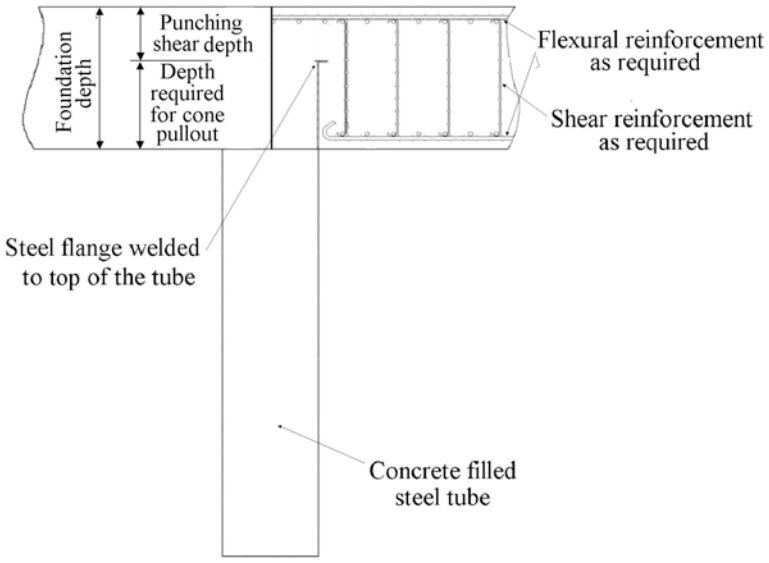

Figure 5.1. Monolithic foundation connection

Figure 5.2. Welded annular ring

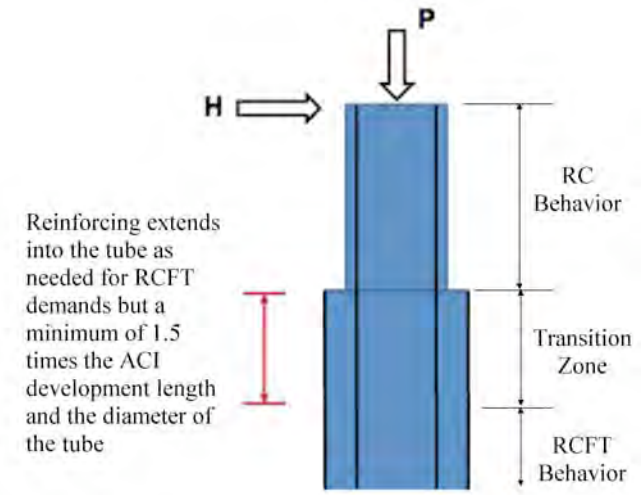

Figure 5.3. RC to RCFT connection

Although CFT columns have been studied by prior researchers, the tubes were typically small (6 inches or less in diameter) and few researchers have studied connections for bridge construction. Therefore an experimental study is critical to the implementation of CFT in bridge construction; the CFT column-to-foundation research has demonstrated this importance. While CFT components are permitted by codes, there is little community consensus on their design. The design expressions vary significantly among codes as shown in the discussion of Chapter 2 of this report.

The objective of this chapter is to present a step-by-step design procedure with validated design expression for a CFT bridge columns and fully restrained connections. The design expressions were validated using the test results describe herein as well as the extensive database gathered as part of this project. This chapter presents a compendium of these design recommendations and hence, there is some repetition of figures and equations provided earlier in this report.

The steps in the design of piles and caissons are as follows:

1. Establish the demands using an appropriate model of the bridge. This demand analysis will require stiffness values and resistance requirements for the piles and caissons. A nonlinear analysis of the bridge system will require a moment-rotation relation for the connection to be implemented as a concentrated rotational spring at the base of the connection (described in the section below on nonlinear analysis modeling) as well as the stiffness and deformation of the soil.
2. Establish the material properties for the concrete fill, steel tube, and fiber-reinforced grout.
3. Determine an initial size of tube to meet constructability, geometric limitations (D/t ratio) and a target axial stress ratio.
4. Design the caisson/pile for combined loading (flexure plus axial load demands) using a P-M interaction curve using the plastic stress distribution method that incorporates buckling.
5. Determine the required development length of the reinforcement into the CFT pile or caisson.

STEP 1: ESTABLISH MATERIAL PROPERTIES

CFT piles and their connections require three types of materials, including the concrete fill, the steel tube, and the reinforcing steel (in the pile cap element). None of the materials are proprietary.

The concrete fill for the CFT member used in the testing was a low-shrinkage, self-consolidating concrete. In the testing, the concrete strength nominal strengths were 42 MPa and 70 MPa (6 ksi and 10 ksi). This is a structural concrete, and the minimum strength is 28 MPa (4 ksi), with an expected strength 25 to 50% larger. The concrete mix must include a low-shrinkage admixture. Low shrinkage concrete is required to ensure the concrete does not shrink relative to the steel tube; a conventional concrete results in an amount of shrinkage that eliminates composite action, thereby comprising the stiffness of the component. A sample concrete mix is provided in Table 5.1.

Table 5.1. Sample concrete mix (used in test specimens)

AASHTO #8 (3/8") Aggregate	1460 lb.
Fine Aggregate	1538 lb.
Type I/II Cement	536 lb.
Type F H.R.W.R.	74.25 oz.
Type A Water Reducer	33.00 oz.
Slag (GGBFS)	289 lb.
Water	270 lb.

As indicated in the table, two admixtures were used: a high-range water reducer (Type F), also called a super plasticizer, to provide the properties required of an SCC mix and a Type A water reducer. In this case, the Type F H.R.W.R. is sold under the name ADVA 170 and the Type A water reducer is sold as WRDA64. Both are manufactured by Grace Construction Products.

Two different steel tubes have been tested. The steel tubes may either be straight seam or spiral welded tubes. Spiral welded tubes offer reduced cost, greater versatility and more rapid fabrication with large diameter tubes, since they can be formed to any diameter from a more limited inventory of materials. Spiral welded tubes are formed from coil steel, which has

different material designations (AISI designations) than commonly used in AASHTO. It is recommended that that a low-carbon, low-alloy steel with a minimum yield stress of 350 MPa (50 ksi) and minimum elongation at break of 15% be employed. The spiral welds must be formed by the double submerged arc process and continuously X-rayed during construction; the weld must be matching metal and meet the minimum toughness requirements of AISC Demand Critical welds (AISC 2005).

The reinforcing steel used in the foundation or cap-beam element is to be the same type of reinforcing steel used in current construction in regions of high seismicity (typically A 706).

STEP 2: ESTABLISH INITIAL TUBE GEOMETRY

There are three different aspects of CFT/RCFT engineering that should be considered when selecting the initial cross section of the tube. First, minimum thickness values may be required for constructability such as driving or corrosion. Second, it may be desirable to limit the axial stress on the member during seismic loading; commonly axial stresses under earthquake loading are limited to 10-20% of the gross capacity. And finally, tubes with very high D/t ratio may compromise their capacity, where as tubes with low D/t ratios may not develop their strength. Therefore aiming towards the D/t limit is encouraged. The following provides D/t limits for primary flexural (columns or piers) and primarily axial (piles or caissons) elements.

To develop the full plastic capacity of CFT or RCFT members, it is necessary to ensure that local buckling does not occur prior to development of the strength of the tube. This is accomplished by providing an upper limit on the D/t ratio. The research has shown that CFT members achieve greater ductility with increased inelastic deformation capacity at the proposed

full strength connection, because much of the inelastic deformation is contributed by yielding of the encased steel in the embedded connection. As a result, the recommended slenderness limit for CFT or RCFT within that full strength connection is:

$$\frac{D}{t} \le 0.22\frac{E}{F_y} \qquad \text{(Eq. 11a)}$$

For CFT and RCFT subjected primarily to axial loading, the recommended slenderness limit is:

$$\frac{D}{t} \le 0.15\frac{E}{F_y} \qquad \text{(Eq. 11b)}$$

STEP 3: STIFFNESS MODELS FOR CFT AND RCFT

The effective stiffness, EI_{eff}, of circular CFT is important, because it is used to evaluate deflections, deformations, buckling capacity, and moment magnification. The prior evaluation of the AISC, ACI, and AASHTO models indicate that none reliable predict the stiffness. A new expression that accounts for the impact of the axial load and effective reinforcing area on the concrete stiffness was developed; this effective stiffness factor is termed C'. Eq. 8 gives the resulting expression.

$$EI_{eff} = E_s I_s + C' E_C I_C \qquad \text{(Eq. 8a)}$$

$$C' = 0.15 + \frac{P}{P_0} + \frac{A_S}{A_S + A_C} < 0.9 \qquad \text{(Eq. 8b)}$$

The subscripts s and c to the steel, concrete section, respectively. The variables E and I are the elastic modulus and moment of inertia.

STEP 4: FLEXURAL STRENGTH AND MATERIAL INTERACTION CURVE

The flexural strength of CFT and RCFT members is determined using the plastic stress distribution method (PSDM), shown in Fig. 5.5 and described previously in Chapter 3. This method can be used to generate a full P-M interaction curve, as shown in Figure 5.5b. For each neutral axis depth, pairs of axial and bending resistances can be determined. Figure 5.5b shows the resulting material interaction curve where the values on the moment (x) axis and axial load (y axis) are normalized to the flexural strength without axial load (M_o) and the axial crush load without moment (P_o) of the member, respectively. Smaller D/t values result in larger resistance, because the area of steel is larger. Larger D/t ratios result in significantly increased bending moment for modest compressive loads, because of the increased contribution of concrete fill as shown in Fig. 5.5b.

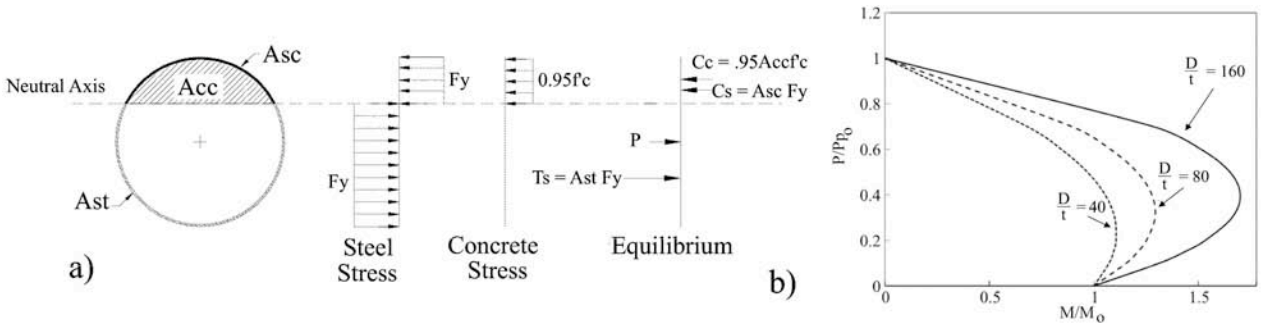

Figure 5.5. Strength determination for CFT; a) Plastic stress distribution method, b) Material-based interaction curves (no buckling)

A closed-form solution for the interaction curve for CFT piles has been derived based upon the geometry described in Fig. 5.6 and is expressed in Equations 9.

$$r_m = r - \frac{t}{2} \qquad \text{(Eq. 9a)}$$

$$\theta = \sin^{-1}\left(\frac{y}{r_m}\right) \qquad \text{(Eq. 9b)}$$

$$c = r_i \cos\theta \qquad \text{(Eq. 9c)}$$

$$P = F_y t r_m \left\{ \left(\pi - 2\theta\right) - \left(\pi + 2\theta\right) \right\} + \frac{0.95 f'_{ct}}{2} \left\{ \left(\pi - 2\theta\right) r_i^2 - 2yc \right\} \qquad \text{(Eq. 9d)}$$

$$M = 0.95 f'_{ct} c \left\{ \left(r_i^2 - y^2 \right) - \frac{c^2}{3} \right\} + 4 F_y t c \frac{r_m^2}{r_i} \qquad \text{(Eq. 9e)}$$

For RCFT members, a similar material interaction curve is expressed by Eqs. 10 with slightly revised geometry as illustrated in Fig. 5.7.

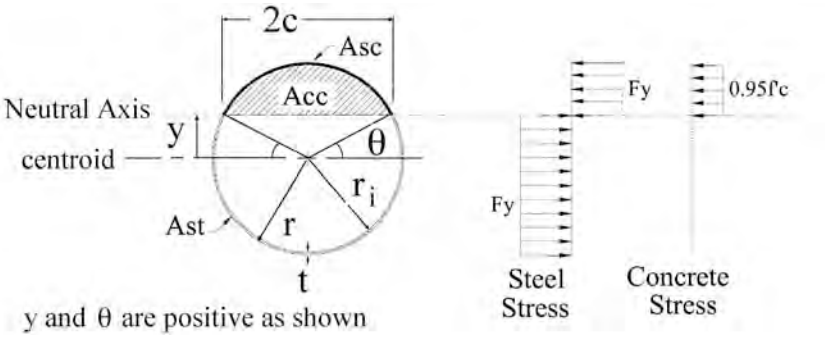

Figure 5-6. Geometry used for closed form derivation of CFT stress distribution prediction

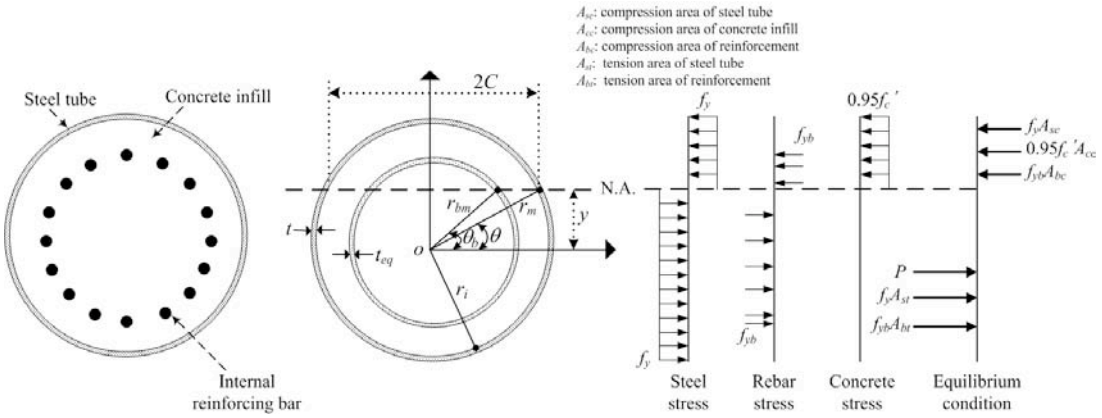

Figure 5.7. Geometry for derivation of plastic stress distribution method for RCFT

$$r_m = r - \frac{t}{2} \qquad \text{(Eq. 10a)}$$

$$\theta_s = \sin^{-1}\left(\frac{y}{r_m}\right) \quad \text{and} \quad \theta_b = \sin^{-1}\left(\frac{y}{r_b}\right) \qquad \text{(Eq. 10b and c)}$$

$$c = r_i \cos\theta_s \text{ and } c_b = r_b \cos\theta_b \qquad \text{(Eq. 10d and e)}$$

$$t_b = \frac{n A_b}{2\pi r_b} \qquad \text{(Eq. 10f)}$$

$$P = F_{ys} t r_m \left\{ (\pi - 2\theta_s) - (\pi + 2\theta_s) \right\} + t_b r_b \left\{ F_{yb}(\pi - 2\theta_b) - \left(F_{yb} - .95 f_c^{'}\right)(\pi + 2\theta_b) \right\}$$

$$+ \frac{0.95 f_c^{'} c}{2} \left\{ (\pi - 2\theta_s) r_i^2 - 2yc \right\} \qquad \text{(Eq. 10g)}$$

$$M = 0.95 f_c^{'} c \left\{ \left(r_i^2 - y^2\right) - \frac{c^2}{3} \right\} + 4 F_{ys} tc \frac{r_m^2}{r_i} + 4 F_{yb} t_b c_b r_b \qquad \text{(Eq. 10h)}$$

A positive value of P implies a compressive force, and y and θ are positive with the sign convention shown in the figures. The variable y varies between plus and minus r_i. The P-M interaction curve is generated by solving the equations for selected points in this range and connection of those points. These formulations can be readily programmed into a spreadsheet to form the interaction curves for both RCFT and CFT.

STEP 5: IMPACT OF COLUMN BUCKLING ON P-M INTERACTION CURVE (OPTION FOR NON-RESTRAINED CFT VERTICAL COMPONENTS)

Piles and caissons are relatively stocky and usually are well confined within the soil. The stiffness of the soil should clearly be adequate to prevent global stability failure. Hence, piles and caissons would not normally affected by P-Δ moment or other secondary effects. As a result, the following steps will not be needed for most applications of CFT or RCFT for these deep foundation elements. However, it is recognized that special circumstances such as scour or other design issues may leave piles and caissons subject to stability and P-Δ moment concerns. In these circumstances, it is necessary to adjust the material interaction curve shown in Fig. 5.5b to

account for stability and slenderness effects. To do this, it is necessary to employ the flexural stiffness, EI_{eff}, of the CFT pier, provided in Eq. 8.

Global column buckling is determined by the equations provided in AISC and repeated here for clarity (Eq. 11):

$$P_{cr} = 0.658^{\frac{P_o}{Pe}} P_o \qquad \text{for stocky columns,} \qquad \text{(Eq. 11a)}$$

$$P_{cr} = 0.877 P_e \qquad \text{for slender columns, and} \qquad \text{(Eq. 11b)}$$

$$P_o = 0.95 f_c^{'} A_c + F_y A_s \qquad \text{(Eq. 11c)}$$

where P_e is the elastic buckling load by the Euler equation, and A_c and A_s are areas of the concrete and steel, respectively.

The interaction curve including stability effects is a modified version of the material interaction curve (Fig. 5.5b), which forms its basis. A series of points are jointed to form the curve. The points are as defined as follows:

- Points *A* and *B* are the axial and flexural capacity by the PSDM.
- Point *C* corresponds to the location on the PSDM interaction curve that results in the same moment capacity as point *B* but with axial load.
- Points *A'* and *C'* are obtained by multiplying the axial load associated with points *A* and *C* by the ratio, $P_{cr}/P_{o,AISC}$.
- Point *D* is located on the PSDM interaction curve and corresponds to one half of axial load which is determined for point *C'*.
- Point *A''* is the intersection of PSDM *P-M* interaction and line parallel with *5*-axis through the point *A'*.

The resulting curve accounts for global buckling of the tube and an example is shown in Fig. 5.9. The axial strength is limited to point *A'* (or the AISC buckling capacity). The stability based *P-M* interaction curve is then constructed by connecting points *A'*, *A''*, *D*, and *B*, as shown in the figure. This interaction curve should then be used for strength design of the CFT member for all load conditions. Seismic design requires that less ductile elements be designed for the expected maximum plastic capacity of the ductile members. Given a specified axial load, the expected maximum bending moment of the CFT will be 125% of the moment obtained from the interaction curve and this is the demand that should be used to design any less-ductile connecting elements.

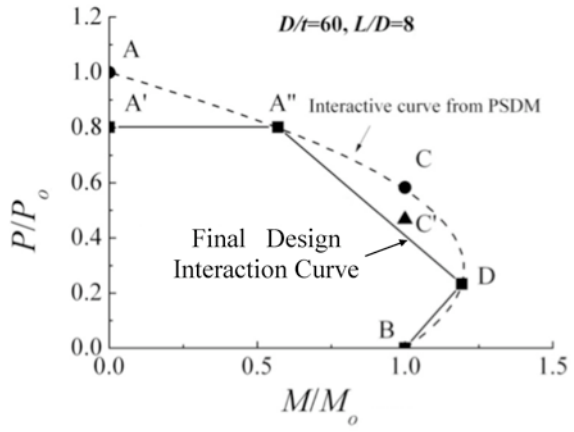

Figure 5.9. Construction of the Stability-Based Interaction Curve for CFT and RCFT

STEP 6: DETERMINE THE SHEAR STRENGTH OF RCFT

Prior research has not evaluated the shear strength of RCFT. This was not studied as part of this research. Such experiments are clearly warranted, but the shear resistance of the composite section clearly cannot be less than the shear resistance of the steel or concrete acting alone. The shear resistance of the steel will invariably be larger than the shear resistance of the

concrete unless the *D/t* ratio of the tube is extremely large (approaching 200). Equation 12 provides the shear resistance of the steel tube alone and is a conservative estimate.

$$V_u \le \phi V_n = \phi 0.6 F_y A_{shear} = \phi 0.6 F_y 0.5 \pi t D \qquad \text{(Eq. 12)}$$

STEP 7: PILE OR CAISSON CONNECTION DESIGN

Two types of connection are discussed for piles or caissons. The full strength connection, illustrated in Fig 5.1, is proposed for connecting piles to pile caps. The partial strength connection, illustrated in Fig. 5.3, is proposed for connection RC pier columns or RC caisson extensions to CFT or RCFT elements.

Full Strength Connection

The foundation connection design for the CFT must consider several different factors. A central part of this research study is the design and detailing of the connecting portion of the CFT to the foundation or cap-beam. The connection design should include:

1. Detailing/sizing of the annular ring
2. Determination of the embedment depth
3. Punching shear evaluation
4. General design (flexure and shear) of the connecting (foundation or cap-beam) element to sustain the CFT column demands.

Detailing of Annular Ring and Embedment Depth

An annular ring is welded to the end of the tube to provide anchorage and stress distribution, as illustrated in Fig. 5.2. The ring is made of steel of the same thickness and yield stress as the steel tube. The ring extends outside the tube 16 times the thickness of the tube and

projects inside the tube 8 times the thickness of the tube. This gives a width of the ring of 25 times the thickness of the tube, as shown in the figure.

The ring is welded to the tube with complete joint penetration (CJP) welds of matching metal or fillet welds on the both the inside and outside of the tube. The fillet welds must be capable of developing the full tensile capacity of the tube, and for this purpose the minimum weld size, w, of the fillets can be defined by Eq. 13a.

$$w \geq \frac{0.764 F_{EXX}}{F_u t} \qquad \text{(Eq. 13)}$$

where F_{EXX} and F_{uu} are the minimum tensile strength of the weld metal and tube steel, respectively. The CJP or fillet welds should as a minimum satisfy the AISC Demand Critical Weld toughness criteria (AISC 2005).

The tube and the annular ring are embedded into the RC pile cap with an embedment depth, l_e, needed to assure ductile behavior of the connection as depicted in Fig. 5.10.
This minimum embedment length is defined as:

$$l_e \geq \sqrt{\frac{D_o^2}{4} + \frac{DtF_u}{6\sqrt{f'_{cf}}}} - \frac{D_o}{2} \qquad \text{(Eq. 14)}$$

The concrete in the pile cap will have a minimum compressive strength, f'_{cf}, in units of psi. The variable D_o is the outside diameter of the annular ring for the embedded connection as shown in the figure, and F_u is the minimum specified tensile strength of the steel. For the grouted connection, D_o is the diameter of the corrugated metal form surrounding the ring, which is typically 50 to 100 mm (2 to 4 in.) larger than the diameter of the annular ring.

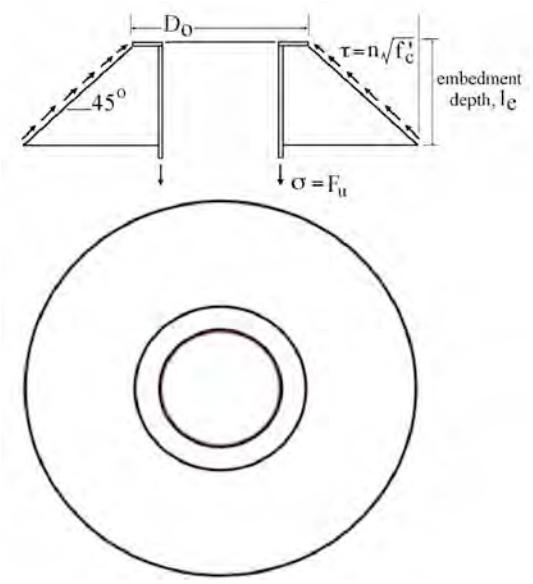

Figure 5.10. Cone pullout requirements for the full strength pile cap connection

The RC pile cap must have adequate concrete depth, *h*, above the concrete filled tube to avoid punching through the pile cap. Several methods may be used for punching shear evaluation, but the current ACI procedure for single shear (ACI 318 2011) is recommended as a conservative approach. In compression, the column carries the axial force (P_u) and the compression force from the moment couple from the same load case. However, unlike the tension case, the data show that a portion of the compressive force is distributed to the foundation through bond. This is similar to the force transfer mechanism for a reinforced concrete column. In compression, the column carries the axial force (P_u) and the compression force from the moment couple from the same load case. However, unlike the tension case, the data show that a portion of the compressive force is distributed to the foundation through bond. This is similar to the force transfer mechanism for a reinforced concrete column.

$$C_{max} = C_s + C_c \qquad \text{(Eq. 15a)}$$

$$d_f = \sqrt{\frac{D^2}{4} + \frac{250 C_{\max}}{\sqrt{f'_{cf}}}} - \frac{D}{2} \qquad \text{(Eq. 15b)}$$

Where C_c and C_s are the compression forces in the concrete and the steel due to the combined bending and axial load as computed by the PSDM for the most extreme combined load case. Using the ACI expression for gives the required total depth of the footing, d_f.

Pile Cap Reinforcement

The pile cap must follow conventional design practice and must be adequate to sustain the foundation design loads. As a result, the concrete, reinforcement and pile cap thickness usually will be identical to that required by normal pile cap design. However, the total concrete pile cap thickness, d_f, also must be large enough to control punching shear and cone pullout of the CFT column, as expressed in Eq. 16a. The width and length of the pile cap, b_f, must be large enough to accommodate the concrete struts of 60 degrees from the vertical originating at the base of the ring, as indicated in Eq. 16b

$$d_f \geq h + l_e \qquad \text{(Eq. 16a)}$$

$$b_f \geq D_o + 3.5 l_e \qquad \text{(Eq. 16b)}$$

The shear and flexural reinforcement in the pile cap must be designed for the normal shear and flexural loadings based upon the bridge loads, the soil conditions, and the expected capacity of the CFT pier. The flexural reinforcement in both directions should be spaced uniformly across the length and width of the footing, but the bottom layer of flexural reinforcement will be interrupted by the concrete tube. The longitudinal bars that are not interrupted by the tube must be designed with adequate capacity to develop the required foundation resistance. The interrupted bars are needed, but these bars do not contribute to the flexural strength of the footing. Figure 5.11 shows the configuration of the longitudinal

reinforcing bars that do not penetrate the tube but are placed within the tube diameter. Each of the bars was hooked using the provisions in ACI 318-08 Chapter 12. The hooked length is equal to $12d_b$, where d_b is the diameter of the longitudinal bar. The hook radius depends on the bar size. Using this detailing for the longitudinal bar permits development of the full yield strength.

The shear reinforcement in the footing must be designed to meet the shear demand. The vertical reinforcement used to resist the shear must meet an additional constraint within the anchorage region of the embedded tube, such that at least two (2) vertical bars intersect the cone depicted in Figures 5.9 and 5.10. Therefore vertical ties spaced no greater than *s* in the region within $1.5l_e$ of the outside of the tube, as defined by Eq. 17.

$$s \le \frac{l_e}{2.5} \qquad \text{(Eq. 17)}$$

In addition, it is noted that the required embedment results in a shear stress in the critical area surrounding the tube (Figure 5.10) of $6\sqrt{f'_c}$ (psi). Assuming the concrete is capable of resisting a shear demand of $2\sqrt{f'_c}$ (psi), the vertical reinforcement required by Eq. 17 should be designed to resist $4\sqrt{f'_c}$ (psi). Additional requirements for the shear demand resulting other load combinations must also be considered.

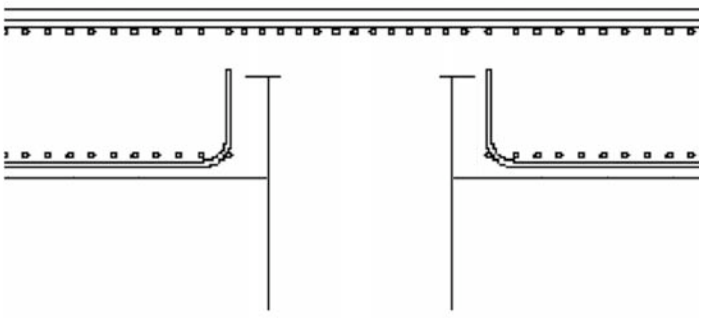

Figure 5.11. Detailing of longitudinal reinforcement adjacent to the tube

RCFT CAISSON-TO-RC PIER COLUMN CONNECTION

The recommended RCFT caisson to RC pier column connection is made as illustrated in Fig. 5.3. As noted earlier, this connection has been analyzed in some detail, but no experimental verification of the connection has been performed. The connection simply extends all tensile reinforcement into the RCFT element for a length greater than or equal to the diameter of the tube or 1.5 times the minimum development of the reinforcement as required by ACI. This detailing will develop the fully ultimate capacity of the RC pier at the top interface of the RCFT caisson. Further, if the internal reinforcement is continued to greater depth within the CFT caisson the full RCFT resistance as described earlier will be developed within the caisson beyond above stated required development length. Two things must be emphasized. First, this recommendation is supported by a comprehensive series of nonlinear analyses, but it has not been verified by experimental research. Second, the benefit of continuing the internal reinforcement with the tube is limited, because this internal reinforcement is far less effective than the steel tube in strengthening the caisson.

As with the proposed full strength pile-to-pile cap connection, the reinforcing in the RC pier must meet all normal design ACI requirements.

DESIGN EXAMPLE

This example employs a large scale CFT or RCFT pile or caisson along with a full strength pile-to-pile cap connection. For this example buckling and stability are unlikely to be considered, since the caisson is fully supported its length. However, to illustrate the use of the stability requirements the example will assume that the caisson is unsupported over a 44 ft height

because of scour. The critical load cases in this example are carried forward from the Ebey Slough example for the CFT caisson included in Chapter 4. In this example, M_u was 12,070 kip-ft, P_u was 800 kips and V_u was 303 kips. The CFT caisson selected for that task was 60 inch diameter tube with 1 inch wall thickness for convenience of handling and installation, but only 0.625 inches of the tube was considered in strength calculations because of potential lose due to corrosion. This example will be continued forward with and RCFT caisson using the following material properties:

Steel Tube: E_s = 29,000 ksi; F_y = 50 ksi

Concrete Fill: f'_c = 4000 psi; E_c = 3,605 ksi

Reinforcing Steel: E_s = 29,000 ksi; F_y = 60 ksi

Design Process

The caisson was designed using the following procedure.

1. Determine the factored load demands (axial, bending and shear) on the columns. This was done from prior example as noted above.
2. Find initial estimate of the column diameter and tube thickness to sustain the axial load such that $P/P_o < 0.1$. Initial estimates of D/t between 80 and 100.
3. Determine the effective stiffness of the column.
4. Establish the material based P-M interaction curve.

Steps 5 through 8 may not be needed for pile or caisson operations, because they are well restrained against lateral deflection because of the soil.

5. Using the effective stiffness, determine the moment magnification factor for the column, δ_s.

6. Magnify the moments by the magnification factor.
7. Determine the required M_n and P_n combinations for each load case, i.e., M_u/ϕ and P_u/ϕ where ϕ=0.75 for most live loads and ϕ=1.0 for seismic load case.
8. Compute the P-M interaction curve considering stability effects.

Steps 9 and 10 will be required for all cases, regardless of P-δ effects.

9. Compare the computed demands and capacities.
10. For the designed column, find the required connection (embedment depth) to the foundation.

Example Steps 1 through 4

The initial size of the tube is estimated using a target axial stress level. For the CFT example, the member was designed with approximately 5% of crush load under maximum load conditions (i.e. 800/16,230=0.0496) and the 0.375" allowance was made for corrosion. Further, a target vD/t ratio of 80 to 100 was used to meet the slenderness requirements. For the case where capacity of the pile-to-pile connection controls the design:

$$D/t \le 0.22\, E/F_y = 0.22\left(29000/50\right) = 127.6$$

If plastic hinging within the pile controls:

$$D/t \le 0.22\, E/F_y = 0.15\left(29000/50\right) = 87$$

If plastic hinging in the pile controls the target D/t ratio becomes approximately 85. With a 1" tube wall thickness for installation and a 0.375-inch reserve for corrosion this implies the RCFT caisson has:

$$D \approx 85 * 0.625 = 53.1"$$

Hence a 54" diameter tube with 1.5% flexural reinforcement placed at a radius of 22 inches is used for the initial design. This percentage of reinforcement requires 22 #11 bars at a radius of 22 inches spaced at approximate 6.25" on the arc of the radius. Equations 9 and 10 of this chapter where then used to define the material based P-M interaction curve for the CFT member described in Chapter 4 and the RCFT member discussed here. The resulting curves are shown in Fig. 5.14. In both cases only 0.625" if the 1" inch wall thickness was used in the strength calculations.

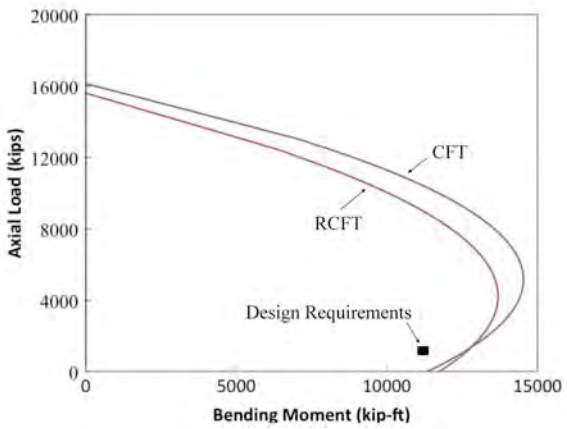

Figure 5.12. Comparison of material based P-M interaction curves for 60" CFT and 54" RCFT

This curve clearly shows that the resistance of the CFT and RCFT are similar. The CFT generally has a bit larger resistance, however it uses 8% less steel and 22% more concrete than the smaller diameter RCFT caisson. Resistance factors must be applied to both interaction curves, but it can be seen that both applications will be adequate after the resistance factor is applied. However, the RCFT has considerably more cost and complexity in the placement of the cage. For these reasons, the use of CFT in encouraged over RCFT for most applications.

The shear capacity of the RCFT and CFT are:

$V_u = 303 \le \phi * 0.5 * 0.625 * 60 * \pi * 0.6 * 50 = 1{,}589 kips$ for CFT application and

$$V_u = 303 \le \phi * 0.5 * 0.625 * 54 * \pi * 0.6 * 50 = 1{,}431 kips$$ for RCFT application.

Both cases easily meet the shear requirements. The P-M interaction curve above and the factored design moment would be adjusted for stability effects for bridge piers (Steps 5 through 8 above), but deflection and buckling of a caisson in the soil is not possible and is not considered in this example.

The nonlinear models described in this chapter can be used to establish analytical models for prediction behavior of both the CFT and RCFT caisson. The plastic capacity is defined based upon P-M interaction curves noted above, and the elastic stiffness is defined by Eqs. 8. That is:

$$C' = 0.15 + \frac{P}{P_0} + \frac{A_S}{A_S + A_C} < 0.9$$

$$EI_{eff} = E_s I_s + C' E_C I_C$$

The stiffness could be calculated for both the full 1" wall thickness for an upper limit or the 0.625" used for the strength calculations for a lower limit on the stiffness. In this example, the full thickness will be used. For CFT:

$$C' = 0.15+.05+(188/2826)=0.265$$

$$EI_{eff} = 29000*3.14*1*59^3 + 0.265*3605*0.049*58^4 = 19.24\ 10^9 \text{ kip-in}^2$$

for RCFT:

$$C' = 0.15+.05+(204/2289)=0.289$$

$$EI_{eff} = 29000*3.14*1*53^3 + 25395*3.14*.247*44^3 + 0.265*3605*0.049*52^4 = 15.58\ 10^9 \text{ kip-in}^2$$

A connection is likely required to a RC bridge pier or a pile cap or similar footing. These connections are based on the concepts described in Fig. 5.3 earlier in the chapter. For the RC bridge pier connection, the flexural and spiral reinforcement would extend into the concrete

filled tube for the larger of 1.5 times the ACI development length equation or the diameter of the tube.

For the full strength embedded pile cap connection shown in Fig. 5.2 the embedment depth and punching requirements of Eqs 14 and 15 are required. In addition the annular ring would be sized to the 1" thickness of the tube, and the footing shear reinforcement in the cone pullout area is required as described earlier in this chapter.

CHAPTER 6

CONCLUSIONS AND FUTURE WORK

The research summarized herein is the first phase of a proposed two-phase research program to investigate connections for CFT and RCFT caissons that are commonly used as substructure components in Washington state bridges. WSDOT is currently using reinforced CFTs as caissons and piles; however, it is discounting the contribution of the steel tube because the engineering models needed to accurately assess their properties and to design their connections do not exist. This research will result in those tools and represents a potential cost savings to the state by reducing the size of these important foundation elements.

This two-phase research program addresses important aspects of the engineering design of these components, including the following: (1) the bond between the steel tube and concrete fill, (2) connections for reinforced CFT caissons. including shear connections and partial strength connections needed for a wide range of seismic bridge applications, and (3) design methods for these connections. This study investigated fundamental design aspects of CFT component behavior, including strength, stiffness, and deformability. In addition, the connection was studied with analytical tools. The analysis provided important information about the behavior of CFT and RCFT and provides a basis for future experimental work on connections. The second phase will study the connections using large-scale experimental methods and will extend the experimental study with parallel continuum analyses. The results from the second phase

will be used to develop engineering models and design expressions for CFT connections. The second phase is discussed as future work at the end of this chapter.

CONCLUSIONS

CFT and RCFT offer significant advantages in practice. They permit rapid and economical construction, since they make optimum use of the material's behavior and can be constructed without formwork, shoring, or internal reinforcement. With self-consolidating concrete (SCC), the concrete fill can be placed without vibration, and this further facilitates the goals of rapid and economical construction.

The research effort described herein has resulted in improved models for predicting the strength, stiffness, and axial load-bending moment interactions for CFT and RCFT components. The research was focused on use of CFT and RCFT for bridge caissons.

A large database of CFT component tests was gathered. Review of the literature indicates that few tests on RCFT have been conducted. The compiled CFT database includes individual components subjected to bending, CFT component tests subjected to axial load, CFT component tests subjected to bending and axial load, and CFT connection tests. The database was used to evaluate a range of commonly used engineering expressions for strength and stiffness as well as D/t ratios. Evaluation of available models and development of new design models using the test results indicated the following:

1. Of the methods available for estimating the flexural strength, the plastic stress method provides the best and simplest estimate.

2. There is considerable uncertainty regarding the strain limit when a fiber-type modeling approach is used to estimate the flexural strength.
3. The effective flexural stiffness of CFT components must account for the impact of concrete cracking and include the effects of the axial load.
4. The AISC method for predicting the axial capacity, including slenderness effects, is accurate.

The test results were used to validate a finite element modeling approach. The model used solid elements for the concrete fill, and shell elements were used to simulate the tube. The concrete-to-steel interface was modeled using gap elements, which accounted for confining effects. The interface elements use a coefficient of friction to simulate the bond between the tube and the concrete fill. The results indicated that the model is capable of simulating the global response, including force-drift and moment rotation, as well as more local response mechanisms including the local slip and tube buckling. This validated modeling approach was used as the fundamental research tool in this study to investigate the response of CFT with internal reinforcement (RCFT) and the response of RCFT to RC pier connections.

Chapter 3 presented the research study approach and findings. The first portion of the study focused on the response of RCFT components. As discussed previously, there are scan data available of RCFT components; therefore, a parametric study was conducted to explore the response and primary engineering properties of RCFT components analytically. The study varied the diameter, D/t ratio, internal reinforcing ratio, diameter of the internal reinforcement, and axial load. The results were used to evaluate the recommended models from the CFT study (presented in Chapter 2). The

results indicated that the CFT models are appropriate for RCFT design. In addition to the previous models, the analytical results were used to evaluate available P-M interaction diagrams and a new, more accurate modeling expression was proposed.

The validated CFT modeling approach was then combined with a model for an RC pier to simulate the response of RC pier-to-RCFT caisson connections. Again, a parametric study was conducted. The CFT model was identical to that used for the RCFT component analysis. An additional modeling requirement was an accurate model for the RC pier, which was validated by using a previous test conducted for WSDOT at the University of Washington. This model was used to conduct a parametric study on the fundamental aspects of the connection geometry, reinforcement, and loading. Specific parameters studied included (1) embedment length of the longitudinal reinforcement, (2) tube diameter, (3) axial load ratio, (4) coefficient of friction between the tube and the concrete fill, (5) tube diameter and D/t ratio, and (6) number of reinforcing bars. The most influential parameter affecting the connection response, including capacity, slip, and cracking, was the length of the embedded reinforcement. Other parameters had a secondary effect, including axial load ratio and the number of reinforcing bars. However, none of these parameters affected the response if the embedment of the reinforcing bars was sufficient.

A primary objective of the research study was to investigate and address 11 fundamental aspects of RCFT and RC pier-to- RCFT caisson connection design. These issues were raised in the initial WSDOT discussions related to this research program and are summarized in Chapter 1. Recommendations are provided in Chapter 4. The

following repeats the 11 issues and, for each, a summary of the recommendation(s) made for each.

1. **Analytical models with hand solution equations**. Use of the plastic stress method is recommended to calculate the flexural strength and combined axial-flexural strength of CFT and RCFT cross-sections. The AISC method is recommended for calculating the axial capacity to account for slenderness effects. A new approach has been developed to estimate the P-M interaction curve.
2. **Design examples using the outcome of the analytical model**. The Ebey Slough drilled shaft was redesigned with the tools.
3. **Single shaft-single column case and CFT pile cap connections**. Design recommendations have been made for both of these connections. The pile-cap connection design was developed from previous research by the authors. The design recommendations for the RC pier-to-RCFT caisson were determined from the analyses.
4. **Analytical model including both steel casing and internal reinforcement**. An extensive analytical study was conducted on RCFT components and connections. The results indicated that the CFT design models are appropriate for RCFT and fully account for the steel casing and the internal reinforcement.
5. **Minimum casing thickness for structural and pile driving**. The minimum thickness needed for structural integrity is established by using the design models. The minimum thickness needed for driving the steel

casing should be determined by the contractor.

6. **Relative ratio of internal reinforcement to steel casing**. The analyses showed that the size and position of the steel casing (or tube) results in a large strength contribution. As a result, even if the tube and internal reinforcing ratios are equal, the tube will contribute more than 50 percent of the strength. Therefore, the amount of internal reinforcement will depend on other factors, including the reinforcement of the RC pier, connection requirements, and cracking control. The tube thickness will largely be controlled by the integrity of the tube during driving.

7. **Connection details for attachment of the steel casing to the pile cap**. The research presented results for the column-to-footing connection and included the use of an annular ring at the end of the tube and a required embedment depth. Several variations have been considered for the column-to-cap beam or other components with partial fixity. However, additional experimental research is needed to develop design recommendation for these components. The RC pier-to-RCFT caisson connection was investigated analytically. The results indicated that sufficient embedment depth is required for the reinforcing steel, and that this embedment depth is at least twice the ACI development length and the tube diameter.

8. **Stress-strain or moment-curvature models for RCFT composite sections**. The research considered alternative approaches to the PSDM. However, those methods proved to be less reliable and more complicated.

A moment-rotation relation was developed for the column-to-footing or column-to-pile cap connection.

9. **Casing manufacturers and availability of type and size**. A new plant owned by Skyline steel has opened in Longview, Washington, and therefore the availability of high-quality spiral welded tubes has increased.
10. **Use of spirally welded steel tubes**. Only spirally welded tubes were used in the experimental investigation, and the results formed the basis of the validated analytical model used in this research study.
11. **Corrosion rate for steel casing**. Discussions suggested that AASHTO and other sources have corrosion rates that would be appropriate for the steel casing used in CFT and RCFT components. The authors suggest using a sacrificial thickness method to account for the impact of corrosion on the strength and stiffness.

FUTURE WORK

The first phase of this project investigated important parameters; the second phase of the project will focus on experimental evaluation of the connections. The second phase will include both experimental and analytical research to further investigate the connections and develop expressions for their design.

The experimental study will investigate the impact of the embedment depth of the reinforcing steel on the connection response. The design of the specimens will be based on the analytical study conducted as part of Phase I. The specimens will be scaled from a full-scale prototype. On the basis of the laboratory capacities, it is expected that the reinforced concrete column will be 16 in. in diameter connected to a 20-in diameter CFT

caisson. The internal reinforcement from the RC column will be embedded into the CFT. The CFT will be anchored to a large reinforced concrete block to transfer the bending, shear, and axial demands.

Instrumentation will be placed to study the response of the embedded reinforcing bars, and conventional resistance strain gauges will be used. In addition, the response of the CFT will be monitored by using a newly purchased vibrating wire gage system. Two types of vibrating wire gages will be used: internal gauges in the concrete and external gages for the steel tube. In addition, conventional resistance strain gauges will be used to monitor the steel tube.

The results from the FE study indicated that the embedment depth of the reinforcing bars must be at least twice the ACI-specified length or the tube diameter. The experimental study will focus on the impact of the embedment depth of the reinforcing steel by specifically investigating the response of a connection with adequate embedment and a connection with inadequate embedment. The experimental results will be compared with the analytical study to verify and improve the modeling capabilities.

The improved model will then be used to extend the study to evaluate several additional important variables. The FE analysis will be used to evaluate a wide range of alternative connections and applications to explore applications for which CFT with or without internal reinforcement will be economical and practical for WSDOT bridge design. In particular, the following parameters and effects will be studied:

- variation in CFT diameter
- variation in RC diameter
- variation in RC pier placement relative to CFT (i.e., the RC pier will be offset to evaluate the impact on response and connection requirements)

- variation in axial load, including loading beyond the “balance” point and tension loading
- full caisson, including termination of tube.

The results will be used to develop design expressions and charts for the required embedment depth as a function of these important parameters. Expressions for CFT piers with and without internal reinforcement will be developed. The research results will be implemented in the WSDOT Bridge Design Manual for design and analysis of future bridge construction projects with pile or shaft foundations, and they will introduce the option of using CFT piers and components for rapid and economical bridge construction.

REFERENCES

AASHTO (2009) “AASHTO LRFD Bridge Design Specification,” American Association of State Highway and Transportation Officials, Washington, D.C.

AASHTO (2007) "AASHTO Guide Specification for LRFD Seismic Bridge Design," American Association of State Highway and Transportation Officials, Washington, D.C.

ABAQUS, (2005) ABAQUS standard user’s manual version 6.5. 2005; Hibbit, Karsson and Sorensen Inc.

ACI (2008) “Building Code Requirements for Structural Concrete and Commentary,” American Concrete Institute, Farmington Hills, MI.

AISC (2005) “Specifications for Structural Steel Buildings” ANSI/AISC Standard 360-05, American Institute of Steel Construction, Chicago, IL.

ATC (1992) "Guidelines for Cyclic Testing of Componenets of Steel Structures," Applied Technology Council, Redwood City, CA.

Bishop, E. S. (2009) “Evaluation of the Flexural Resistance and Stiffness Models for Circular Concrete-filled Steel Tube Members Subjected to Combined Axial-Flexural Loading,” a thesis submitted in partial fulfillment of Master of Science in Civil Engineering, University of Washington, Seattle, WA.

Boyd, P.F., Cofer, W.F., and Mclean, D.I., (1995) “Seismic Performance of Steel-Encased Concrete Columns under Flexural Loading.” *ACI Structural Journal*, Vol. 92, No. 3, pp. 355–364.

Chronister, A. (2007). “Experimental Investigation of High Strength Concrete Filled Steel Tubes in Embedded Column Base Foundation Connections.” Unpublished data , University of Washington, Seattle, WA.

Elchalakani, M., Zhao, X.L., and Grzebieta, R.H. (2001) “Concrete-Filled Circular Steel Tubes Subjected to Pure Bending,” *Journal of Constructional Steel Research*, Vol. 57, pp. 1141-1168.

Elremaily, A., and Azizinamini, A. (2002) “Behavior and Strength of Circular Concrete-Filled Tube Columns,” *Journal of Constructional Steel Research*, Vol. 58, pp. 1567-1591.

Fujimoto, T., Mukai, A., Nishiyama, I., and Sakino, K., (2004) “Behavior of Eccentrically-Loaded Concrete-Filled Steel Tubular Columns,” *Journal of Structural Engineering,* Vol. 130, No. 2, pp. 203-212.

Furlong, R.W. (1967), “Strength of Steel-Encased Concrete Beam Columns,” *Journal of the Structural Division*, ASCE, Vol. 93, No. ST5, pp. 113-124.

Han, L.H, Lu, H., Yao, G.H., and Liao, F.Y. (2006) “Further Study on the Flexural Behaviour of Concrete-Filled Steel Tubes,” *Journal of Constructional Steel Research*, Vol. 62, pp. 554-565.

Hseih, J.C. (2011) private email communication, March 16, 2011.

Inai, E., Mukai, A., Kai, M., Tokinoya, H., Fukumoto, T., Mori, K. (2004). "Behavior of Concrete-Filled Steel Tube Beam Columns." *Journal of Structural Engineering* . Vol. 130, No 2, pp. 189-202.

Kingsley, A. (2005). “Experimental and Analytical Investigation of Embedded Column Base Connections for Concrete Filled High Strength Steel Tubes.” a thesis submitted in partial fulfillment of Master of Science in Civil Engineering, University of Washington, Seattle, WA.

Lee, Jason R. (2011) "Experimental Investigation of Embedded Connections for Concrete-Filled Steel Tube Columns Subjected to Combined Axial-Flexural Loading," a thesis

submitted in partial fulfillment of Master of Science in Civil Engineering, University of Washington, Seattle, WA.

Mander, J.B., Preistley, M.J.N., and Park, R. (1988). "Theoretical Stress-Strain Model for Confined Concrete," *ASCE Journal of Structural Engineering*, Vol. 57, No. 8, pp.1804-1826.

Marson, J. and Bruneau, M. (2004) "Cyclic Testing of Concrete-Filled Circular Steel Bridge Piers Having Encased Fixed-Base Detail," *ASCE Journal of Bridge Engineering*, Vol. 9, No. 1, pp. 14-23.

Mazzoni, S., McKenna, F., and Fenves, G.L. (2005) "Open System for Earthquake Engineering Simulation User Manual; Version 1.6.0," Pacific Earthquake Engineering Research Center, University of California, Berkeley. (http://opensees.berkeley.edu

Moon, J, Roeder, C.W., Lehman, D.E., and Lee, H-E (2011) "Finite Element Modeling and Behavior of Circular Concrete-Filled Tubes Subjected to Bending," submitted for publication review, *Engineering Structures*, Elsevier.

Morino, S., Sakino, K., Mukai, A., and Yoshioka, K., (1997) *Experimental Studies of CFT Column Systems – U.S.-Japan Cooperative Earthquake Research*, ASCE, New York, NY, pp. 1106-1110

O'Shea, M.D., and Bridge, R.Q., (2000) "Design of Circular Thin-Walled Concrete Filled Steel Tubes" *Journal of Structural Engineering*, Vol. 126, No. 11, pp. 1295-1303

Prion, H.G.L., and Boehme, J. (1994) "Beam-Column Behaviour of Steel Tubes Filled with High Strength Concrete," *Canadian Journal of Civil Engineering*, Vol. 21, pp. 207-218.

Roeder, C.W, Lehman, D.E., and Thody, R. (2009) "Composite Action in CFT Components and Connections," AISC, *Engineering Journal*, Chicago, IL.

Roeder, C.W., Lehman, D.E., and Bishop, E. (2010) "Strength and Stiffness of Circular Concrete Filled Tubes," ASCE, *Journal of Structural Engineering*, Vol 136, No 12, pgs 1545-53.

Roeder, C.W., Cameron, B., and Brown, C.B., (1999) Composite action in concrete filled tubes, *Structural Engineering*, ASCE, Vol 125, No. 5, May 1999, pgs 477-84.

Schneider SP. (1998) Axially loaded concrete-filled steel tubes.'' J Struct Engrg ASCE; 124(10): 1125–38.

Thody, R. (2006). "Experimental Investigation of the Flexural Properties of High-Strength Concrete-Filled Steel Tubes." a thesis submitted in partial fulfillment of Master of Science in Civil Engineering, University of Washington, Seattle, WA.

Wheeler, A., and Bridge, R., (2006) "The Behavior of Circular Concrete-Filled Thin-Walled Steel Tubes In Flexure," *Composite Construction in Steel and Concrete V*, Proceedings of the 5th International Conference, Vol. 39, pp. 412-423.

Williams, T.S. (2006). "Experimental Investigation of High Strength Concrete Filled Steel Tubes in Embedded Column Base Foundation Connections." a thesis submitted in partial fulfillment of Master of Science in Civil Engineering, University of Washington, Seattle, WA.

Zhang, G.W., Xiao, Y., and Kunnath, S., (2009) "Low-Cycle Fatigue Damage of Circular Concrete-Filled Tube Columns," *ACI Structural Journal*, Vol. 106, No. 2, pp 151-159